A Curved Beam Element and Its Application to Traffic Poles

by

Cheng Zhang

A Thesis

Submitted to the Faculty of Graduate Studies

in Partial Fulfillment of the Requirements

for the Degree of

MASTER OF SCIENCE

Department of Mechanical and Industrial Engineering

University of Manitoba

Winnipeg, Manitoba

THE UNIVERSITY OF MANITOBA

FACULTY OF GRADUATE STUDIES

*****

COPYRIGHT PERMISSION PAGE

A CURVED BEAM ELEMENT AND ITS APPLICATION TO TRAFFIC POLES

BY

CHENG ZHANG

A Thesis/Practicum submitted to the Faculty of Graduate Studies of The University of Manitoba in partial fulfillment of the requirements of the degree

of

MASTER OF SCIENCE

Abstract

Curved traffic poles may vibrate noticeably when excited by the wind. The finite element method can be utilized to analyze these beam-like structures. A three-node, curved beam element has been developed for the static and dynamic analysis of curved poles. Shear deformation as well as rotary inertia effects are included. Furthermore, reduced integration is used to prevent the shear locking problem. Several examples are used to verify the accuracy and computational efficiency of this element. The results agree well with exact solutions or results taken from the literature. The element is used to analyze the wind induced vibrations of curved traffic poles. Natural frequencies and the corresponding mode shapes are computed. Time integration is utilized to compute the dynamic response of curved poles having hexagonal and octagonal cross-sections. The initiation of galloping is investigated and critical wind speeds are found.

Acknowledgements

I would like to express my deep gratitude to my thesis advisors, Profs. N. Popplewell and A. H. Shah, for their academic guidance, knowledge and experience throughout this work. I am also grateful to Mr. B. Barrett for his effort in doing all the aerodynamic experiments. The helpful discussions with Mr. Q. Zhang, Mr. M. Lu, Mr. W. Flather and Mr. H. Bai, are appreciated greatly. I would also like to thank Dr. R. Derksen for serving as an examiner. The financial support provided by NSERC is acknowledged gratefully.

I would like to thank Manitoba Hydro's research committee for providing continuous financial support to the graduate students working in this area.

Finally, special thanks are due to my parents, my family as well as my friends for their support and encouragement throughout my M. Sc. Program.

Table of Contents

List of Figures

List of Tables

Nomenclature

A	area of a cross-section
a_{c0}, a_{c1}	proportional constants in structural damping matrix
a_n	frequency coefficients
$\bar{a}, \bar{b}$	constants in equation (A.2)
a_0, a_1, a_2 b_0, b_1, b_2 c_0, c_1, c_2	constants in N_i
b	width of a beam
$[B]_\varepsilon, [B]_{\gamma\zeta}$ $[B]_{\gamma\eta}, [B]_t$	strain matrices
C_D, C_S	drag and side force coefficients for a straight pole, respectively
C_D^*, C_S^*, C_L^*	drag, side and lift force coefficients, respectively, for the curved part CD
$C_{MR}^*, C_{MP}^*, C_{MY}^*$	rolling, pitching and yawing moment coefficients, respectively, for the curved part CD
C_{DC}, C_{SC}, C_{LC}	drag, side and lift force coefficients for the curved model BE, respectively
$C_{MRC}, C_{MPC}, C_{MYC}$	rolling, pitching and yawing moment coefficients for the curved model BE, respectively

$[C]$	structural damping matrix
d	diameter of a circular cross-section
D	dimension of a hexagonal or octagonal cross-section
D_1	dimension of a hexagonal cross-section
e	eccentricity
E	Young's modulus
f_s	frequency of a complete cycle of vortex shedding
F_0	distributed load
$\{F\}$	distributed load vector
F_D, F_S, F_L	drag, side and lift forces per unit length, respectively
F_{MR}, F_{MP}, F_{MY}	rolling, pitching and yawing moments per unit length, respectively
F_ζ, F_η, F_x	forces per unit length in the ζ, η and x directions, respectively
$F_{m\zeta}, F_{m\eta}, F_{mx}$	moments per unit length about the ζ, η and x axes, respectively
F_X, F_{MX}	force and moment per unit length in the X direction
G	shear modulus
h	thickness of a beam
I	moment of inertia of a cross-section
I_ζ, I_η	moments of inertia of a cross-section about the ζ and η axes, respectively
J	polar moment of inertia of a cross-section
$k_i \ (i = 1, 2, \cdots 5)$	stiffness constant

k_s	shear correction factor
k_t	torsion factor for a cross-section
K_t	torsional constant of a cross-section
$[k]$	stiffness matrix of an element
$[k]_\varepsilon, [k]_\gamma, [k]_t,$ $[k]_{membrane}, [k]_{bending}$	component matrices in the element stiffness matrix
$[K]$	structural stiffness matrix
$[\hat{K}]$	matrix in the Newmark-β method
L	length of a beam
L_e	length of a finite element
L_0, L_1, L_2, L_3, L_R	lengths of different parts of the curved pole model
L_{BE}	total length of the curved model BE
$L_{C0}, L_{C1}, L_{C2}, L_{C3},$ L_{C4}, L_{C5}, L_{C6}	constants related to the lengths of different parts of the curved model
$m_i \ (i = 1, 2, \cdots 5)$	lumped mass
M_R, M_P, M_Y	rolling, pitching and yawing moments, respectively
M_x	moment about the x axis
$[m]$	mass matrix of an element
$[m]_I, [m]_{II}, [m]_{III}$	components of the element mass matrix

$[M]$	structural mass matrix
N_i	shape functions
$[N_q]$	displacement matrix of a point
$[N_u],[N_v],[N_w]$ $[N_{\theta_\zeta}],[N_{\theta_\eta}],[N_{\theta_\xi}]$	component matrices in the displacement matrix of a point
$[N_\phi]$	component matrix in the twist angle
$\{p\}$	vector of local loads acting on an element
$\{p_e\}$	equivalent load vector of an element
$\{p_p\}$	concentrated load vector of an element
P	concentrated force
P_D, P_S, P_L	drag, side and lift forces, respectively
P_ζ	concentrated force in the ζ direction
P_η	concentrated force in the η direction
$\{P\}$	load vector acting on a structure
$\{\hat{P}\}$	matrix in the Newmark-β method
$\{q\}$	nodal displacement vector of an element
$\{Q\},\{\dot{Q}\},\{\ddot{Q}\}$	nodal displacement, velocity and acceleration vectors
$\{\bar{Q}\}$	amplitude column
$\{\hat{Q}\},\{\bar{Q}\}$	matrices in the Newmark-β method

$\bar{r}$	cross-sectional radius of gyration ($\bar{r}^2 = I / A$)
R	radius of curvature
Re	Reynolds number
s	arc length
S_t	Strouhal number
t	time
T	kinetic energy of an element
T_b	beating period
T_n	natural period of the n th mode
T_I, T_{II}, T_{III}	components of the kinetic energy of an element
U_{crit}	critical wind speed
U_E	total strain energy of an element
U_f	free stream speed
$U_\varepsilon, U_\gamma, U_t$	components of the total strain energy of an element
U_{wind}	wind speed
U_{rel}	relative wind speed
u, v, w	displacements in the local coordinate system located at the beam's centroidal axis
U, V, W	displacements at point (s, ζ, η) in the local coordinate system
$\dot{V}_X, \dot{V}_Y$	velocities in the X and Y directions, respectively
x	local coordinate

$\bar{X}, \bar{Y}, \bar{X}', \bar{Y}'$	the global coordinate systems used in Appendix A
X, Y, Z	global coordinate system
X', Y'	global coordinate system used in Appendix E
α	angle
$\bar{\alpha}$	wind's angle of attack used in formulae
$\bar{\alpha}_m$	air stream's angle of attack used in experiments ($\bar{\alpha}_m = \bar{\alpha} + 90^\circ$)
$\bar{\alpha}_v$	direction of the relative wind
β_1, β_2	parameters in the Newmark-β method
$\gamma_{s\zeta}$	shear strain in the $s-\zeta$ plane
$\gamma_{s\eta}$	shear strain in the $s-\eta$ plane
δ	damping ratio
ε	longitudinal strain
$\bar{\varepsilon}$	offset angle of the wind's direction
ζ, η	local coordinate system
$\theta, \bar{\theta}$	angles used in Appendix A
θ_x	rotation about the x axis
θ_X	rotation about the X axis
θ_Y	rotation about the Y axis
θ_ζ	rotation about the ζ axis
θ_η	rotation about the η axis

μ	Poisson's ratio
ν_{air}	kinematic viscosity of air
ξ	natural coordinate
ρ	material density
ρ_{air}	air density
φ	phase angle
ϕ	angle between the x and X axes
ϕ_t	twist about the x axis
ω_n	circular natural frequency of the n th mode

Chapter 1

Introduction

1.1 Description of the Problem

Traffic poles are exposed to wind. Hence they experience wind induced vibration which may result in their failure. A few years ago, several light poles on Provincial Highway No. 59, located by the floodway near Winnipeg, Manitoba, cracked close to their bases due to wind loads. These poles were replaced before failure. Because a light pole has a curved part, it is difficult to find an analytical method to deal with the dynamic response. To analyze the wind induced vibrations of curved poles, the finite element method, which is a powerful approximate technique, can be used. The purpose of this thesis is to derive a curved beam element and provide a procedure to analyze the dynamic response of curved traffic poles when they are excited by the wind.

1.2 Literature Review

Much effort has been devoted since the 1970s to develop a curved finite element. R. K. Wen et al [1], for example, derived a two-node, curved beam element but excluded the shear deformation. Other researchers [2-14] included the shear deformation. However, mostly two-node elements were considered for which an unknown radius of

curvature, R, cannot be found easily. Although three or more node curved elements [2-8] have also been formulated, they require either R to be given explicitly [4], or the displacements in the plane of curvature be excluded [3,7], or a shell based derivation [5] may make them unsuitable for slender poles. An unconventional approach has also been advanced [8,13] in which the curvatures at three nodes are reduced to displacements and rotations at two nodes. Although the scheme is used easily, its derivation is laborious and the mass matrix, as well as the external load vector, detrimentally involve trigonometric functions.

Another problem observed for curved beam elements is that shear and membrane locking may happen. This phenomenon can occur for deep thin arches where an element becomes very stiff so that the computed displacements may be too small. It happens because shear and membrane energies are overestimated when full integration is used in the finite element displacement method [15]. Several procedures, including reduced integration [15-17], curvature based elements [8,13] and a hybrid displacement-stress formulation [14], are able to remedy the locking problem [8-10,13-15].

Although the above developments have been achieved, very little research has been performed with three dimensional, curved beam elements to analyze the wind induced vibrations of traffic poles.

1.3 Present Work

A three-node, curved beam element is developed in this thesis that is based purely upon simple polynomial approximations. It permits general motions and includes shear

deformation as well as rotary inertia effects. Reduced integration, which is implemented easily in the finite element displacement method, is utilized to avoid locking. Exact solutions and previously published results for several static and dynamic examples are used to assess the element's performance. Finally, as an application of the element, the free vibration and dynamic response of traffic poles under wind loads are analyzed. Aerodynamic loads are formulated for the curved pole by using the data derived from wind tunnel experiments. Direct time integration is used to obtain a dynamic response. In addition, the initiation of galloping is investigated.

Chapter 2

Formulation of Three-node Curved Beam Element

2.1 Element's Geometry

Consider the element of a beam illustrated in Figure 2.1(a) whose cross section is assumed to be symmetrical about both the ζ and η axes. The centroidal axis, s, curves in the ζ, x plane with a radius of curvature R. When R is not given specifically, it can be approximated by using a circular sector that passes through the element's three nodes. Details are given more conveniently in Appendix A. This method is easy and can reasonably approximate the curvature.

2.2 Displacement Functions

Suppose that u, v and w are the displacements at the centroidal axis in the ζ, η and x directions, respectively. The $\theta_\zeta, \theta_\eta$ and θ_x are the total rotations of a cross section about the ζ, η and x directions, respectively. The displacement functions of the three-node element are assumed to be:

$$u = \sum_{i=1}^{3} N_i u_i \qquad v = \sum_{i=1}^{3} N_i v_i \qquad w = \sum_{i=1}^{3} N_i w_i$$

and

$$\theta_\zeta = \sum_{i=1}^{3} N_i \theta_{\zeta i} \qquad \theta_\eta = \sum_{i=1}^{3} N_i \theta_{\eta i} \qquad \theta_x = \sum_{i=1}^{3} N_i \theta_{xi} \tag{2.1}$$

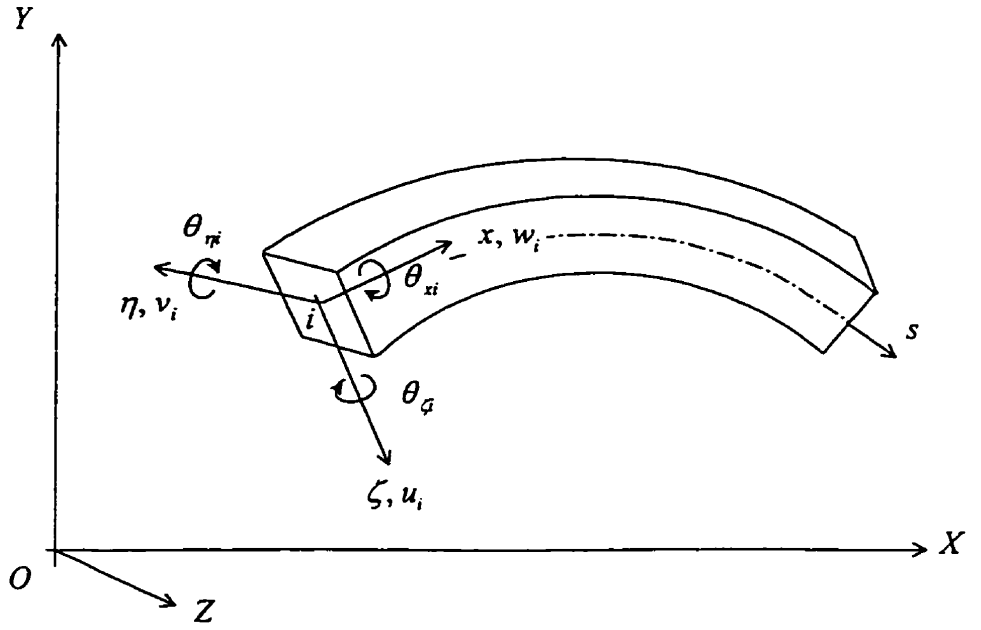

(a)

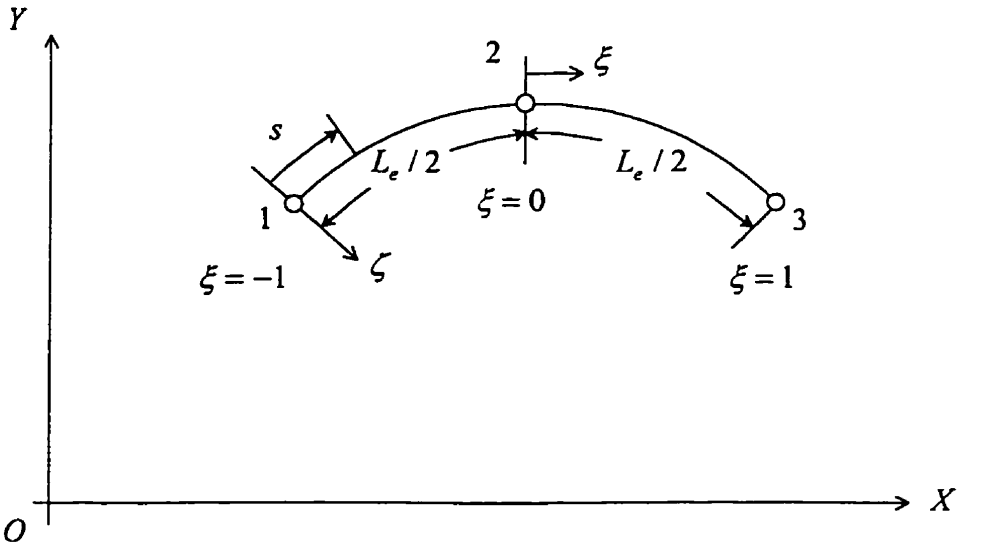

(b)

Figure 2.1 Curved beam element showing (a) the displacements of node i, and (b) the global coordinate system, $OXYZ$, and the natural coordinate ξ.

where, for example, u_i is the ζ displacement at the left side of the element, i.e. node i.

N_1, N_2, N_3 are shape functions. Furthermore, the following standard relation is adopted:

$$s = \sum_{i=1}^{3} N_i s_i \ . \tag{2.2}$$

Next, assume that:

$$\begin{aligned} N_1 &= a_0 + a_1\xi + a_2\xi^2 \\ N_2 &= b_0 + b_1\xi + b_2\xi^2 \\ N_3 &= c_0 + c_1\xi + c_2\xi^2 \end{aligned}$$

where a_i, b_i and c_i, $i = 0, 1, 2,$ can be determined from the following conditions:

$$\begin{array}{lll} N_1(-1) = 1 & N_1(0) = 0 & N_1(1) = 0 \\ N_2(-1) = 0 & N_2(0) = 1 & N_2(1) = 0 \\ N_3(-1) = 0 & N_3(0) = 0 & N_3(1) = 1 \ . \end{array}$$

Hence;

$$\begin{array}{lll} a_0 = 0 & a_1 = -1/2 & a_2 = 1/2 \\ b_0 = 1 & b_1 = 0 & b_2 = -1 \\ c_0 = 0 & c_1 = c_2 = 1/2 & \end{array}$$

so that

$$\begin{aligned} N_1 &= -\frac{1}{2}\xi + \frac{1}{2}\xi^2 \\ N_2 &= 1 - \xi^2 \\ N_3 &= \frac{1}{2}\xi + \frac{1}{2}\xi^2 \ . \end{aligned} \tag{2.3}$$

On the other hand,

$$s = N_2 s_2 + N_3 s_3 = (1 - \xi^2)s_2 + \frac{1}{2}\xi(1 + \xi)s_3$$

From Figure 2.1 (b),

$$s_3 = L_e \text{ and } s_2 = \frac{L_e}{2}$$

where L_e is the length of the element, hence

$$s = \frac{L_e}{2}(1+\xi)\,. \tag{2.4}$$

2.3 Strain Energy and Stiffness Matrix of the Element

Consider next a typical point (s,ζ,η) of the element whose displacements in the ζ,η and x directions take the form [2,13]:

$$\begin{aligned} U(s,\zeta,\eta) &= u(s) \\ V(s,\zeta,\eta) &= v(s) \\ W(s,\zeta,\eta) &= w(s) - \zeta\theta_\eta + \eta\theta_\zeta . \end{aligned} \tag{2.5}$$

The corresponding longitudinal and shear strains (i.e. ε, $\gamma_{s\zeta}$ and $\gamma_{s\eta}$) can be written as [1,2]:

$$\varepsilon = \frac{dW}{ds} - \frac{U}{R} + \eta\left(\frac{\theta_x}{R}\right) = \left(\frac{dw}{ds} - \frac{u}{R}\right) - \zeta\frac{d\theta_\eta}{ds} + \eta\left(\frac{d\theta_\zeta}{ds} + \frac{\theta_x}{R}\right) \tag{2.6}$$

$$\gamma_{s\zeta} = \frac{du}{ds} - \theta_\eta + \frac{w}{R} \tag{2.7}$$

and

$$\gamma_{s\eta} = \frac{dv}{ds} + \theta_\zeta \ . \tag{2.8}$$

Equations (2.6) through (2.8) can be expressed in terms of ξ as:

$$\varepsilon = \left(\frac{dw}{d\xi}\frac{d\xi}{ds} - \frac{u}{R}\right) + \eta\left(\frac{d\theta_\zeta}{d\xi}\frac{d\xi}{ds} + \frac{\theta_x}{R}\right) - \zeta\frac{d\theta_\eta}{d\xi}\frac{d\xi}{ds} = [B]_\varepsilon\{q\} \tag{2.9}$$

$$\gamma_{s\zeta} = \frac{du}{d\xi}\frac{d\xi}{ds} - \theta_\eta + \frac{w}{R} = [B]_{\gamma\zeta}\{q\} \tag{2.10}$$

and

$$\gamma_{s\eta} = \frac{dv}{d\xi}\frac{d\xi}{ds} + \theta_\zeta = [B]_{\gamma\eta}\{q\} \ . \tag{2.11}$$

Here $\{q\}$ is the vector of the element's nodal displacements, so that:

$$\{q\} = \begin{Bmatrix} q_1 \\ q_2 \\ q_3 \end{Bmatrix} \tag{2.12}$$

where

$$[q]_i = \left[u_i \ \theta_{\zeta i} \ v_i \ \theta_{\eta i} \ w_i \ \theta_{xi}\right]^T \quad \text{for } i = 1, 2, 3.$$

$[B]_\varepsilon$, $[B]_{\gamma\zeta}$ and $[B]_{\gamma\eta}$ are the element's strain matrices, details of which are given in Appendix B.1. In addition, the twist about the x axis is ϕ_t [3,18,19] so that :

$$\frac{d\phi_t}{ds} = \frac{d\theta_x}{ds} - \frac{\theta_\zeta}{R} = \frac{d\theta_x}{d\xi}\frac{d\xi}{ds} - \frac{\theta_\zeta}{R} = [B]_t\{q\} \tag{2.13}$$

where $[B]_t$ is given again in Appendix B.1.

For convenience, the total strain energy of the element is decomposed into the three components:

$$U_E = U_\varepsilon + U_\gamma + U_t \tag{2.14a}$$

where the membrane and bending energy is:

$$U_\varepsilon = \int_{L_e}\int_A \frac{E}{2}\varepsilon^2 dA ds \tag{2.14b}$$

the shear energy is:

$$U_\gamma = k_s A \int_{L_e} \frac{G}{2}\left(\gamma_{s\zeta}^2 + \gamma_{s\eta}^2\right) ds \tag{2.14c}$$

and the torsional energy is:

$$U_t = \int_{L_e} \frac{GK_t}{2}\left(\frac{d\phi_t}{ds}\right)^2 ds\,. \tag{2.14d}$$

The A and K_t are the area and torsional constant of a cross-section; E and G are the Young's modulus and shear modulus, respectively. When the cross-section is circular, K_t is simply J, the polar moment of inertia about the beam's centroidal axis. On the other hand, k_s is a standard shear correction factor that accommodates a variable shear strain over different cross sectional shapes. For example, k_s is 5/6 for a rectangle, 0.9 for a circle, and 0.5 for a circular, thin-walled cross section [20,21].

By combining equations (2.9) through (2.14) in a conventional manner, equation (2.14a) can be rewritten in the matrix form:

$$U_E = \frac{1}{2}\{q\}^T[k]\{q\} \tag{2.15}$$

in which the element stiffness matrix, $[k]$, is given by the component matrices:

$$[k] = [k]_\varepsilon + [k]_\gamma + [k]_t \tag{2.16a}$$

where

$$[k]_\varepsilon = \int_{L_e}\int_A E[B]_\varepsilon^T[B]_\varepsilon\, dA ds = [k]_{membrane} + [k]_{bending}\,. \tag{2.16b}$$

The $[k]_{membrane}$ and $[k]_{bending}$ contain terms involving only EA or EI, respectively, where I is the moment of inertia of the beam's cross-section. Furthermore,

$$[k]_{\gamma} = k_s GA \int_{L_e} \left([B]_{\gamma\zeta}^T [B]_{\gamma\zeta} + [B]_{\gamma\eta}^T [B]_{\gamma\eta} \right) ds \tag{2.16c}$$

and

$$[k]_t = \int_{L_e} GK_t [B]_t^T [B]_t ds . \tag{2.16d}$$

Because it is difficult to calculate the above integrals analytically, numerical integration is used. Gaussian Quadrature [20] is employed here to calculate the component stiffness matrices. Full three-point integration is used to compute $[k]_{bending}$ and $[k]_t$. However, when full three-point integration is used to calculate $[k]_{membrane}$ and $[k]_{\gamma}$, locking will happen. Then the widely employed reduced integration method [15,17] is utilized, i.e., two-point integration is used to obtain $[k]_{membrane}$ and $[k]_{\gamma}$.

2.4 Kinetic Energy and Mass Matrix of the Element

The element's kinetic energy, T, can be divided in an analogous fashion to the strain energy, so that:

$$T = T_{\mathrm{I}} + T_{\mathrm{II}} + T_{\mathrm{III}} \tag{2.17a}$$

where

$$T_{\mathrm{I}} = \frac{1}{2} \int_{L_e} \rho A \left[(\dot{u})^2 + (\dot{v})^2 + (\dot{w})^2 \right] ds \tag{2.17b}$$

$$T_{II} = \frac{1}{2}\int_{L_e} \rho\left[I_\eta\left(\dot{\theta}_\eta\right)^2 + I_\zeta\left(\dot{\theta}_\zeta\right)^2\right] ds \tag{2.17c}$$

and

$$T_{III} = \frac{1}{2}\int_{L_e} \rho K_t\left(\dot{\phi}_t\right)^2 ds\,. \tag{2.17d}$$

A dot superscript indicates a differentiation with respect to time, t. The I_ζ and I_η are the moments of inertia of a cross-section of the beam about the ζ and η axes, respectively, whereas ρ is the beam's density. Finally,

$$T = \frac{1}{2}\{\dot{q}\}^T[m]\{\dot{q}\} \tag{2.18}$$

and the form of the mass matrix, $[m]$, is given in Appendix B.1. Its elements are computed by employing three-point integration again.

2.5 Equations of Motion

The equations of motion can be formulated for an element by using, say, Lagrange's equation. For an undamped structure, they take the standard form:

$$[m]\{\ddot{q}\} + [k]\{q\} = \{p\} \tag{2.19}$$

where $\{p\}$ is the load vector corresponding to $\{q\}$. The overall structural matrices, $[K]$ and $[M]$, are assembled conventionally [20] from the element matrices and the resulting equations of motion take the usual form:

$$[M]\{\ddot{Q}\} + [K]\{Q\} = \{P\}\,. \tag{2.20}$$

$\{Q\}$ is the vector of the structure's nodal displacements and $\{P\}$ is the corresponding load vector. For static problems, $\{\ddot{Q}\} = \{0\}$ so that the last equation becomes

$$[K]\{Q\} = \{P\}. \tag{2.21}$$

On the other hand, harmonic motion is assumed for free vibrations so that:

$$\{Q\} = \{\overline{Q}\}\cos(\omega t - \varphi) \quad \text{and} \quad \{P\} = \{0\}$$

where $\{\overline{Q}\}$ is the amplitude vector, ω is the circular natural frequency and φ is the phase angle. Then equation (2.20) reduces to:

$$([K] - \omega^2[M])\{\overline{Q}\} = \{0\}. \tag{2.22}$$

Equations (2.21) and (2.22) are solved numerically by invariably utilizing double precision arithmetic and the IMSL programs DLSASF and DGVCSP, respectively [22].

2.6 Equivalent Loads

The load vector for an element is

$$\{p\} = \{p_e\} + \{p_p\} \tag{2.23}$$

where $\{p_e\}$ is the equivalent load vector arising from the distributed loads and $\{p_p\}$ is a concentrated load vector.

Next, suppose that the distributed loads (forces and moments per unit length) at cross-section s are:

$$\{F\} = \left[F_\zeta \; F_{m\zeta} \; F_\eta \; F_{m\eta} \; F_x \; F_{mx}\right]^T \tag{2.24}$$

and assume that:

$$\begin{Bmatrix} u \\ \theta_\zeta \\ v \\ \theta_\eta \\ w \\ \theta_x \end{Bmatrix} = [N_q]\{q\} \tag{2.25}$$

where

$$[N_q] = \begin{Bmatrix} [N_u] \\ [N_{\theta_\zeta}] \\ [N_v] \\ [N_{\theta_\eta}] \\ [N_w] \\ [N_{\theta_x}] \end{Bmatrix}. \tag{2.26}$$

The $[N_u]$ through $[N_{\theta_x}]$ are given in Appendix B.1. Then, the load vector $\{p_e\}$ is formulated in a conventional way as:

$$\{p_e\} = \int_0^{L_\zeta} [N_q]^T \{F\} ds \tag{2.27a}$$

where

$$\{p_e\} = [p_{e1}\ p_{e2} \cdots p_{e18}]^T \tag{2.27b}$$

and

$$p_{ei} = \int_0^{L_\zeta} \left(N_{ui} F_\zeta + N_{\theta_\zeta i} F_{m\zeta} + N_{vi} F_\eta + N_{\theta_\eta i} F_{m\eta} + N_{wi} F_x + N_{\theta_x i} F_{mx} \right) ds \qquad (i = 1, 2, \cdots 18). \tag{2.27c}$$

2.7 Formulae for Plane Problems

In engineering structures, plane problems (i.e. ones in which all the loads are exerted in a single plane, for example in the $\zeta - x$ plane of Figure 2.2) are very common. See, for instance, Example 3.2 which is considered later in Chapter 3. In this situation, only u, θ_η and w are needed, and

$$u = \sum_{i=1}^{3} N_i u_i \qquad \theta_\eta = \sum_{i=1}^{3} N_i \theta_{\eta i} \qquad w = \sum_{i=1}^{3} N_i w_i \tag{2.28}$$

where N_1, N_2, N_3 are identical to before.

From equation (2.9), the longitudinal strain reduces to:

$$\varepsilon = \left(\frac{dw}{d\xi}\frac{d\xi}{ds} - \frac{u}{R} \right) - \zeta \frac{d\theta_\eta}{d\xi}\frac{d\xi}{ds} = [B]_\varepsilon \{q\}. \tag{2.29}$$

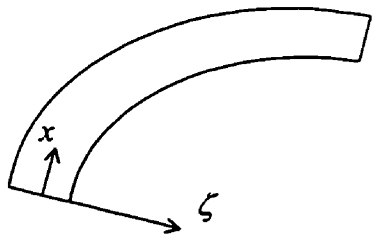

Figure 2.2 Two dimensional curved beam element.

From equation (2.10), the shear strain is:

$$\gamma_{s\zeta} = \frac{du}{d\xi}\frac{d\xi}{ds} - \theta_\eta + \frac{w}{R} = [B]_{\gamma\zeta}\{q\} \tag{2.30}$$

where

$$\{q\} = \left[u_1 \ \theta_{\eta 1} \ w_1 \ u_2 \ \theta_{\eta 2} \ w_2 \ u_3 \ \theta_{\eta 3} \ w_3 \right]^T. \tag{2.31}$$

$[B]_\varepsilon$ and $[B]_{\gamma\zeta}$ are given in Appendix B.2.

The strain energy of the element is:

$$U_E = U_\varepsilon + U_\gamma = \int_{L_e}\int_A \frac{E}{2}\varepsilon^2 dA ds + k_s GA\int_{L_e}\frac{1}{2}\gamma_{s\zeta}^2 ds = \frac{1}{2}\{q\}^T[k]\{q\} \tag{2.32}$$

where

$$[k] = [k]_\varepsilon + [k]_\gamma \tag{2.33}$$

$$[k]_\varepsilon = \int_{L_e}\int_A E[B]_\varepsilon^T[B]_\varepsilon dA ds \qquad (i, j = 1, 2, \cdots 9) \tag{2.34}$$

and

$$[k]_\gamma = k_s GA\int_{L_e}[B]_{\gamma\zeta}^T[B]_{\gamma\zeta} ds \qquad (i, j = 1, 2, \cdots 9). \tag{2.35}$$

The corresponding kinetic energy is

$$T = \frac{1}{2}\int_{L_e}\rho A\left[(\dot{u})^2 + (\dot{w})^2\right]ds + \frac{1}{2}\int_{L_e}\rho I_\eta(\dot{\theta}_\eta)^2 ds = \frac{1}{2}\{\dot{q}\}^T[m]\{\dot{q}\} \tag{2.36}$$

where $[m]$ is given in Appendix B.2.

The equivalent load vector is:

$$\{p_e\} = \int_0^{L_e}[N_q]^T\{F\}ds \tag{2.37a}$$

where

$$\{p_e\} = [p_{e1}\ p_{e2}\ \cdots\ p_{e9}]^T \tag{2.37b}$$

and

$$\{F\} = [F_\zeta\ F_x]^T \tag{2.38}$$

$$\begin{Bmatrix} u \\ w \end{Bmatrix} = [N_q]\{q\} \quad \text{and} \quad [N_q] = \begin{Bmatrix} [N_u] \\ [N_w] \end{Bmatrix}. \tag{2.39}$$

$[N_u]$ and $[N_w]$ are detailed in Appendix B.2.

If $\{F\}$ is constant for an element, the following results can be obtained from equation (2.37):

$$\begin{aligned} p_{e1} &= \frac{F_\zeta L_e}{6} & p_{e2} &= 0 & p_{e3} &= \frac{F_x L_e}{6} \\ p_{e4} &= \frac{2F_\zeta L_e}{3} & p_{e5} &= 0 & p_{e6} &= \frac{2F_x L_e}{3} \\ p_{e7} &= \frac{F_\zeta L_e}{6} & p_{e8} &= 0 & p_{e9} &= \frac{F_x L_e}{6} \end{aligned} \tag{2.40}$$

2.8 Summary

The formulae of the three-node curved beam element have been derived by using the finite element displacement method. There are six degrees of freedom at each node. Shear deformation and rotary inertia effects are considered. Reduced integration method is employed to avoid locking. For convenience, the formulae for plane problems are also presented.

Chapter 3

Examples

Computer programs STATIC and FREEVIB are written in FORTRAN 77. STATIC is for the static analysis, FREEVIB is for free vibrations. Details are given in Appendix C. The following illustrative examples are used to assess the proposed, three-node element's performance.

3.1 Static Problems

Example 3.1 Cantilevered Beam under a Concentrated Force

A straight, uniform cantilevered beam, having length L, is subjected to a concentrated static force, P, applied at the free end, as shown in Figure 3.1. The force lies in the $\zeta-\eta$ plane but its line of action does not coincide with the centroid of the beam's cross section. Therefore, the beam will bend and twist simultaneously. The exact Timoshenko based solution at the free end is [21,23]:

$$u=\frac{P_\zeta L^3}{3EI_\eta}+\frac{P_\zeta L}{k_s GA} \qquad v=\frac{P_\eta L^3}{3EI_\zeta}+\frac{P_\eta L}{k_s GA}$$

and

$$\theta_\zeta=\frac{P_\eta L^2}{2EI_\zeta} \qquad \theta_\eta=\frac{-P_\zeta L^2}{2EI_\eta} \qquad \theta_x=\frac{M_x L}{Gk_t hb^3} \tag{3.1}$$

where P_ζ and P_η are the components of P in the ζ and η directions, respectively, and M_x is the moment of P about the x axis. k_t is the torsion factor. The following data are used here: $E = 200\,GPa$, Poisson's ratio $\mu = 1/3$, $h = 20\,mm$, $b = 10\,mm$, $k_t = 0.229$, $\alpha = 30^\circ$ and $P = 50\,N$. Moreover, for the rectangular cross-section considered, k_s equals $5/6$ [21]. Table 3.1 lists the Timoshenko solution and data obtained at the free end with the proposed element for two beam lengths, L. It can be seen that merely one element produces data that is virtually identical to the Timoshenko solution.

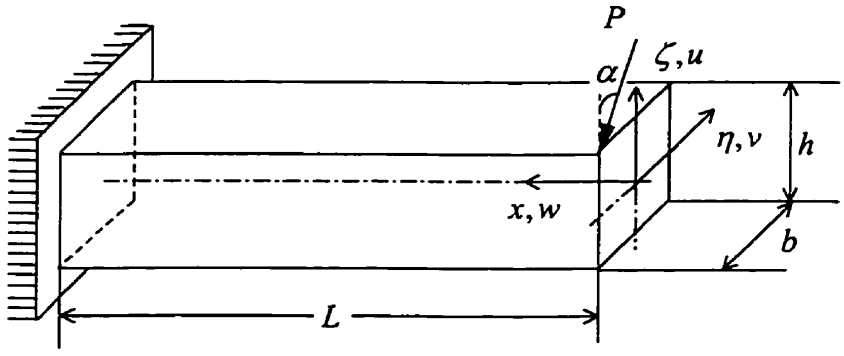

Figure 3.1 Cantilevered straight beam.

Table 3.1 Tip deflections for Example 3.1

	$L/h=4$		$L/h=10$	
	Timoshenko solution [21,23]	FEM 1 element	Timoshenko solution [21,23]	FEM 1 element
$u\ (mm)$	5.81259×10^{-3}	5.81259×10^{-3}	8.72755×10^{-2}	8.72755×10^{-2}
$\theta_\zeta(rad)$	2.40000×10^{-4}	2.39999×10^{-4}	1.50000×10^{-3}	1.50000×10^{-3}
$v\ (mm)$	1.29560×10^{-2}	1.29560×10^{-2}	2.00390×10^{-1}	2.00390×10^{-1}
$\theta_\eta(rad)$	1.03920×10^{-4}	1.03920×10^{-4}	6.49500×10^{-4}	6.49499×10^{-4}
$\theta_x\ (rad)$	1.26935×10^{-4}	1.26935×10^{-4}	3.17337×10^{-4}	3.17337×10^{-4}

Example 3.2 Cantilevered Quarter Circle under an In-plane Force

The straight beam of the previous example is replaced by the uniform quarter circle configuration shown in Figure 3.2 (a). The quarter circle has a square cross section and its material and dimensional properties are: $E/G=2.6$, $\mu=0.3$, $k_s=5/6$, $h=25.4\ mm$, $b=25.4\ mm$. It is cantilevered and a static in-plane force, $P=44.48\ N$, is applied at the free end, B. When the beam is moderately thick (so that conventional beam theory can be used), the analytical deflections at B can be found, by using Castigliano's theorem, to be [21]:

$$u=\frac{\pi PR^3}{4EI}+\frac{\pi PR}{4GAk_s}+\frac{\pi PR}{4EA}$$

$$w=\frac{PR^3}{2EI}+\frac{PR}{2GAk_s}-\frac{PR}{2EA}$$

and

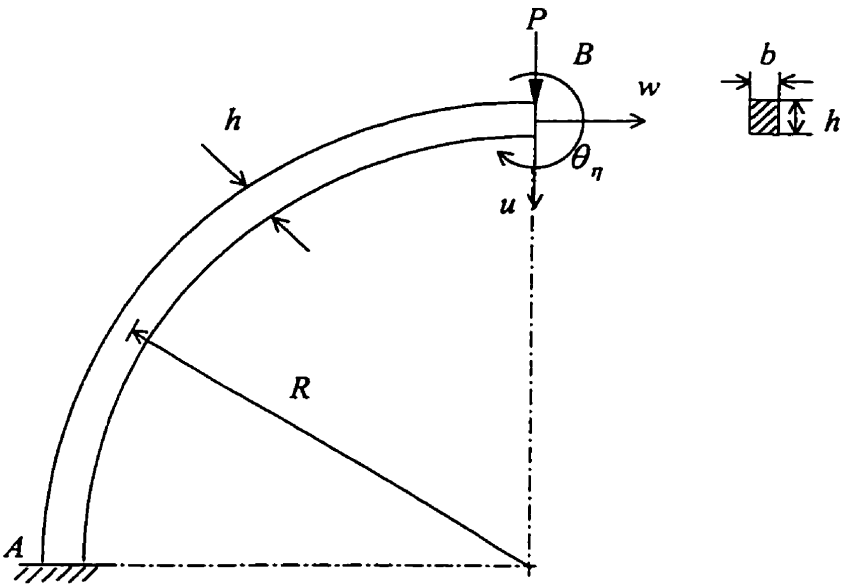

(a)

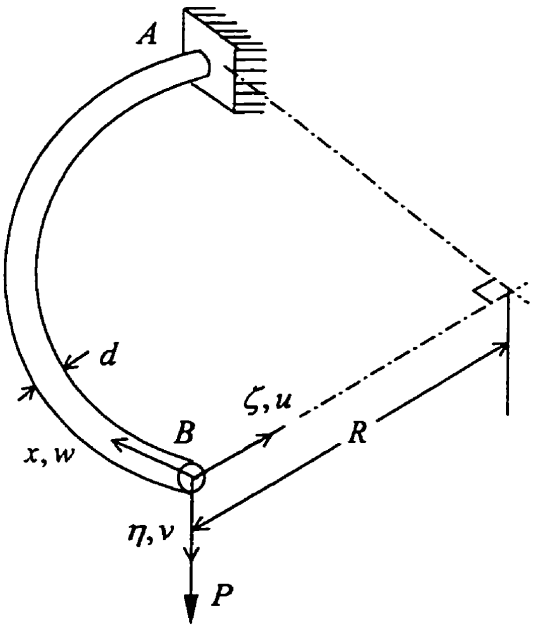

(b)

Figure 3.2 Cantilevered quarter circle under (a) an in-plane force, and (b) an out-of -plane force.

$$\theta_\eta = \frac{PR^2}{EI}. \tag{3.2}$$

These formulae are used to determine the ratio of the deflection, computed with an increasing number of elements, to the corresponding analytical deflection at B. The ratios are presented in Figure 3.3 for different ratios of R/h. It can be seen that tip deflection ratios are similar for a given number of elements and R/h ratio. Rapid convergence is evident and excellent agreement usually occurs with the use of only three elements.

Example 3.3 Cantilevered Quarter Circle under an Out-of-plane Force

A quarter circle which has a circular cross-section is shown in Figure 3.2 (b). It is subjected to an out-of-plane force. The related data are: $E = 200\,GPa$, $\mu = 1/3$, $k_s = 0.9$, $d = 20\,mm$, $P = 5\,N$. By using Castigliano's theorem, the analytical deflections at the free end are [21]:

$$v = \frac{\pi PR^3}{4EI} + \frac{\pi PR}{2k_sGA} + \frac{PR^3}{GJ}\left(\frac{3\pi}{4} - 2\right)$$

$$\theta_\zeta = \frac{PR^2}{2EI} + \frac{PR^2}{2GJ}$$

and

$$\theta_x = \frac{-\pi PR^2}{4EI} + \frac{PR^2}{GJ}\left(1 - \frac{\pi}{4}\right). \tag{3.3}$$

Figure 3.4 shows the deflection ratios at the free end for $R/d = 10$ and 100. It can be seen, again, that the agreement is excellent and three elements give accurate results.

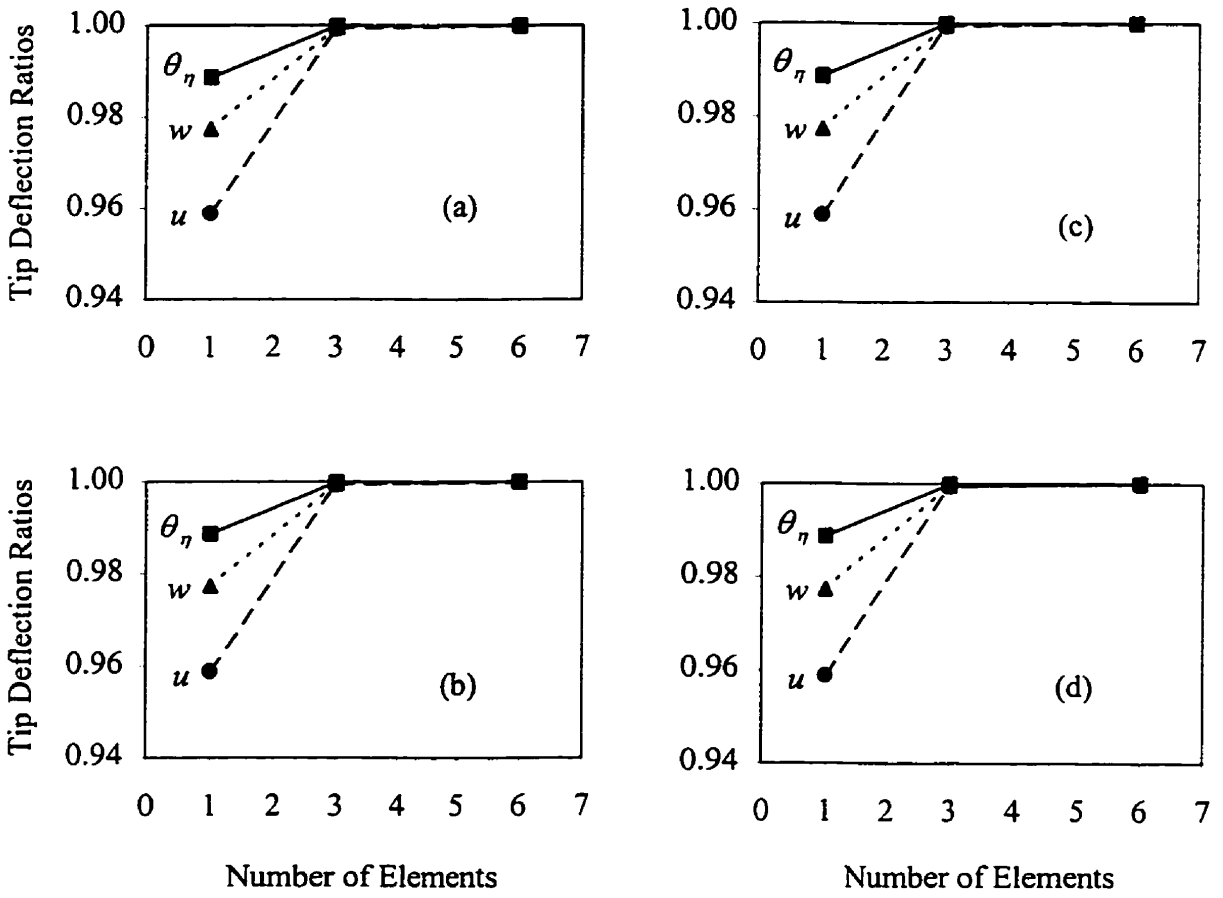

Figure 3.3 Tip deflection ratios for Example 3.2; (a) $R/h = 10$; (b) $R/h = 20$; (c) $R/h = 50$ and (d) $R/h = 100$.

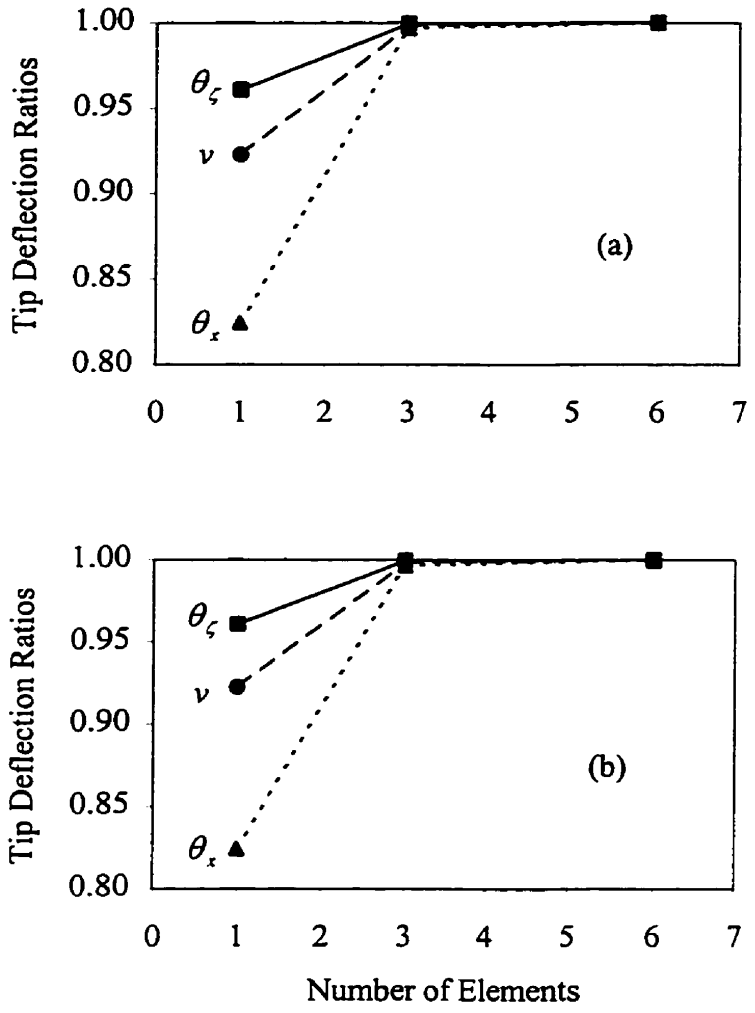

Figure 3.4 Tip deflection ratios for Example 3.3; (a) $R/d = 10$ and (b) $R/d = 100$.

3.2 Free Vibrations

In the following Examples 3.4 and 3.5, $E/G = 2.6667$ and $k_s = 5/6$. The natural frequency coefficient, $a_n = \omega_n \sqrt{\rho AL^4/(EI)}$, is used and the density, ρ, is chosen so that the ratio $\rho AL^4/(EI)$ is one.

Example 3.4 A Straight, Simply-supported Beam

The natural frequency coefficients of the freely vibrating, simply supported square beam illustrated in Figure 3.5 are computed by using the proposed element. Numerical values are listed in Tables 3.2 and 3.3 when $E = 200\ GPa$, $b = 10\ mm$ and $h = 10\ mm$. Two slenderness ratios, $L/\bar{r} = 10$ and 50, are assumed. The $\bar{r}$ is the beam's cross-sectional radius of gyration. The tables also list the corresponding Timoshenko solutions [24] and the lowest results (i.e., the best results) obtained with the three-node, straight beam element which is labeled T2CL6 in reference [24]. The total number of degrees of freedom (DOF) is also given because it is more indicative of the

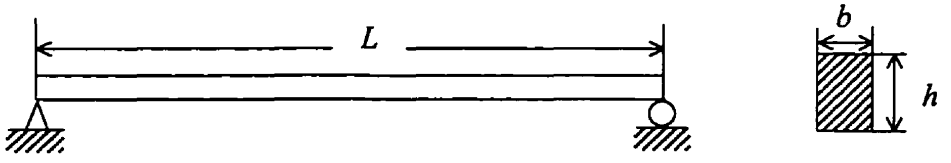

Figure 3.5 A simply supported beam.

Table 3.2 Frequency coefficients, a_n, for Example 3.4; $L / \bar{r} = 10$

Mode number n	Timoshenko solution [24]	Reference [24] 10 elements (40 DOF)	Number of present elements 4 (16 DOF)	10 (40 DOF)	20 (80 DOF)
1	8.36487	8.36493	8.37004	8.36490	8.36477
2	25.1965	25.1990	25.3759	25.2008	25.1960
3	43.7750	43.7980	44.9466	43.8092	43.7754
4	55.9016	55.9017	55.8981	55.8981	55.8981
5	62.5090	62.6100	64.3453	62.6452	62.5150
6	65.9577	65.9581	65.9459	65.9541	65.9543
7	81.0880	81.3980	87.5918	81.4751	81.1107
8	87.5880	87.6010	92.8102	87.5861	87.5852
9	99.4830	100.230	114.433	100.374	99.5402
10	113.430	113.600	123.904	113.456	113.433

computational effort involved. With the use of ten elements, the present element usually produces slightly greater natural frequencies than T2CL6. Both elements generally generate somewhat higher natural frequencies than the Timoshenko solution, especially at the large $L / \bar{r} = 50$ ratio. However, Table 3.3 demonstrates that progressively increasing the number of present elements (and, presumably, also increasing the number of the T2CL6 elements) quickly reduces the differences.

Table 3.3 Frequency coefficients, a_n, for Example 3.4; $L / \bar{r} = 50$

Mode number n	Timoshenko solution [24]	Reference [24] 10 elements (40 DOF)	Number of present elements 4 (16 DOF)	10 (40 DOF)	20 (80 DOF)	30 (120 DOF)
1	9.78902	9.78909	9.79647	9.78922	9.78903	9.78902
2	38.2444	38.2485	38.6628	38.2560	38.2451	38.2445
3	82.9860	83.0310	86.9903	83.1057	82.9936	82.9874
4	140.950	141.190	153.861	141.544	140.991	140.960
5	209.120	209.950	272.542	211.072	209.251	209.146
6	284.900	287.160	447.611	289.899	285.239	284.962
7	366.230	371.430	697.204	377.025	366.988	366.374
8	451.550	462.130	1397.45	472.113	453.053	451.852
9	539.730	559.260	1407.75	574.924	542.418	540.275
10	629.910	665.530	1431.09	665.509	634.397	630.835

Example 3.5 In-plane Vibration of a Semicircular Arch

Figure 3.6 shows a semicircular arch for which $E = 206.85\ GPa$, $b = 25.4\ mm$ and $h = 25.4\ mm$. Natural frequencies are computed for slenderness ratios of $\pi R / \bar{r} = 10$ and 50. Results calculated with the proposed element are compared with data taken from references [9] and [25]. Sixty two-node, curved beam elements and thirty straight, three-node Timoshenko elements are employed, respectively, in these references. The comparisons are given in Tables 3.4 and 3.5. Four significant figures are used to conform with the values given in references [9] and [25]. These tables

demonstrate that the present element gives comparable natural frequencies to the two-node curved beam element but with noticeably fewer elements (and a fewer number of degrees of freedom).

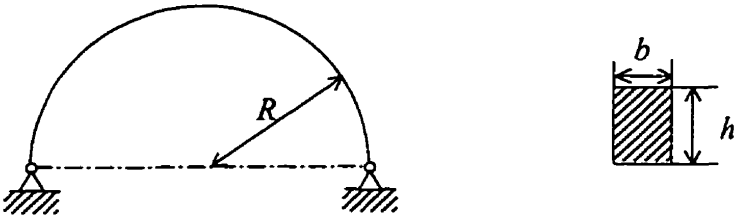

Figure 3.6 A semicircular arch.

Table 3.4 Frequency coefficients, a_n, for Example 3.5; $\pi R / \bar{r} = 10$

Mode number n	Reference [25] 30 elements (179 DOF)	Reference [9] 60 elements (179 DOF)	Number of present elements 4 (23 DOF)	10 (59 DOF)	20 (119 DOF)
1	12.87	12.79	12.90	12.79	12.78
2	24.69	24.64	24.87	24.63	24.63
3	38.13	37.98	38.93	37.99	37.96
4	40.01	39.90	40.49	39.90	39.88
5	57.62	57.13	58.59	57.18	57.08
6	60.42	59.87	60.99	59.89	59.87
7	60.83	60.47	61.63	60.48	60.44
8	73.40	72.80	76.46	72.91	72.73
9	81.03	80.74	85.97	80.86	80.64
10	85.18	84.74	88.53	84.78	84.68

Table 3.5 Frequency coefficients, a_n, for Example 3.5; $\pi R / \bar{r} = 50$

Mode number n	Reference [25] 30 elements (179 DOF)	Reference [9] 60 elements (179 DOF)	Number of present elements 4 (23 DOF)	10 (59 DOF)	20 (119 DOF)
1	21.60	21.53	21.85	21.54	21.53
2	62.57	62.35	65.54	62.44	62.34
3	120.8	120.3	132.8	120.7	120.3
4	146.3	146.4	150.7	146.6	146.4
5	199.6	199.2	219.0	200.8	199.1
6	212.0	212.1	258.3	212.5	212.0
7	278.2	277.7	350.2	282.0	277.6
8	335.4	334.8	430.0	337.8	334.6
9	368.8	368.9	509.3	376.0	368.7
10	439.5	438.2	643.7	455.0	438.0

Example 3.6 Out-of-plane Vibration of a Simply Supported Quarter Circle

The circular natural frequencies are calculated for the example shown in Figure 3.7. The related properties are: $E = 100\ GPa$, $h = 10\ mm$, $b = 20\ mm$, $GK_t / (EI_\zeta) = 0.5$, $L / \sqrt{I_\zeta / A} = 200$, $\rho = 0.0001\ kg / mm^3$ and $k_s = 5/6$. The results are presented in Table 3.6 in comparison with the analytical solutions given in reference [26], the results obtained by applying a Green function with the parameters $n = 10$, $m = 40$ [27], and FEM results [27] from the use of thirty two-node elements. It can be seen from this table that the natural frequencies obtained by using fifteen of the proposed elements are lowest except for the first frequency.

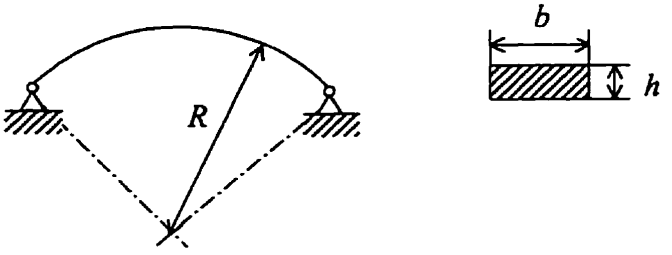

Figure 3.7 A simply supported, quarter circle.

Table 3.6 Natural frequencies, $\omega_n\,(rad/s)$, for Example 3.6

Mode number n	Reference [26]	Reference [27]	FEM [27] (89 DOF)	Number of present elements		
				5 (29 DOF)	10 (59 DOF)	15 (89 DOF)
1	0.82750	0.82777	0.82865	0.82810	0.82760	0.82758
2	4.77787	4.78273	4.77674	4.79969	4.77413	4.77268
3	11.50907	11.52565	11.49200	11.75883	11.49628	11.48070
4	20.95914	20.99236	20.89887	22.30823	20.95754	20.87423
5	33.11698	33.08505	32.97106	36.55892	33.23572	32.93339
6	47.97960	47.54485	47.64135	63.38276	48.52077	47.66273

3.3 Concluding Remarks

From the above examples, it can be seen that the results computed by using the curved beam element agree well with published results. However, the present element is somewhat inferior to the best, currently available three-node straight element for straight beams. On the other hand, it is advantageous from a computational perspective to use the three-node curved element for curved beams.

Chapter 4

Wind Induced Vibrations of Traffic Poles

4.1 Introduction

Traffic poles are beam-like structures that often have both straight and curved parts. They are flexible so that a wind may cause them to vibrate. This behavior may be due to either vortex shedding or to galloping [28]. Vortex shedding is the periodic formation and shedding of vortices, as shown in Figure 4.1 [29]. The shedding causes the pressure on each side of an object to be alternately reduced and increased. Then appreciable vibrations of the body may result, especially if the object has a natural frequency close to the vortex shedding frequency. Galloping, on the other hand, is a self excited oscillation that involves a large amplitude and low (0.1 to 3 Hz) frequencies. It is induced by aerodynamic instabilities that stem from an object's cross-sectional asymmetry. Rectangular or D cross-sections are particularly susceptible to galloping [29].

Wind loading research has developed over the past four or so decades and it has been used in practical problems [28-35]. However, only the most pertinent recent examples are given here. A flexible, square sectioned, slender cantilever beam has been examined in [30]. In the analysis, experimentally obtained, quasi-static air forces were used in a Galerkin analysis to obtain the beam's deflection at its tip. In reference

[31], the effect of dynamic wind loads was found on compliant towers. However, the calculation of the wind loads was performed by using equivalent static loads. The finite element method (FEM) has also been used. The authors in [32], for example, proposed a one degree-of-freedom, non-linear model of self limiting cyclic wind loads for the analysis of flexible structures subjected to vortex shedding. A numerical simulation of the dynamic response of broadcasting antennas under wind loads was performed by using the FEM [33]. The researchers in [28] analyzed the free vibrations of traffic poles, which had only straight parts, by using two-node beam elements. Flather [35] also analyzed a curved traffic pole by using two-node, straight beam elements. On the other hand, experiments have been performed in a wind tunnel to understand the vibration inducing mechanism for cantilevered poles [30]. The authors in reference [28] did more experimental research about cantilevered traffic poles by performing water table, tow tank and full scale field experiments. They found that vortex shedding at Reynolds numbers (Re) in the range from 300 to 3×10^5 (called the subcritical region) occurs at a Strouhal number around 0.2. The Strouhal number is in this neighborhood for most traffic light poles. From their experiments, they observed that large amplitude vibrations of cantilevered traffic poles are caused by galloping, not by pure vortex shedding. Furthermore, they found that galloping is most likely to occur in a steady wind when the wind direction is within $\pm7.5^\circ$ of normal to the cantilever signal arm. The associated wind speed is typically from 4.5 to 13.4 m/s.

Curved beam finite elements are needed to deal with curved poles. However, research about the dynamic response of curved poles has been very scanty. Furthermore,

a three-dimensional analysis is necessary. This is because the most dangerous situation (for the initiation of galloping) seems to be when the wind's direction is approximately normal to the curved pole's plane and vibrations are observed in this plane [28].

In this chapter, the previously discussed three-node curved beam element, whose displacements are in three dimensions, is used to analyze the wind induced vibrations of curved light poles. The initiation of galloping is investigated. Vortex shedding is not discussed further. Critical wind speeds, which correspond to the magnitude of a steady wind speed that is just large enough to initiate galloping, are found for poles having a hexagonal or octagonal cross-section. The wind's direction is approximately normal to the curved pole's plane of curvature. The effects of structural damping and the wind's direction are also investigated.

4.2 Reynolds and Strouhal Numbers

The two most influential effects in an air flow are due to the air's viscosity and inertia. The Reynolds number, Re, is a non-dimensional parameter which is a measure of the ratio of the inertial to viscous forces. Re is given as:

$$\mathrm{Re} = U_f D / \nu_{air} \tag{4.1}$$

where U_f is the free stream velocity. D is the width of the structure perpendicular to the air flow and ν_{air} is the kinematic viscosity of air. Re is an index of the type of flow that may be expected to occur. The air flow around a circular cylinder, for example, is shown in Figure 4.1. Each flow situation is identified by a Reynolds number region. At $\mathrm{Re} \cong 1$,

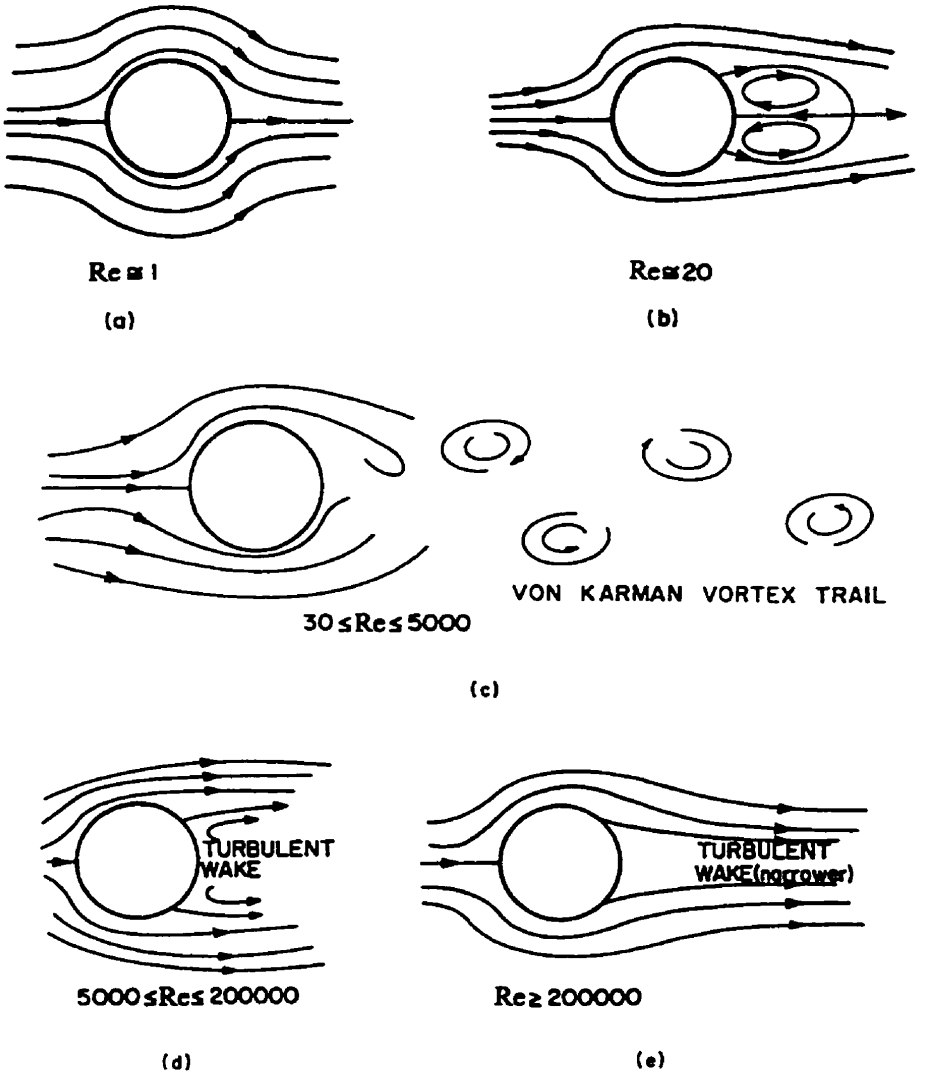

Figure 4.1 Flow past a circular cylinder at different Reynolds number, Re [29].

the flow remains attached to the cylinder. At Re ≅ 20, the flow remains symmetrical but separation occurs and large wake eddies are formed. For 30 ≤ Re ≤ 5000, alternating vortices are shed from the cylinder that form a clear "vortex trail" downstream of the cylinder. When $5000 \leq \mathrm{Re} \leq 2\times10^5$, the transition to turbulent flow occurs in the wake. The wake narrows appreciably for $\mathrm{Re} \geq 2\times10^5$.

The phenomenon of vortex-shedding can be described in terms of a non-dimensional Strouhal number, S_t, defined as:

$$S_t = \frac{f_s D}{U_f} \tag{4.2}$$

where f_s is the frequency of a complete cycle of vortex shedding. The Strouhal number is a function of Reynolds number, surface roughness and the free stream turbulence. Figure 4.2 illustrates the relationship between the Strouhal and Reynolds numbers for circular cylinders having either a smooth or a rough surface.

When the wind speed is around 10 m/s, for example, the Reynolds number is approximately between 6.7×10^4 and 2×10^5 (i.e. in the subcritical range) for the 100 mm to 300 mm pole diameters considered here. Then the airflow is turbulent in the wake, as shown in Figure 4.1. The corresponding Strouhal number is seen from Figure 4.2 to be about 0.2.

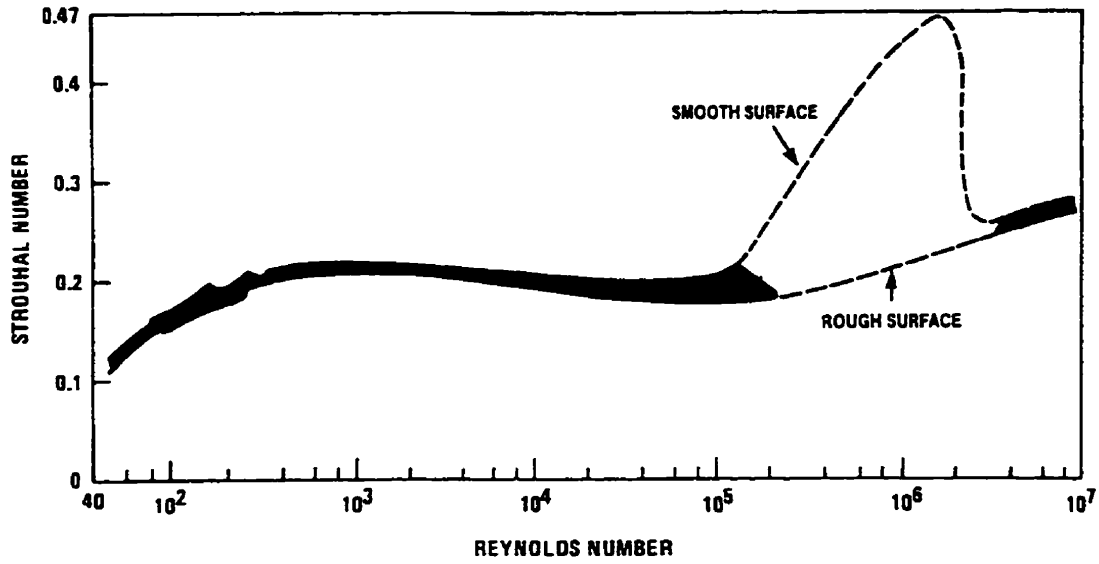

Figure 4.2 Relationship between the Strouhal and Reynolds numbers for circular cylinders [34].

4.3 Description of Light Poles

The tapered steel light pole shown in Figure 4.3 is analyzed next. It consists of three parts, two straight parts, AC and DE, as well as a curved part, CD, which is a quarter of a circle. Hexagonal and octagonal cross-sections are analyzed. A lamp, which is not shown in Figure 4.3, is usually attached to the tip of the pole. The mass of the lamp considered here is $39\ kg$. Other related data are:

$$E = 200\ GPa \qquad G = 80\ GPa \qquad k_s = 0.5$$

$$\rho_{steel} = 7850\ kg/m^3 \qquad \rho_{air} = 1.19\ kg/m^3$$

$$D_A = 232\ mm \qquad D_B = 154\ mm \qquad D_C = 119.2\ mm$$

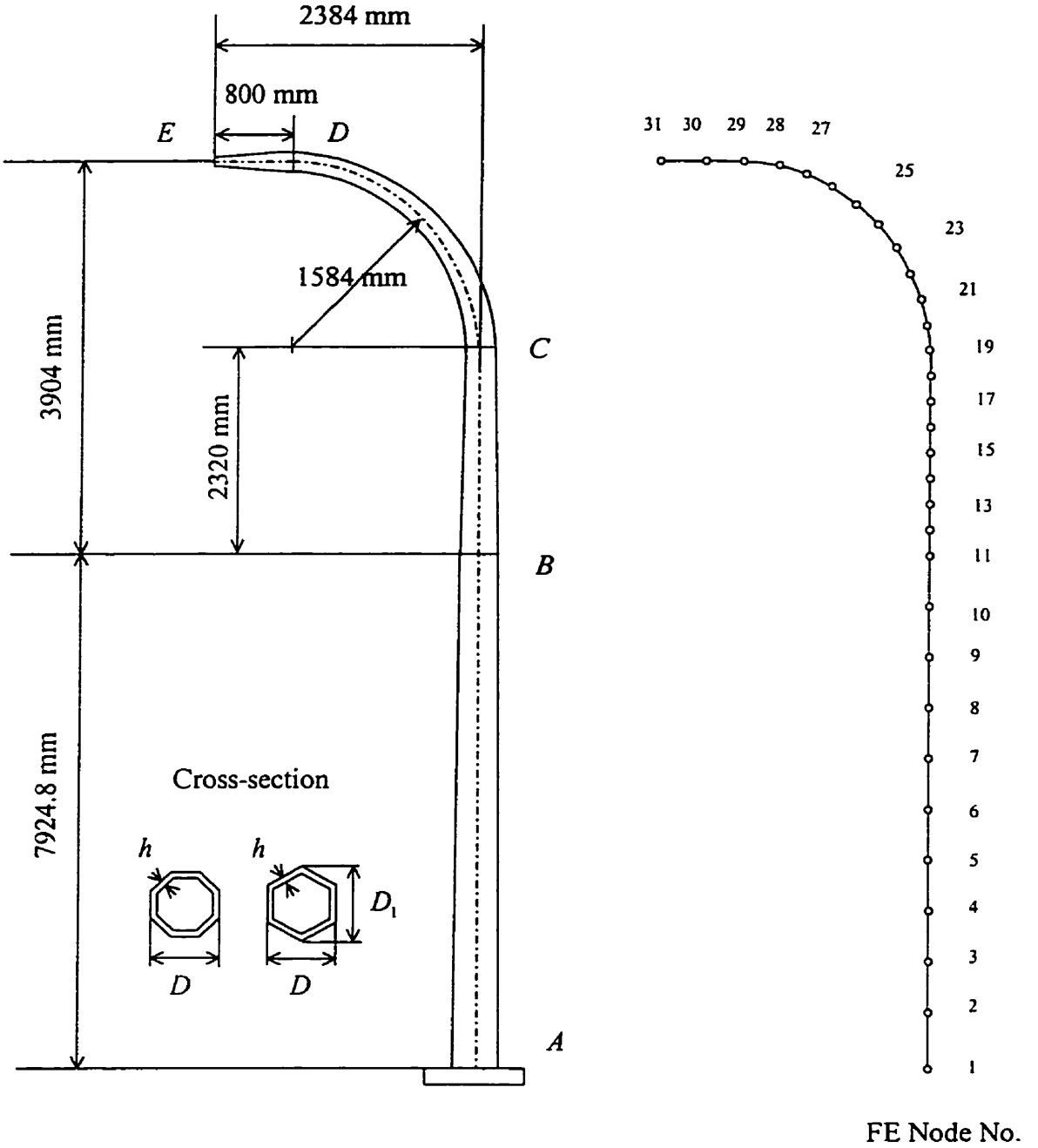

Figure 4.3 A curved light pole.

$$D_D = 82\ mm \qquad D_E = 70\ mm$$

$$h_{AB} = 4.55\ mm \qquad h_{BE} = 3.04\ mm.$$

where D_A, D_B, D_C, D_D and D_E are the values of D at cross-sections A, B, C, D and E, respectively. Moreover, h_{AB} and h_{BE} are the pole's constant thickness for part AB and BE, respectively. When the wind's direction is normal to the structural plane ABE, the dimension D illustrated in Figure 4.3 is perpendicular to the wind's direction.

4.4 Equations of Motion

By using the conventional theory [36] for the whole structure, the form of the equations of motion can be derived as:

$$[M]\{\ddot{Q}\} + [C]\{\dot{Q}\} + [K]\{Q\} = \{P\} \tag{4.3}$$

where $[M]$, $[C]$ and $[K]$ are the global structural mass, damping and stiffness matrix, respectively. The $\{Q\}$, $\{\dot{Q}\}$ and $\{\ddot{Q}\}$ are the nodal displacement, velocity and acceleration vectors, respectively. $\{P\}$ is the corresponding nodal load vector. When the external loads are aerodynamic forces and moments, $\{P\}$ is a function of the nodal displacements and velocities which, in turn, are functions of time. (See the later Section 4.7.)

4.5 Damping Matrix

It is difficult to experimentally measure the damping matrix $[C]$. Therefore, several approximate methods are employed. In this thesis, the most common approximate

form of proportional or Rayleigh damping [37] is used. Then $[C]$ is given by:

$$[C] = a_{c0}[M] + a_{c1}[K] \tag{4.4}$$

where a_{c0} and a_{c1} are constants which can be evaluated from:

$$\begin{Bmatrix} a_{c0} \\ a_{c1} \end{Bmatrix} = \frac{2\omega_m \omega_n}{\omega_n^{\,2} - \omega_m^{\,2}} \begin{bmatrix} \omega_n & -\omega_m \\ -1/\omega_n & 1/\omega_m \end{bmatrix} \begin{Bmatrix} \delta_m \\ \delta_n \end{Bmatrix}. \tag{4.5}$$

Here δ_m and δ_n are the measured damping ratios for two modes having the natural frequencies ω_m and ω_n, respectively. If $\delta_m = \delta_n = \delta$, then equation (4.5) simplifies to:

$$\begin{Bmatrix} a_{c0} \\ a_{c1} \end{Bmatrix} = \frac{2\delta}{\omega_m + \omega_n} \begin{Bmatrix} \omega_m \omega_n \\ 1 \end{Bmatrix}. \tag{4.6}$$

4.6 Aerodynamic Experiments

Wind tunnel experiments are performed to obtain the aerodynamic coefficients of the wind load by applying a quasi-steady theory. Full-scale experiments could not be performed due to the limited dimensions of the working cross-section of the available wind tunnel. Therefore, the tests are carried out on geometrically similar but smaller models. According to the similarity requirements [29], the Reynolds number is kept approximately the same for both the model and (full scale) prototype poles. Because the taper of the pole shown in Figure 4.3 is small (about 1:150), constant cross-sectional pole models (not tapered poles) are used for simplicity. As the maximum wind speed obtainable in the wind tunnel is about 32 m/s, and 4m/s is at the lower end of the range of wind speeds observed to produce galloping in practice, the scale one-eighth for the model is realistic. However, if one model is made for the complete pole, it would be too big to

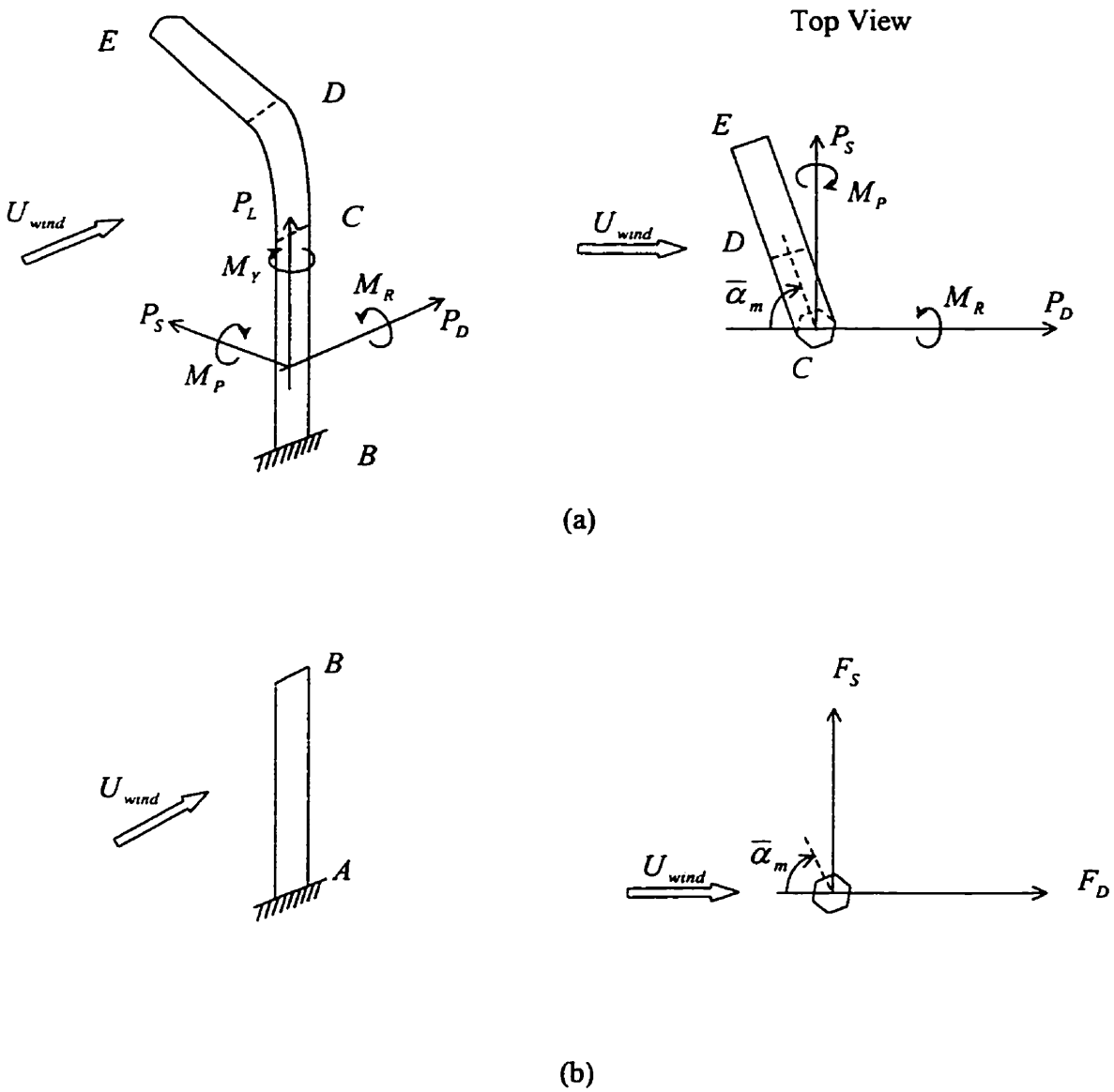

Figure 4.4 Showing (a) the total aerodynamic forces acting on the curved, rigid pole; and (b) the aerodynamic forces per unit length of a straight, rigid pole.

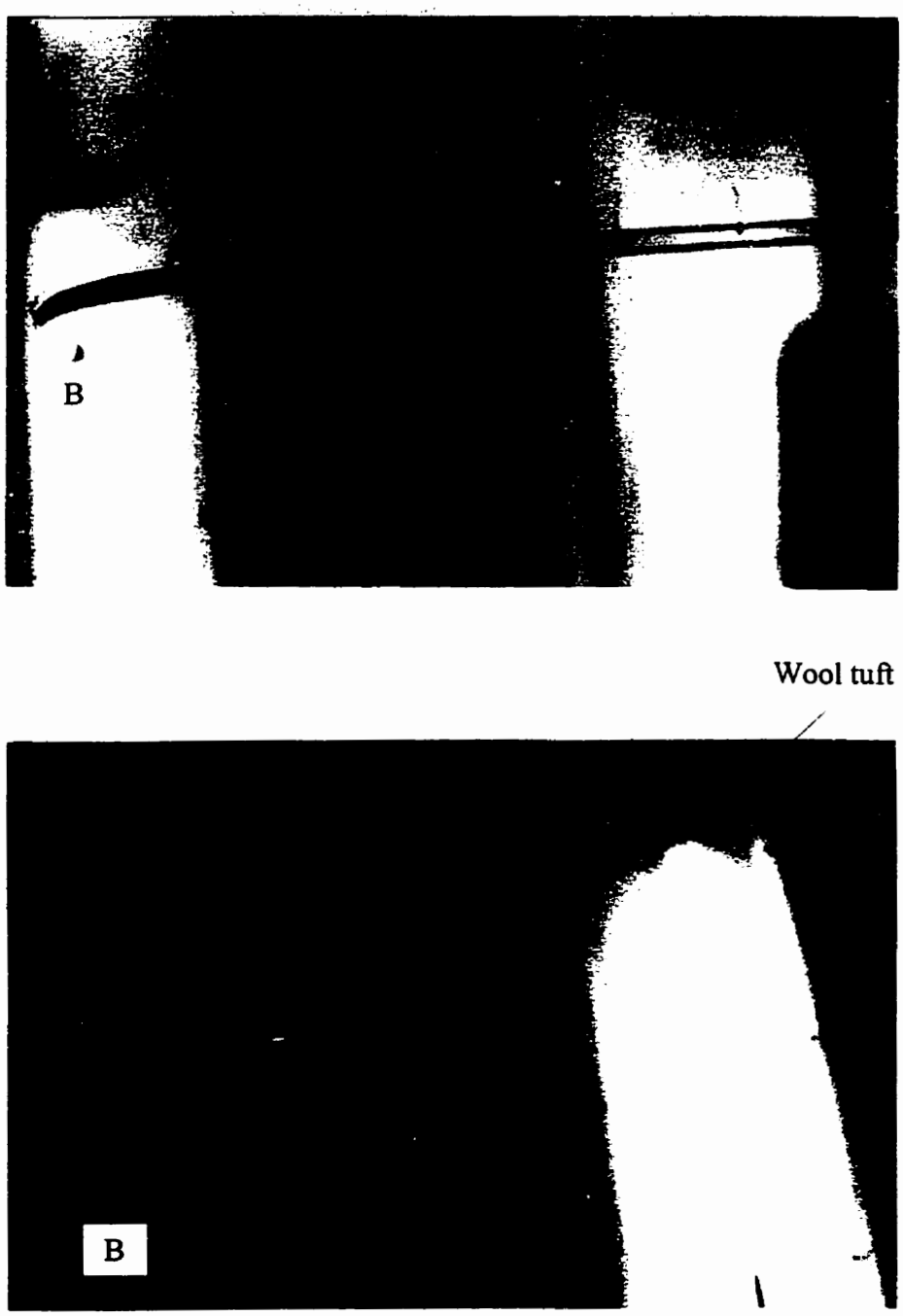

Figure 4.5 A curved pole positioned in the wind tunnel at $\overline{\alpha}_m = 90^\circ$.

put in the wind tunnel. Consequently, to use the one-eighth or so scaling, a model had to be wind tunnel tested in two separate components. The two components consist of one component which corresponds to the combined curved-straight part shown as part BE in Figure 4.3; the other component is for the solely straight part, AB. They are illustrated in Figures 4.4 (a) and 4.4 (b), respectively. The interaction of the airflow between parts AB and BE is assumed to be negligible. Figure 4.5 shows a wool tufted model in the wind tunnel. The relatively straight tufts around point B suggest that the assumption is reasonable.

The drag force, P_D, shown in Figure 4.4 (a), is defined along the wind's direction. The lift force, P_L, is vertical and the horizontal side force, P_S, is perpendicular to both P_D and P_L. These forces are usually given in terms of aerodynamic coefficients by:

$$P_D = \frac{1}{2}\rho_{air}U_{wind}^2 DC_{DC}L_{BE}$$

$$P_L = \frac{1}{2}\rho_{air}U_{wind}^2 DC_{LC}L_{BE} \tag{4.7}$$

$$P_S = \frac{1}{2}\rho_{air}U_{wind}^2 DC_{SC}L_{BE} \ .$$

ρ_{air} is the density of air, U_{wind} is the free stream air speed, and D is a typical dimension of the pole's cross-section. However, the wind's angle of attack on the model pole is varied so that the model's dimension normal to the airflow varies with the wind direction. For example, it varies between D and D_1 for the hexagonal cross-section presented in Figure 4.3. For convenience, D is taken as the (constant) distance between any two opposite flat sides for both the hexagonal and octagonal cross-sections. Furthermore, L_{BE}

in equation (4.7) is the total outside periphery length of the curved model BE. C_{DC}, C_{LC} and C_{SC} are the drag, lift and side force coefficients for the curved model BE. The rolling, yawing and pitching moments, M_R, M_Y and M_P respectively, are the corresponding moments about these three directions. They are given by:

$$M_R = \frac{1}{2}\rho_{air}U_{wind}^2 D^2 C_{MRC} L_{BE}$$

$$M_Y = \frac{1}{2}\rho_{air}U_{wind}^2 D^2 C_{MYC} L_{BE} \tag{4.8}$$

$$M_P = \frac{1}{2}\rho_{air}U_{wind}^2 D^2 C_{MPC} L_{BE}$$

where C_{MRC}, C_{MYC} and C_{MPC} are the rolling, yawing and pitching moment coefficients for the curved model BE. Similarly, there are drag and side forces for the straight pole model AB. However, the measured moments are negligible, regardless of the cross-section, so that only the forces per unit length are shown in Figure 4.4. They are given by:

$$F_D = \frac{1}{2}\rho_{air}U_{wind}^2 DC_D$$

and

$$F_S = \frac{1}{2}\rho_{air}U_{wind}^2 DC_S \tag{4.9}$$

where C_D and C_S are the drag and side force coefficients for the straight model AB.

The aerodynamic forces and moments are non-dimensionalized to obtain the aerodynamic coefficients. Both hexagonal and octagonal cross-sections are tested. Measured data are shown in Figures 4.6 through 4.8 when the wind speed is 31.4 m/s and the Reynolds number is 2.7×10^4 (i.e. in the subcritical range). The reference angle,

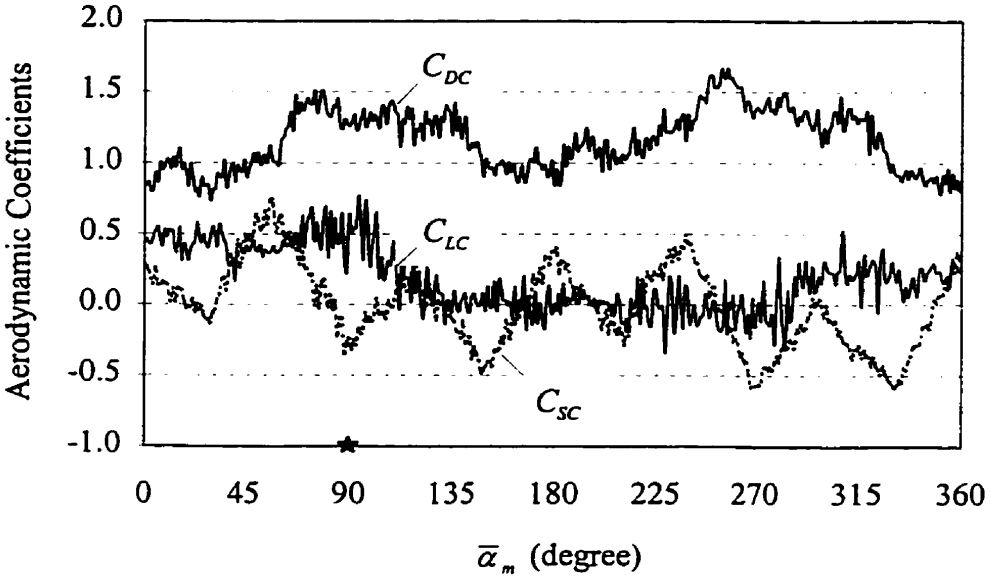

(a)

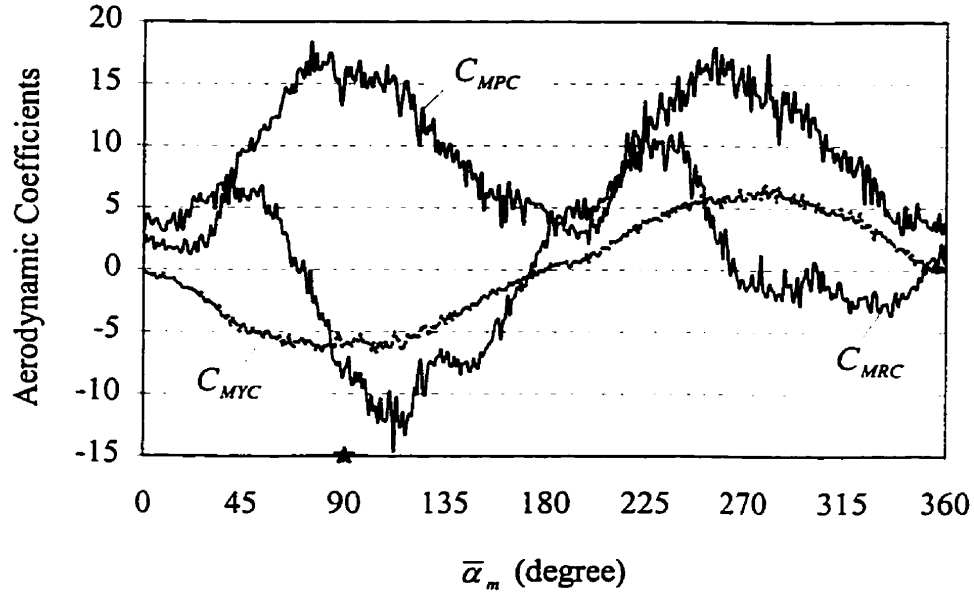

(b)

Figure 4.6 Aerodynamic coefficients for the hexagonal curved model *BE*.

★The analyzed position.

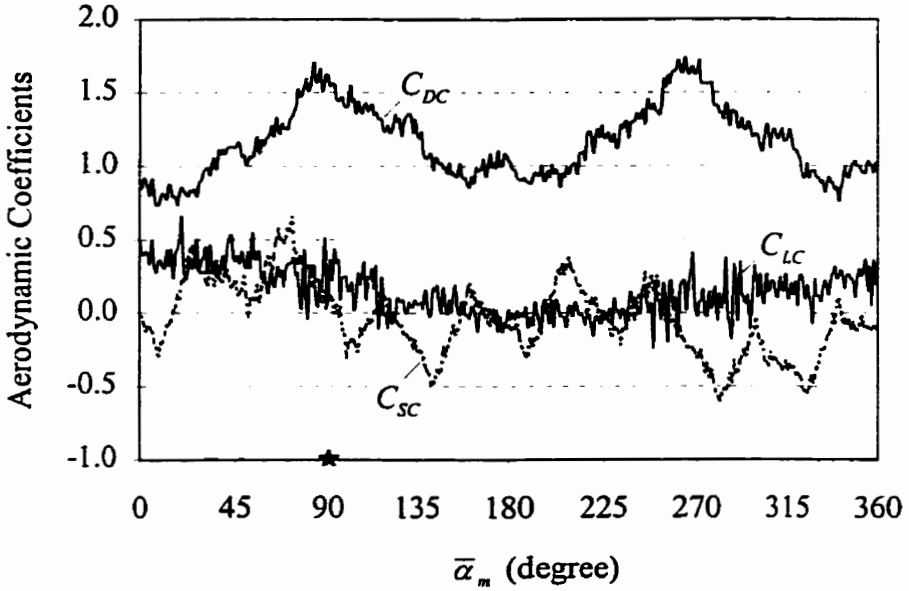

(a)

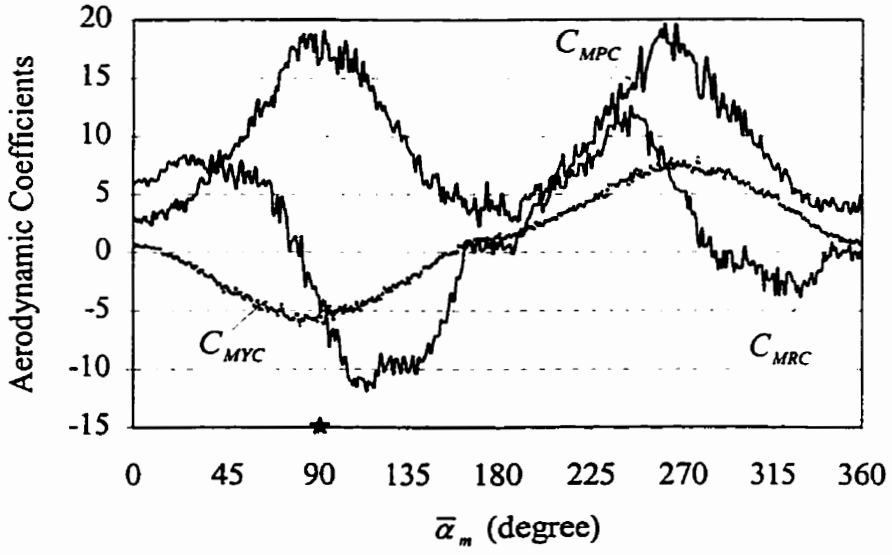

(b)

Figure 4.7 Aerodynamic coefficients for the octagonal curved model BE .

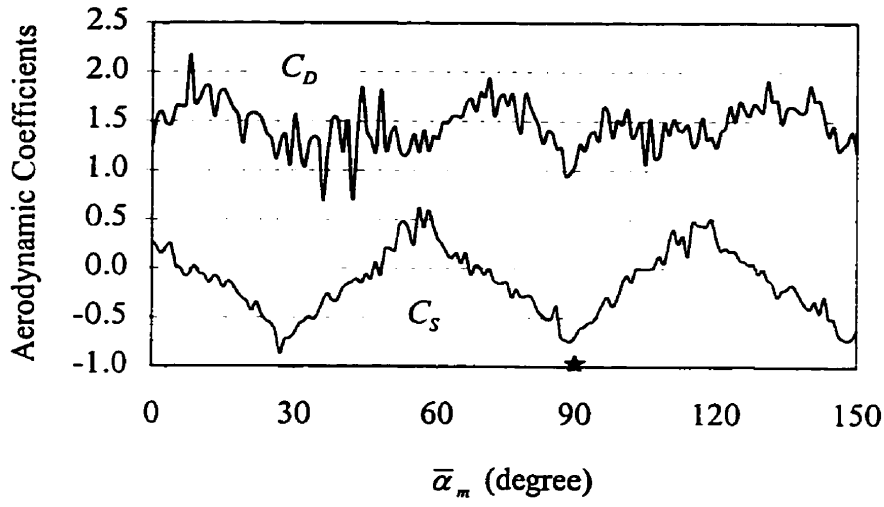

(a)

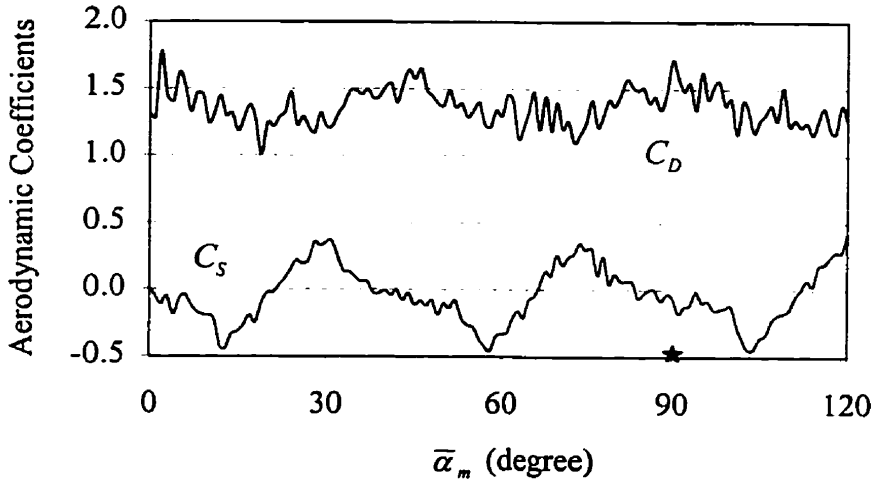

(b)

Figure 4.8 Aerodynamic coefficients for straight poles having a (a) hexagonal; and (b) octagonal cross-section.

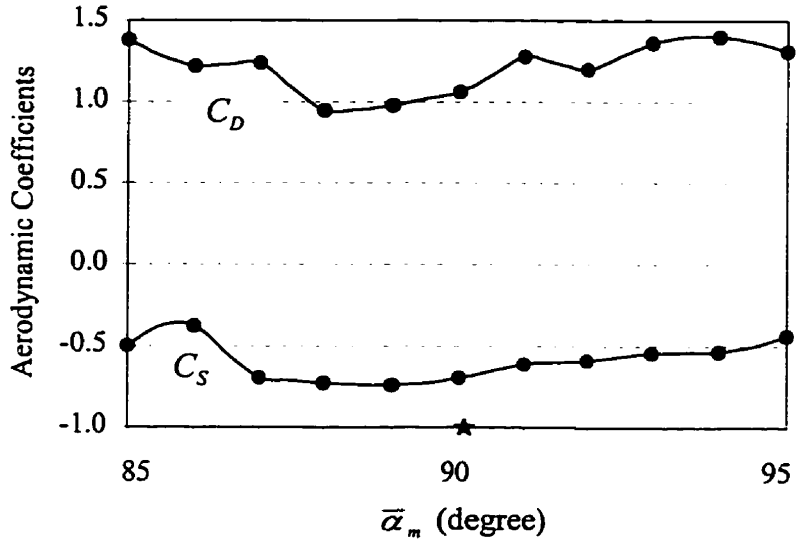

(a)

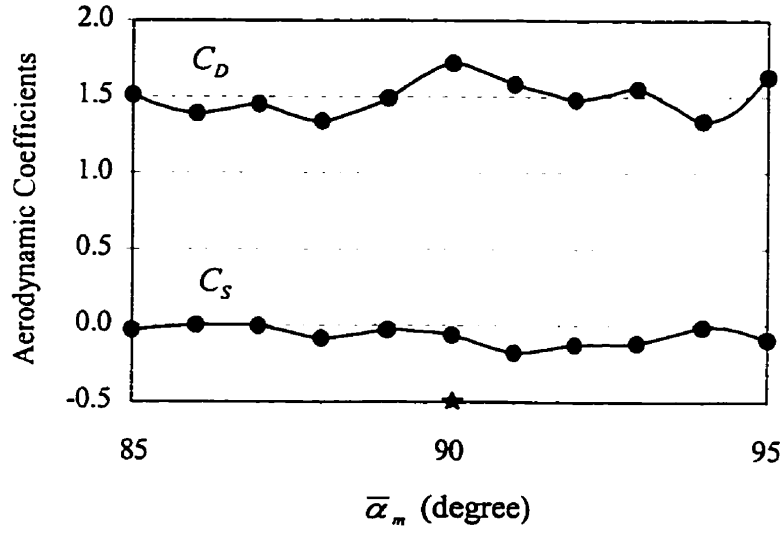

(b)

Figure 4.9 Cubic spline interpolation for the aerodynamic coefficients of a straight pole having a (a) hexagonal; and (b) octagonal cross-section. — cubic spline interpolation, ● experimental data, ★ the analyzed position.

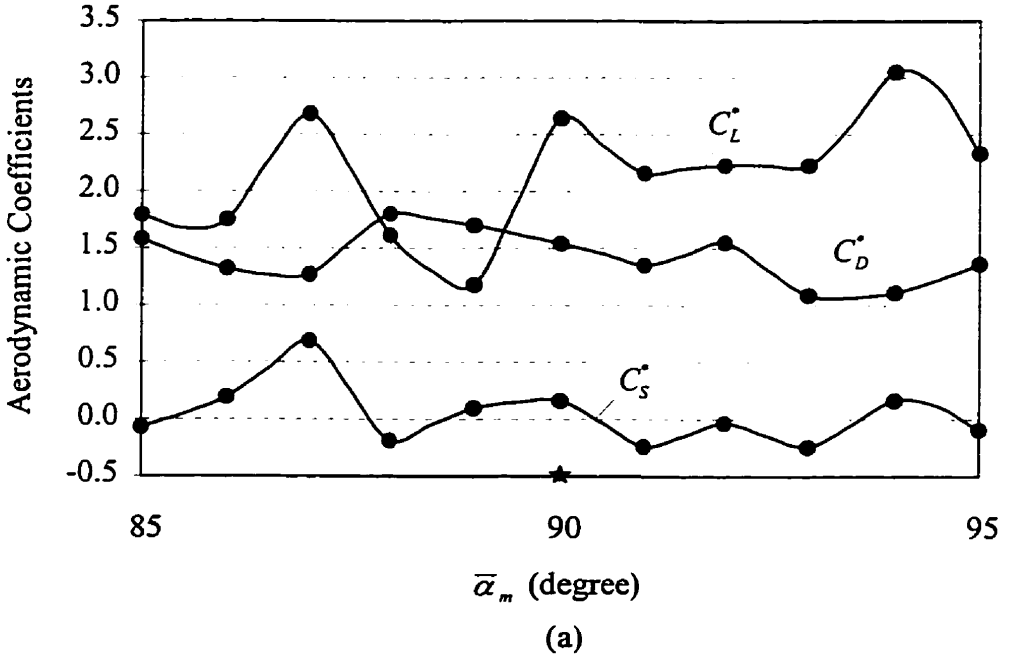

(a)

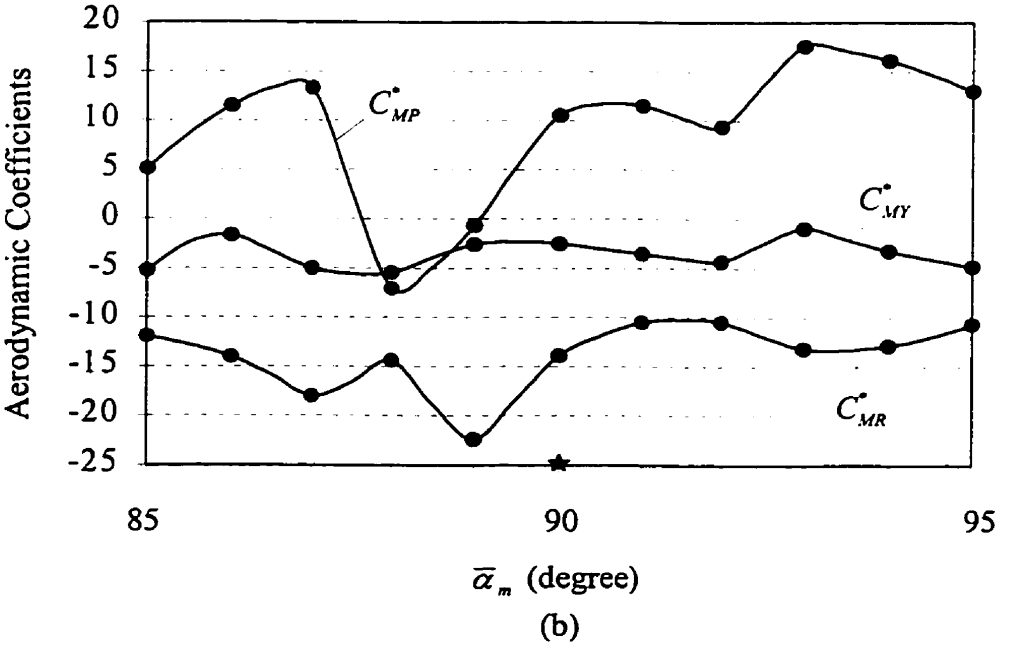

(b)

Figure 4.10 Cubic spline interpolation for the calculated aerodynamic coefficients of the curved part, *CD* , having a hexagonal cross-section. — cubic spline interpolation, •• calculated data.

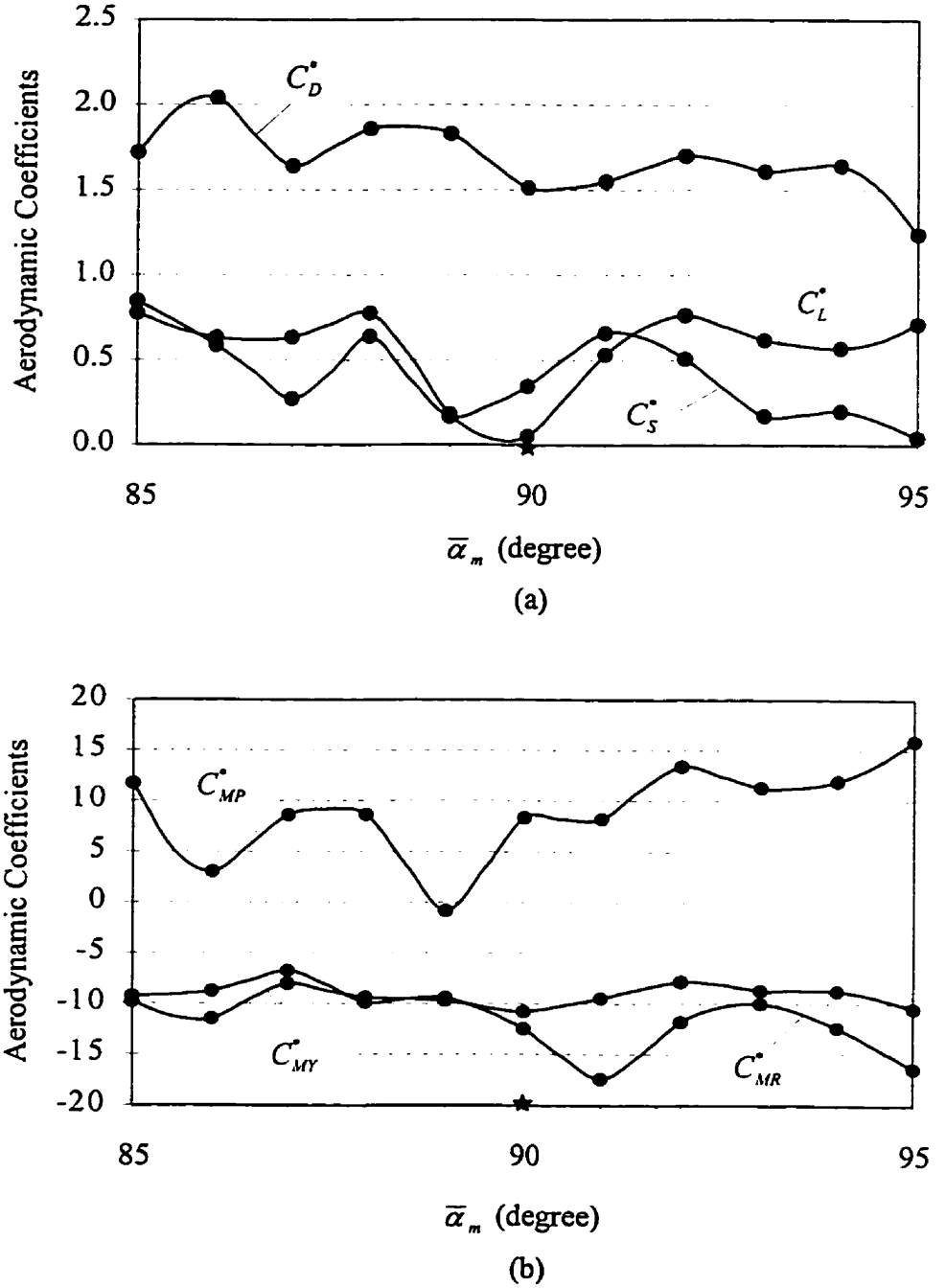

Figure 4.11 Cubic spline interpolation for the calculated aerodynamic coefficients of the curved part, *CD* , having a octagonal cross-section. — cubic spline interpolation, • calculated data.

$\overline{\alpha}_m = 0°$, for the curved model is taken to correspond to the position when part ED in Figure 4.4 is along the wind's direction and the wind blows from point E to point D. In addition, two opposite flat sides (of either the hexagonal or octagonal cross-section) are perpendicular to the wind's direction at $\overline{\alpha}_m = 0°$ for both the curved and straight model.

It can be seen from Figures 4.6 through 4.8 that the trends of these curves are similar for the hexagonal and octagonal poles. Theoretically, the data at $\overline{\alpha}_m = 0°$ and $360°$ should be the same. However, there are small differences between these two angles in these figures. The drift is likely due to a temperature change during the wind tunnel experiments, even though the wind tunnel and its instrumentation was run for several hours before starting an experiment. In this thesis, only the positions around $\overline{\alpha}_m$ equal $90°$ are analyzed because the pole is most susceptible then to galloping. (A star is used in the figures to highlight this particular orientation.)

Next, because the measured aerodynamic coefficients for the curved model BE include the effects of the straight parts BC and DE, the aerodynamic coefficients for the purely curved part CD of the model are calculated by subtracting the effects of the straight parts from the measured coefficients. Details of the calculations required to compute the aerodynamic coefficients for the curved part CD are given more conveniently in Appendix E. The cubic spline interpolation program given in IMSL [22], DCSAKM, is used to curve fit the measured and calculated data. These curves are presented in Figures 4.9 through 4.11 in the range of $\overline{\alpha}_m$ around $90°$. The effects on the aerodynamic coefficients of various Reynolds numbers and a lamp located at the tip of a

pole are investigated. In the experiment, a tubular section is mounted coaxially at the tip of the curved pole model to simulate a lamp. The tube has a length of about 20 mm, its inside diameter is approximately equal to the maximum dimension of the cross-section of the model, and its thickness is about 2 mm. The related figures are given in Appendix F. The aerodynamic effect of the lamp simulator is small. On the other hand, because the wind speed in the wind tunnel could not be changed over a large range, the effects of Reynolds number could not be analyzed realistically over a large range.

4.7 Aerodynamic Loads

The $\{P\}$ term in equation (4.3) is created by the wind load. The most dangerous situation, in which the wind's direction is essentially perpendicular to the curved pole's structural plane (i.e. $\bar{\alpha}_m = 90^\circ$ in Figure 4.4), is analyzed. First, because the pole is so slender and its Reynolds number is in the subcritical range, it is reasonable to suppose that the airflow does not reattach to a downstream part of the pole [29] at $\bar{\alpha}_m \approx 90^\circ$. Indeed, the similar orientation of the wool tufts shown in Figure 4.5 suggests that the wind pressure is distributed quite uniformly over the model. Therefore, a uniform pressure assumption is adopted in the finite element model.

A curved pole can be divided into three parts: the vertical straight part AC shown in Figure 4.12, as well as the curved part CD and the horizontal straight part, DE. The $X-Y-Z$ shown in Figure 4.12 corresponds to the global coordinate system and the $x-\zeta-\eta$ is the local coordinate system. The x and ζ are along the tangential

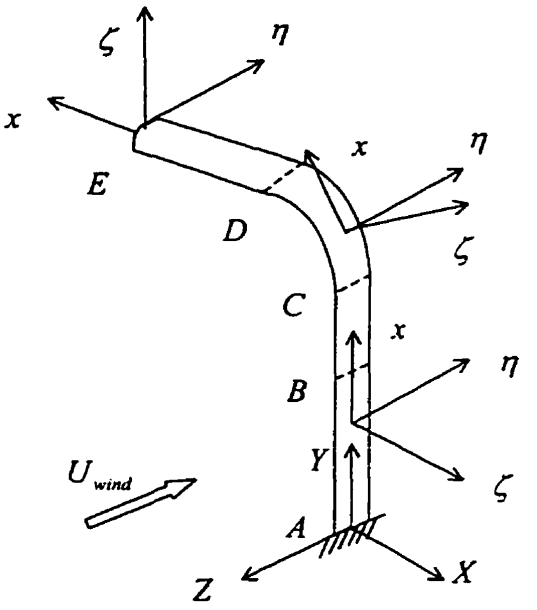

Figure 4.12 Global and local coordinate systems.

and normal directions of the centroidal axis of the pole, respectively, and η is perpendicular to the $x-\zeta$ plane. Let the angle between the wind's direction and the structural plane (the $X-Y$ plane) be $90^\circ \pm |\bar{\varepsilon}|$. $|\bar{\varepsilon}| \le 1^\circ$ is a small offset angle. The following derivation presents the formulae for calculating the nodal forces that are needed in the finite element analysis for the curved pole.

(a) The vertical part AC

The forces acting over a unit length of the vertical part, AC, of the vibrating pole are shown in Figure 4.13. When $\bar{\varepsilon} = 0$, U_{wind} is perpendicular to the ζ direction. Due to the pole's dynamic rotation, θ_x, induced by the wind, the local coordinate plane $\zeta - \eta$, which corresponds to the pole's static configuration, instantaneously takes the

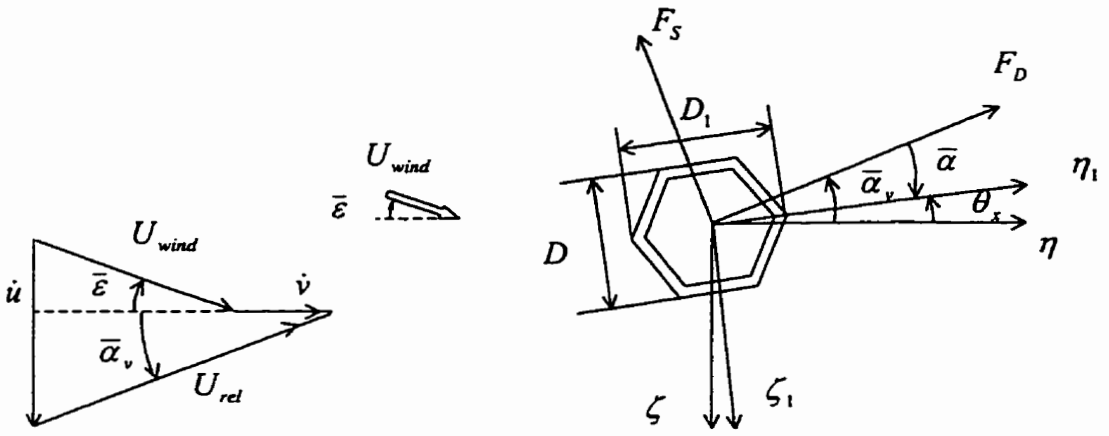

Figure 4.13 Aerodynamic forces per unit length acting on AC.

orientation $\zeta_1 - \eta_1$ illustrated in Figure 4.13. Consequently, a vibrating pole experiences a relative wind, U_{rel}, as suggested in Figure 4.13. The magnitude of U_{rel} and its direction, $\bar{\alpha}_v$, with respect to the original $\zeta - \eta$ system are [38]:

$$\begin{aligned} U_{rel}^2 &= (\dot{u} - U_{wind}\sin\bar{\varepsilon})^2 + (U_{wind}\cos\bar{\varepsilon} + \dot{v})^2 \\ &\equiv (\dot{u} - U_{wind}\bar{\varepsilon})^2 + (U_{wind} + \dot{v})^2 \end{aligned} \tag{4.10a}$$

and

$$\bar{\alpha}_v = \frac{\dot{u} - U_{wind}\sin\bar{\varepsilon}}{U_{wind}\cos\bar{\varepsilon} + \dot{v}} \cong \frac{\dot{u} - U_{wind}\bar{\varepsilon}}{U_{wind} + \dot{v}} \cong \frac{\dot{u}}{U_{wind} + \dot{v}} - \bar{\varepsilon}. \tag{4.10b}$$

In the above formulae, the approximations $\sin\bar{\varepsilon} \cong \bar{\varepsilon}$ and $\cos\bar{\varepsilon} \cong 1$ are reasonably used because $|\bar{\varepsilon}| \le 1^\circ$. Also, it is assumed that $U_{wind} >> |\dot{v}|$ because the later numerical computations indicate that U_{wind} for galloping is typically around 13 m/s and $|\dot{v}|$ is about 0.1m/s. Then

$$\frac{U_{wind}}{U_{wind}+\dot{v}} \cong 1. \tag{4.11}$$

The wind's instantaneous angle of attack, $\bar{\alpha}$, is :

$$\bar{\alpha} = \bar{\alpha}_v - \theta_x . \tag{4.12}$$

$\bar{\alpha}$ and $\bar{\varepsilon}$ are taken to be positive in the plan view's clockwise direction but $\bar{\alpha}_v$ and θ_x are positive in the counterclockwise direction, as indicated in Figure 4.13. On the other hand, the relation between $\bar{\alpha}$ and the $\bar{\alpha}_m$ used experimentally is: $\bar{\alpha} = \bar{\alpha}_m - 90^\circ$.

The drag and side force per unit length are:

$$F_D = \frac{1}{2}\rho_{air} U_{rel}^2 D C_D$$

and

$$F_S = \frac{1}{2}\rho_{air} U_{rel}^2 D C_S \tag{4.13}$$

where C_D and C_S are the drag and side force coefficients for the straight pole, respectively. They are shown in Figure 4.9 where $85^\circ \le \bar{\alpha}_m \le 95^\circ$, i.e., $-5^\circ \le \bar{\alpha} \le 5^\circ$. Next, the forces per unit length along the ζ_1 and η_1 directions are:

$$F_{\zeta_1} = -F_D \sin\bar{\alpha} - F_S \cos\bar{\alpha}$$

and

$$F_{\eta_1} = F_D \cos\bar{\alpha} - F_S \sin\bar{\alpha} . \tag{4.14a}$$

From the numerical calculations, the rotation θ_x is about 0.3° when the wind speed is around 13 m/s. Hence, θ_x is small and the directions ζ and η are used for the ζ_1 and η_1 directions in the calculations, i.e.

$$F_{\zeta_1} \cong F_{\zeta} \quad \text{and} \quad F_{\eta_1} \cong F_{\eta} \ . \tag{4.14b}$$

(b) The curved part CD

Consider the unit arc length shown in Figure 4.14 which is used to analyze the aerodynamic forces acting on the curved part CD. The ϕ in this figure is the angle between the x and X axes. Because the aerodynamic forces are given in the X, η and Y directions (see Appendix E), first find the velocities and rotations about the X and Y axes. They are:

$$\begin{aligned} \dot{V}_X &= \dot{u}\sin\phi - \dot{w}\cos\phi \\ \dot{V}_Y &= \dot{u}\cos\phi + \dot{w}\sin\phi \end{aligned} \tag{4.15a}$$

and

$$\begin{aligned} \theta_X &= \theta_\zeta \sin\phi - \theta_x \cos\phi \\ \theta_Y &= \theta_\zeta \cos\phi + \theta_x \sin\phi \ . \end{aligned} \tag{4.15b}$$

Next

$$\begin{aligned} U_{rel}^2 &= \left(\dot{V}_X - U_{wind}\sin\bar{\varepsilon}\right)^2 + \left(U_{wind}\cos\bar{\varepsilon} + \dot{v}\right)^2 \\ &\cong \left(\dot{V}_X - U_{wind}\bar{\varepsilon}\right)^2 + \left(U_{wind} + \dot{v}\right)^2 \end{aligned} \tag{4.16a}$$

and

$$\bar{\alpha}_v = \frac{\dot{V}_X - U_{wind}\sin\bar{\varepsilon}}{U_{wind}\cos\bar{\varepsilon} + \dot{v}} \cong \frac{\dot{V}_X}{U_{wind} + \dot{v}} - \bar{\varepsilon} \tag{4.16b}$$

$$\bar{\alpha} = \bar{\alpha}_v - \theta_Y . \tag{4.17}$$

The aerodynamic forces per unit arc length are:

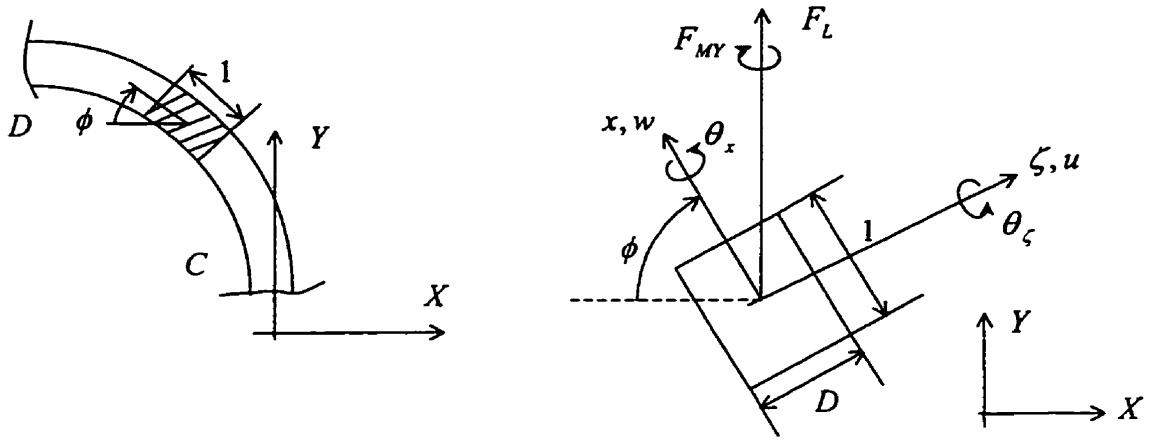

Figure 4.14 Aerodynamic forces per unit arc length of CD when observed along the wind's direction.

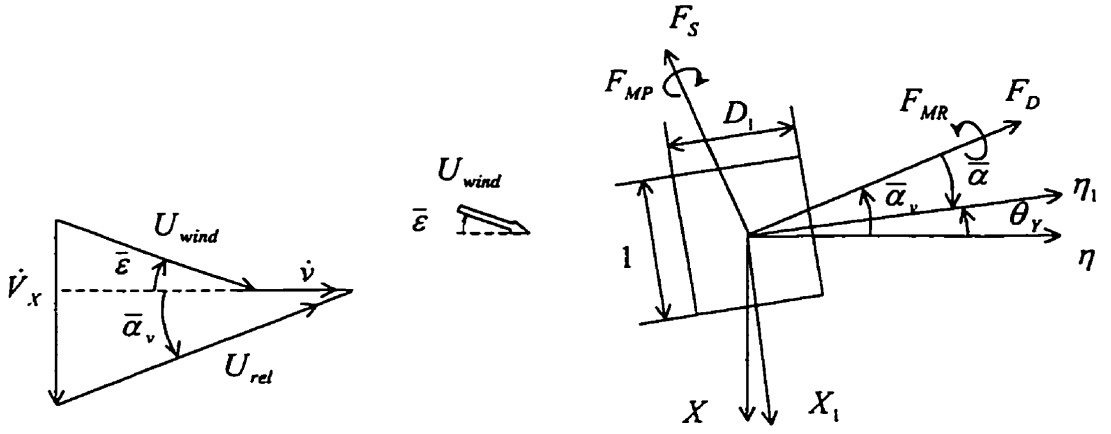

Figure 4.15 Aerodynamic forces per unit arc length of CD when observed from the top of the pole.

$$F_D = \frac{1}{2}\rho_{air} U_{rel}^2 D C_D^*$$

$$F_S = \frac{1}{2}\rho_{air} U_{rel}^2 D C_S^* \sin\phi \tag{4.18}$$

and

$$F_L = \frac{1}{2}\rho_{air} U_{rel}^2 D C_L^* \cos\phi$$

where F_L is the lift force, while C_D^*, C_S^* and C_L^* are the drag, side and lift force coefficients for the curved part CD, respectively. Similarly, the rolling, pitching and yawing moments per unit arc length are:

$$F_{MR} = \frac{1}{2}\rho_{air} U_{rel}^2 D^2 C_{MR}^*$$

$$F_{MP} = \frac{1}{2}\rho_{air} U_{rel}^2 D^2 C_{MP}^* \cos\phi \tag{4.19}$$

$$F_{MY} = \frac{1}{2}\rho_{air} U_{rel}^2 D^2 C_{MY}^* \sin\phi$$

where C_{MR}^*, C_{MP}^* and C_{MY}^* are the rolling, pitching and yawing moment coefficients for the curved part CD, respectively. These coefficients are presented in Figures 4.10 and 4.11. Next, the aerodynamic force and moment per unit arc length along the X_1 direction are:

$$F_{X_1} = -F_D \sin\bar{\alpha} - F_S \cos\bar{\alpha}$$

and

$$F_{MX_1} = F_{MR} \sin\bar{\alpha} - F_{MP} \cos\bar{\alpha}\,. \tag{4.20}$$

Finally, the forces and moments per unit arc length in the ζ, η_1 and x directions can be obtained as:

$$\begin{aligned} F_\zeta &= F_{X_1} \sin\phi + F_L \cos\phi \\ F_{\eta_1} &= F_D \cos\overline{\alpha} - F_S \sin\overline{\alpha} \\ F_x &= -F_{X_1} \cos\phi + F_L \sin\phi \end{aligned} \tag{4.21}$$

and

$$\begin{aligned} F_{m\zeta} &= F_{MX_1} \sin\phi - F_{MY} \cos\phi \\ F_{m\eta_1} &= -F_{MR} \cos\overline{\alpha} - F_{MP} \sin\overline{\alpha} \\ F_{mx} &= -F_{MX_1} \cos\phi - F_{MY} \sin\phi \ . \end{aligned} \tag{4.22}$$

As before, the direction η is used for η_1 in the calculations because the rotation θ_Y is small again. For instance, when the wind speed is around 13 m/s, θ_Y is about 0.25°.

(c) The horizontal part DE

The forces acting on a unit length of the horizontal part DE are shown in Figure 4.16. The $\zeta - \eta$ system still corresponds to the static position of the pole. As for the vertical part AC,

$$U_{rel}^2 = \dot{u}^2 + \left(U_{wind} + \dot{v}\right)^2 \tag{4.23a}$$

and

$$\overline{\alpha}_v \cong \frac{\dot{u}}{U_{wind} + \dot{v}} \tag{4.23b}$$

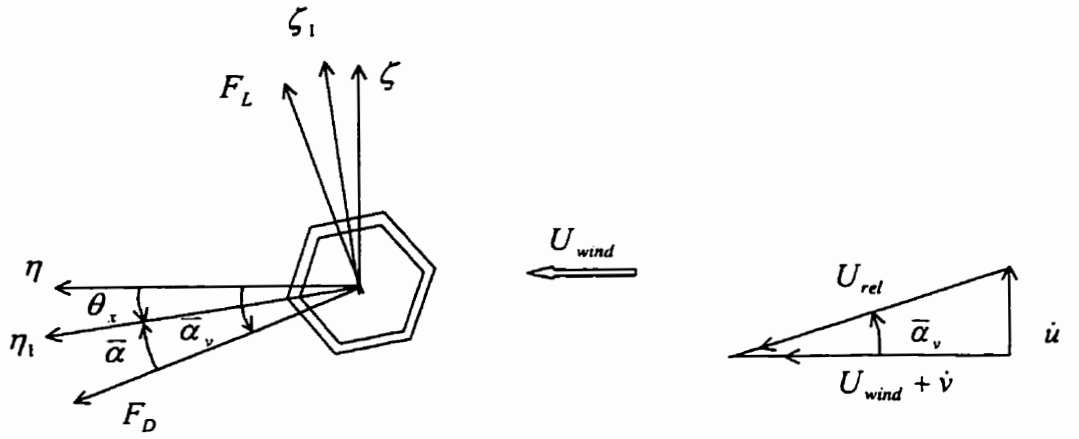

Figure 4.16 Aerodynamic forces per unit length of DE.

with

$$\bar{\alpha} = \bar{\alpha}_v - \theta_x \tag{4.24}$$

and

$$\begin{aligned} F_D &= \frac{1}{2}\rho_{air} U_{rel}^2 D C_D \\ F_L &= \frac{1}{2}\rho_{air} U_{rel}^2 D C_S \ . \end{aligned} \tag{4.25}$$

C_D and C_S are the same as before. The forces per unit length in the ζ_1 and η_1 directions are:

$$F_{\zeta_1} = -F_D \sin\bar{\alpha} + F_L \cos\bar{\alpha}$$

and

$$F_{\eta_1} = F_D \cos\bar{\alpha} + F_L \sin\bar{\alpha} \ . \tag{4.26}$$

As before, the directions ζ and η are used for ζ_1 and η_1, respectively.

The equivalent consistent load acting on an element can be obtained by using equation (2.27) and numerical integration. However, to simplify the calculations a lumped load vector [38] is utilized to avoid the numerical integration and save computational time. It is given by:

$$\{p_e\} = \frac{L_e}{4}\left[F_{\zeta 1}F_{m\zeta 1}F_{\eta 1}F_{m\eta 1}F_{x1}F_{mx1}\ 2\left(F_{\zeta 2}F_{m\zeta 2}F_{\eta 2}F_{m\eta 2}F_{x2}F_{mx2}\right)\ F_{\zeta 3}F_{m\zeta 3}F_{\eta 3}F_{m\eta 3}F_{x3}F_{mx3}\right]^T . \tag{4.27}$$

The equivalent load vector of an element can be calculated now by using the above formula. Then the load vector $\{P\}$, which is required in equation (4.3), can be assembled from the element load vectors.

4.8 Direct Time Integration

Because $\{P\}$ is a function of the nodal displacements and velocities which are related to time, it is not easy to decouple equation (4.3) to a set of independent, single degree of freedom systems in order to employ modal superposition. Here step-by-step, direct numerical integration is used. The standard Newmark-β method [36,39] is chosen. The following formulae are pertinent to this method.

For a damped structure, the equations of motion at instant t_j are:

$$[M]\{\ddot{Q}\}_j + [C]\{\dot{Q}\}_j + [K]\{Q\}_j = \{P\}_j . \tag{4.28}$$

Similarly, at instant $t_{j+1} = t_j + \Delta t_j$, the equations of motion become:

$$[M]\{\ddot{Q}\}_{j+1} + [C]\{\dot{Q}\}_{j+1} + [K]\{Q\}_{j+1} = \{P\}_{j+1} . \tag{4.29}$$

On the other hand, according to the Newmark-β method [36,39]:

$$\{\dot{Q}\}_{j+1} = \{\dot{Q}\}_j + \left[(1-\beta_1)\{\ddot{Q}\}_j + \beta_1\{\ddot{Q}\}_{j+1}\right]\Delta t_j \tag{4.30}$$

and

$$\{Q\}_{j+1} = \{Q\}_j + \{\dot{Q}\}_j \Delta t_j + \Delta t_j{}^2\left[\left(\frac{1}{2}-\beta_2\right)\{\ddot{Q}\}_j + \beta_2\{\ddot{Q}\}_{j+1}\right] \tag{4.31}$$

It can be shown from equation (4.31) that:

$$\{\ddot{Q}\}_{j+1} = \frac{1}{\beta_2(\Delta t_j)^2}\left[\{Q\}_{j+1} - \{Q\}_j\right] - \frac{1}{\beta_2 \Delta t_j}\{\dot{Q}\}_j - \left(\frac{1}{2\beta_2} - 1\right)\{\ddot{Q}\}_j. \tag{4.32}$$

Substituting equation (4.32) into equation (4.30) gives:

$$\{\dot{Q}\}_{j+1} = \frac{\beta_1}{\beta_2 \Delta t_j}\left[\{Q\}_{j+1} - \{Q\}_j\right] - \left(\frac{\beta_1}{\beta_2} - 1\right)\{\dot{Q}\}_j - \Delta t_j\left(\frac{\beta_1}{2\beta_2} - 1\right)\{\ddot{Q}\}_j. \tag{4.33}$$

For convenience, define the vectors:

$$\{\hat{Q}\}_j = \frac{1}{\beta_2(\Delta t_j)^2}\{Q\}_j + \frac{1}{\beta_2 \Delta t_j}\{\dot{Q}\}_j + \left(\frac{1}{2\beta_2} - 1\right)\{\ddot{Q}\}_j \tag{4.34}$$

$$\{\breve{Q}\}_j = \frac{\beta_1}{\beta_2 \Delta t_j}\{Q\}_j + \left(\frac{\beta_1}{\beta_2} - 1\right)\{\dot{Q}\}_j + \Delta t_j\left(\frac{\beta_1}{2\beta_2} - 1\right)\{\ddot{Q}\}_j \tag{4.35}$$

Now rewrite equations (4.32) and (4.33) in the form:

$$\{\ddot{Q}\}_{j+1} = \frac{1}{\beta_2 \Delta t_j{}^2}\{Q\}_{j+1} - \{\hat{Q}\}_j \tag{4.36}$$

and

$$\{\dot{Q}\}_{j+1} = \frac{\beta_1}{\beta_2 \Delta t_j}\{Q\}_{j+1} - \{\breve{Q}\}_j. \tag{4.37}$$

Then substitute equations (4.36) and (4.37) into equation (4.29) to yield:

$$\left[\hat{K}\right]\{Q\}_{j+1} = \left\{\hat{P}\right\}_{j+1} \tag{4.38a}$$

in which

$$\left[\hat{K}\right] = [M]\frac{1}{\beta_2 \Delta t_j{}^2} + \frac{\beta_1}{\beta_2 \Delta t_j}[C] + [K] \tag{4.38b}$$

and

$$\left\{\hat{P}\right\}_{j+1} = \{P\}_{j+1} + [M]\left\{\hat{Q}\right\}_j + [C]\left\{\breve{Q}\right\}_j . \tag{4.38c}$$

$\{Q\}_{j+1}$ can be obtained from equation (4.38), then $\left\{\ddot{Q}\right\}_{j+1}$ and $\left\{\dot{Q}\right\}_{j+1}$ can be calculated from equations (4.36) and (4.37).

From reference [40], the Newmark-β method is unconditionally stable provided:

$$\beta_1 \geq \frac{1}{2} \text{ and } \beta_2 \geq \frac{1}{4}\left(\beta_1 + \frac{1}{2}\right)^2 . \tag{4.39}$$

It is recommended in reference [36] to take $\beta_1 = 0.6$ and $\beta_2 = 0.3025$. A commonly used time step is $\Delta t = T_n / 10$ [36], where T_n is the natural period of the nth mode. In this thesis, $\Delta t = 0.02$ s ($< T_2 / 10$ for the analyzed poles) is used because the lowest two frequency modes dominate a pole's deflection. (See Section 4.11.)

The initial conditions corresponding to the displacements, velocities and loads at time $t_0 = 0$ should be known to begin the numerical integration procedure. From equation (4.28):

$$\left\{\ddot{Q}\right\}_0 = [M]^{-1}\left(\{P\}_0 - [K]\{Q\}_0 - [C]\left\{\dot{Q}\right\}_0\right) . \tag{4.40}$$

If the mass matrix $[M]$ is singular so that its inverse dose not exist, vector $\{\ddot{Q}\}_0$ may be taken as the null vector [36].

4.9 Tapered Poles

The cross-section of a tapered pole considered here varies almost linearly along its centroidal axis. Then A, I_ζ, I_η and J are functions of ξ in formulating the properties of a finite element. Hence, these variables must be included inside the related integrals when the element stiffness and mass matrices are calculated.

4.10 Additional Masses

Only the mass of a pole alone is considered in the previous derivation of the mass matrix. However, there are usually lights or signs mounted on a traffic pole. A light's size is usually small in comparison with that of a pole observed on streets. Therefore, these lights are considered as lumped, point masses that are added at the translational degree of freedom of a coincident node. The mass moments of inertia of the light are neglected because the lights are considered to be points so that their effect on the corresponding rotational degree of freedom is negligible [35].

4.11 Numerical Results

4.11.1 Free Vibrations

Natural frequencies are computed for the pole shown in Figure 4.3 by using the program FREEVIB. Fifteen elements are used to model this light pole, i.e. there is a total of 31 nodes. Figure 4.3 shows the distribution of the nodes and Table 4.1 gives the resulting six lowest natural frequencies, ω_n, for the hexagonal and octagonal cross-sections. It can be seen that the introduction of a 39 *kg* lamp (or about 17% of the mass of the pole alone) not unexpectedly reduces the ω_n. However, the percentage reduction of a particular ω_n is similar, regardless of the cross-sectional shape. (Note that the corresponding natural frequencies for a circular cross-section are given in Appendix D.)

The six lowest frequency mode shapes are shown in Figures 4.17 and 4.18 for the octagonal light pole. The corresponding mode shapes for the hexagonal cross-section are very similar, except that the lowest two mode shapes (corresponding to ω_1 and ω_2) are interchanged if there is no lamp. The modal coupling between the out-of-plane and the in-plane vibrations is small. Typically it is less than six orders of magnitude. When a 39 *kg* lamp is added, the coupling is decreased for the octagonal cross-section but it remains nearly the same for the hexagonal cross-section. In addition, if there is no lamp, more modal coupling exists for the octagonal cross-section than for the hexagonal cross-section, but the opposite is true when the lamp is introduced.

Table 4.1 Lowest natural frequencies, $\omega_n\ (rad/s)$, for the light pole

Mode number	Hexagonal cross-section		Octagonal cross-section	
n	With a lamp	Without a lamp	With a lamp	Without a lamp
1	7.42958 out-of-plane*	11.27796 in-plane	7.48227 out-of-plane	11.68140 out-of-plane
2	7.57063 in-plane	11.44675 out-of-plane	7.74687 in-plane	11.68540 in-plane
3	21.64227 in-plane	40.94778 out-of-plane	22.13030 in-plane	41.84075 out-of-plane
4	25.22781 out-of-plane	41.16205 in-plane	25.67305 out-of-plane	42.66639 in-plane
5	52.25575 in-plane	79.08447 out-of-plane	53.89742 in-plane	80.86093 out-of-plane
6	61.46298 out-of-plane	85.77957 in-plane	62.67030 out-of-plane	88.97935 in-plane

* predominant motion

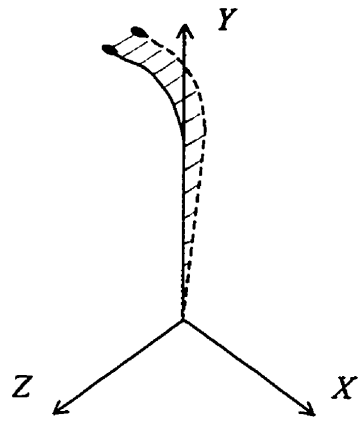

$\omega_1 = 7.48227\ rad / s$ (out-of-plane)

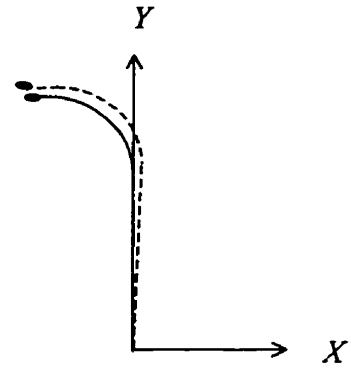

$\omega_2 = 7.74687\ rad / s$ (in-plane)

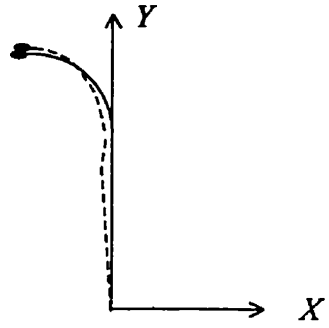

$\omega_3 = 22.13030\ rad / s$ (in-plane)

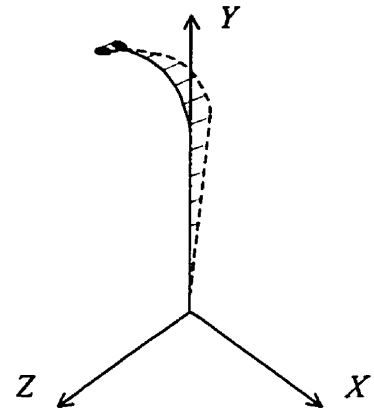

$\omega_4 = 25.67305\ rad / s$ (out-of-plane)

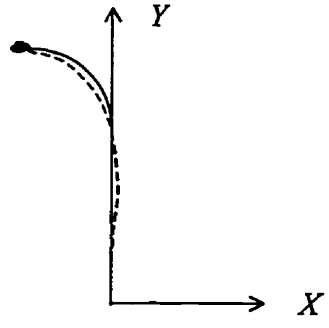

$\omega_5 = 53.89742\ rad / s$ (in-plane)

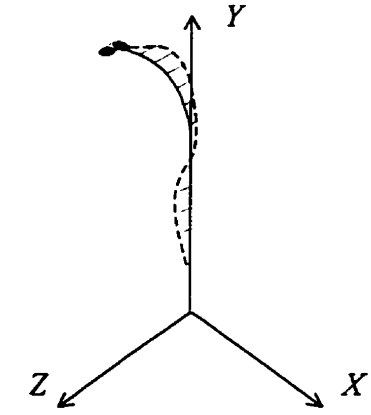

$\omega_6 = 62.67030\ rad / s$ (out-of-plane)

Figure 4.17 The six lowest frequency mode shapes for the octagonal light pole with a lamp.

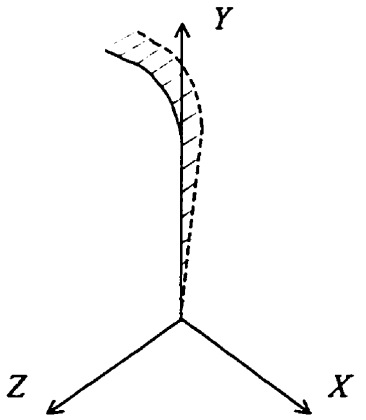

$\omega_1 = 11.68140\ rad / s$ (out-of-plane)

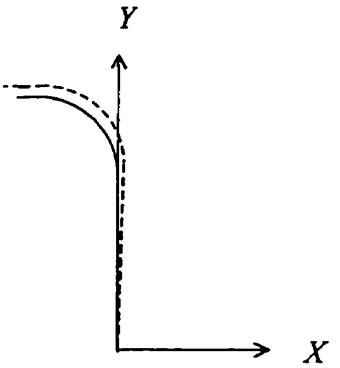

$\omega_2 = 11.68540\ rad / s$ (in-plane)

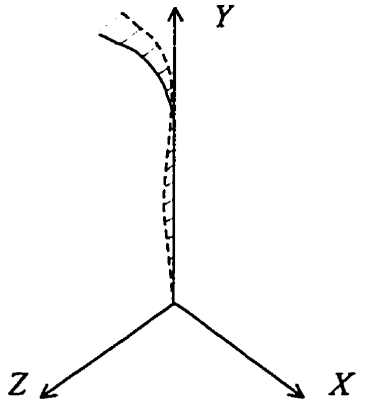

$\omega_3 = 41.84075\ rad / s$ (out-of-plane)

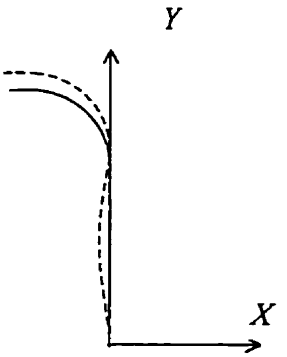

$\omega_4 = 42.66639\ rad / s$ (in-plane)

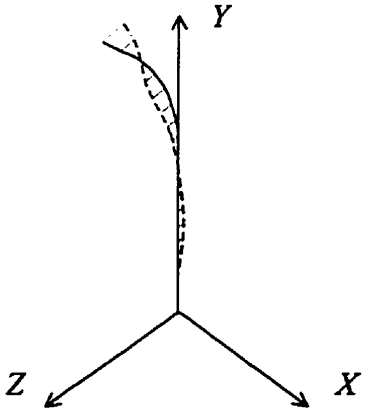

$\omega_5 = 80.86093\ rad / s$ (out-of-plane)

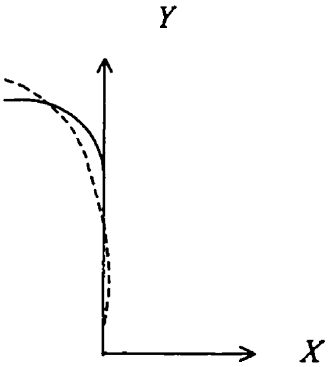

$\omega_6 = 88.97935\ rad / s$ (in-plane)

Figure 4.18 The six lowest frequency mode shapes for the octagonal light pole without a lamp.

4.11.2 Dynamic Responses

Program DYNA is written to compute the dynamic response for wind loads. (The details are given in Appendix C.) Figures 4.19 and 4.20 show the dynamic responses under a steady wind speed of $9\ m/s$. It can be seen from these figures that there are both out-of-plane and in-plane deformations and beating appears. The period of the beating, T_b, is given by [41]:

$$T_b = \frac{2\pi}{\omega_2 - \omega_1}. \tag{4.41}$$

Measurements from the two figures indicate that:

$$T_b \approx 3.7s \quad \omega_1 \approx 7.4\ rad/s \text{ and } \omega_2 \approx 9\ rad/s. \tag{4.42}$$

The above data is compatible with equation (4.41) so that the two lowest frequency mode shapes, one predominantly out-of-plane and the other largely in-plane, dominate the dynamic deflections. A similar beating phenomenon also exists for the dynamic responses under other wind speeds. Then the lowest two natural frequencies are comparable in value and, regardless of the vibrational plane, they are both bending modes. The third and higher mode shapes are invariably involved very little in the dynamic deflection. On the other hand, most of the structural damping is likely to occur at the base of the welded pole, regardless of whether the motion is largely in-plane or out-of-plane. Therefore, it is reasonable to assume $\delta_1 = \delta_2$ and Rayleigh damping.

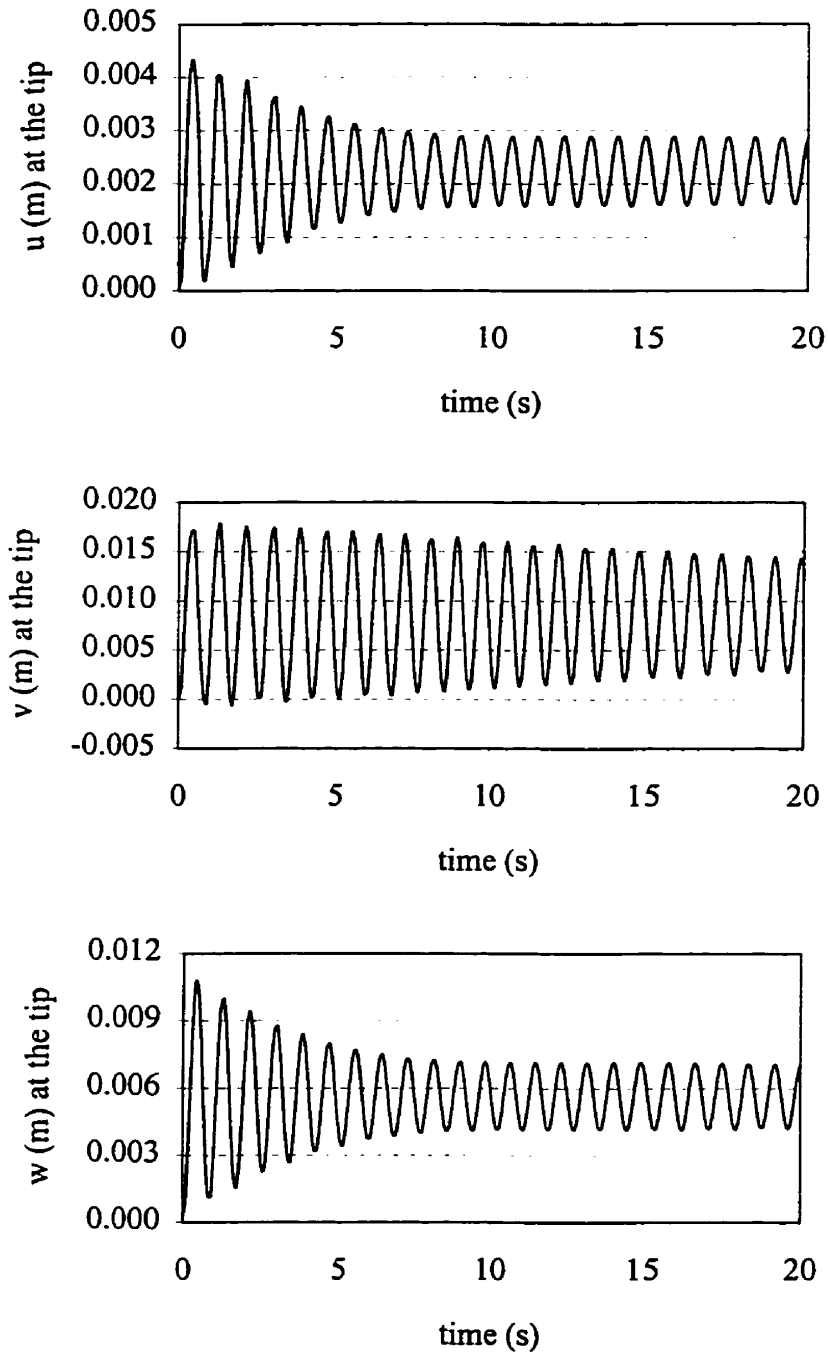

Figure 4.19 Dynamic deflections for the hexagonal light pole with a lamp when $\delta = 0.002$, $\bar{\varepsilon} = 0.5^{\circ}$ and $U_{wind} = 9\ m/s$.

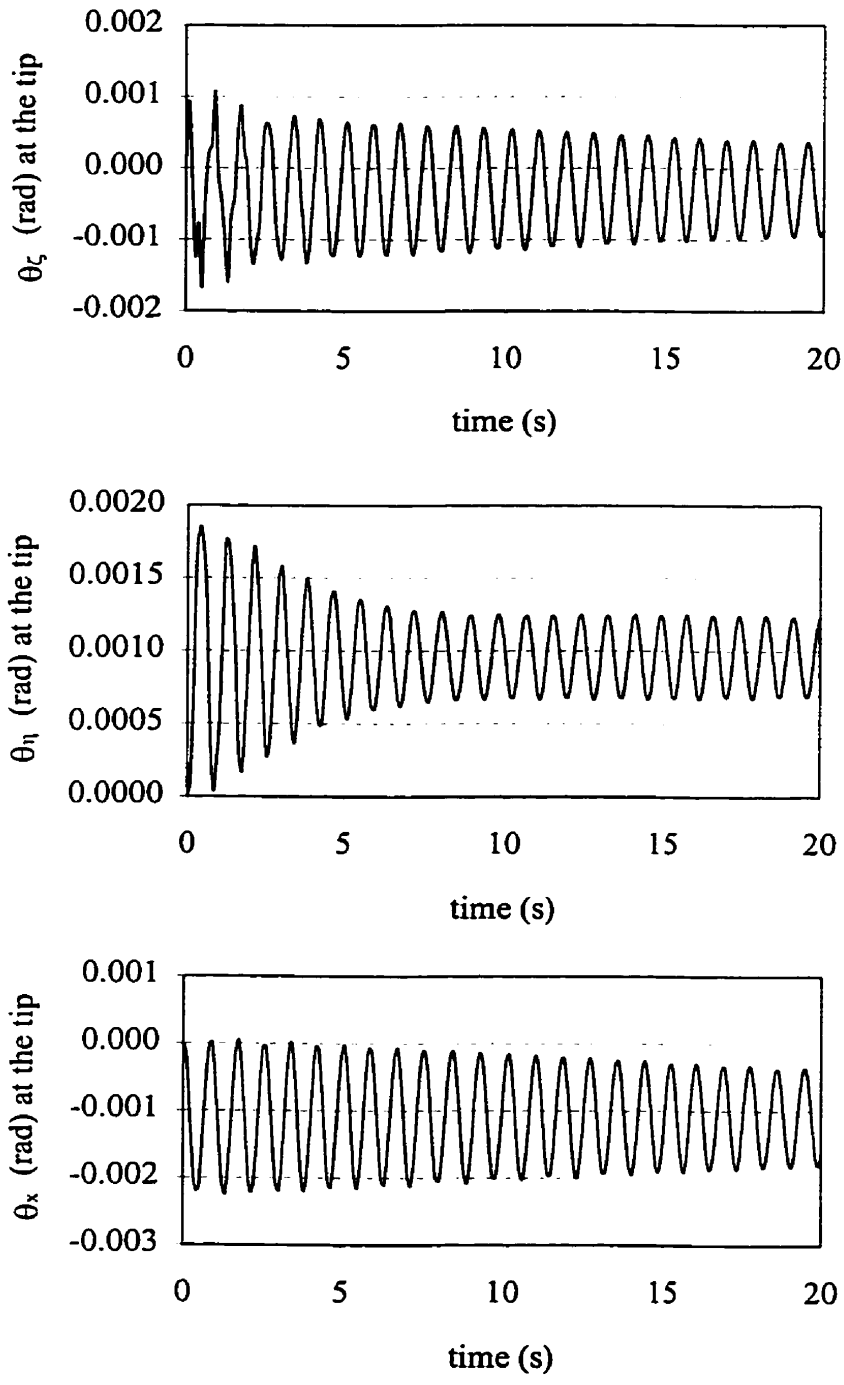

Figure 4.20 Dynamic rotations for the hexagonal light pole with a lamp when $\delta = 0.002$, $\bar{\varepsilon} = 0.5^{\circ}$ and $U_{wind} = 9\ m/s$.

4.11.3 Investigation of Galloping

Whether a light pole is stable or not at a given wind speed, i.e. whether galloping is initiated or not, can be shown computationally. The critical wind speed, U_{crit}, can be found by gradually incrementing the wind speed, U_{wind}, in steps of 0.1 m/s. The procedure is illustrated in Figure 4.21. Convergence of the along wind, temporal deflection, v, at the pole's tip is found, for example, for different values of U_{wind} until U_{wind} reaches 13.5 m/s. From a visual inspection, further increases in U_{wind} make v diverge. Therefore U_{crit} is 13.5 m/s.

Figures 4.22 and 4.23 show the deformation at the critical speed. Figures 4.24 through 4.27 present the displacement histories at the four critical wind speeds. Figures 4.28 and 4.29 show how the critical wind speed changes with structural damping ratio and the wind's direction. The accuracy of the critical wind speed is about ± 0.1 m/s and the dynamic deflections are computed for the first 40 seconds. For the octagonal pole with a lamp, U_{crit} is greater than 20 m/s when $\delta = 0$, $\bar{\varepsilon} = -0.5^{\circ}$. Therefore, this case is not shown in Figure 4.29. The effect of the wind's direction is given in Table 4.2.

Figures 4.24 through 4.27 show that $|w|/|u|$ is about 2.5 at all the four critical wind speeds. This ratio is reasonably consistent with the comparable ratios found in the two lowest frequency modes. Moreover, the correlation between the ratio of v and the approximate average drag force per unit length is consistent with that observed in Example D.2. For example, $v \approx 0.03\,m$ in Figure 4.24 and the average drag force per unit length is about $12\,N/m$ so that the ratio is $0.03/12 = 0.0025\,m^2/N$. In Example

D.2, on the other hand, $v \approx 0.005\,m$ and $F_0 = 2N/m$, which give the same $0.0025\,m^2/N$ ratio. This result also suggests that the displacement in the wind's direction, v, is created mainly by the drag force.

Comparing Figure 4.28 with Figure 4.29, the critical wind speeds are generally seen to be slightly lower for the hexagonal than for the octagonal cross-section. Hence, the octagonal cross-section is somewhat more stable. This observation is intuitively reasonable because a straight circular pole is more stable compared with other cross-sectional shapes and the octagon is closer to a circle than a hexagon. As expected [34], the critical wind speed increases with a larger damping ratio, δ. Furthermore, Table 4.2 indicates that the initiation of galloping is very sensitive to even a small change in the wind's direction from the 90° orientation. When a lamp is added, the critical wind speed usually increases except for the 89° and 89.5° directions in the case of the hexagonal cross-section.

The critical wind speed usually diminishes when the sum of the slope of C_L^* versus $\overline{\alpha}$ plus C_D^* is negative (i.e. $dC_L^*/d\overline{\alpha} + C_D^* < 0$). The trend suggests that the classical Den Hartog criterion [29] (i.e. $dC_L/d\overline{\alpha} + C_D < 0$) can still be used as an indication of the initiation of galloping. However, a hexagonal pole with a lamp is an anomalous case, i.e. the galloping initiation in this case is not completely dependent upon $dC_L^*/d\overline{\alpha} + C_D^*$. This phenomenon may be due to the coupling of the aerodynamic forces and moments. Its clarification requires further investigation.

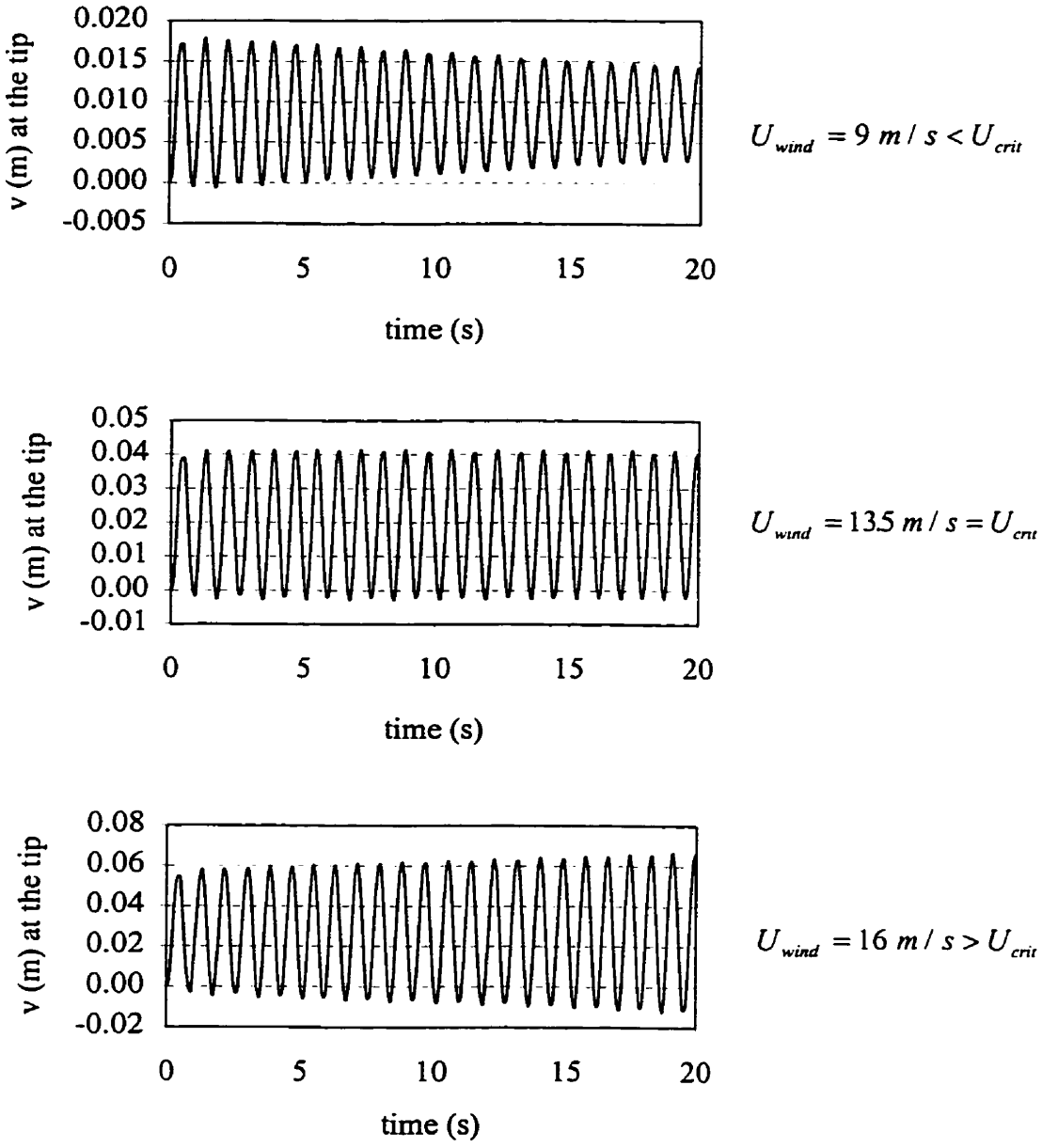

Figure 4.21 Showing the dynamic behavior of different wind speeds for the hexagonal light pole with a lamp when $\delta = 0.002$ and $\bar{\varepsilon} = 0.5°$.

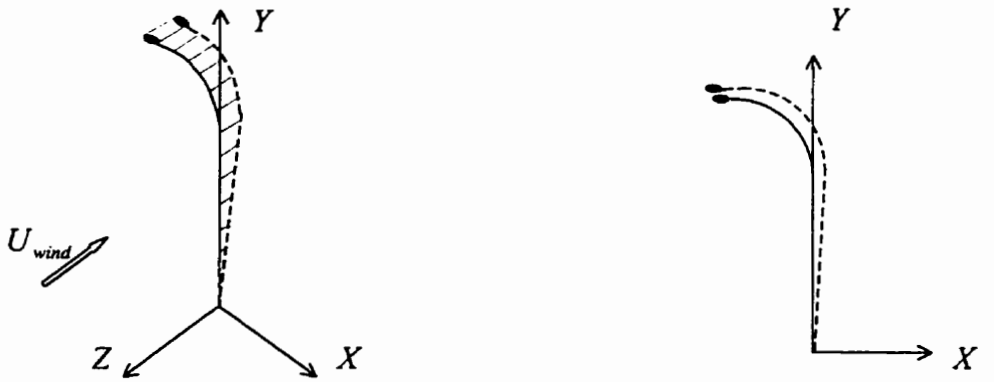

Out-of-plane In-plane

(a) $t = 2s$

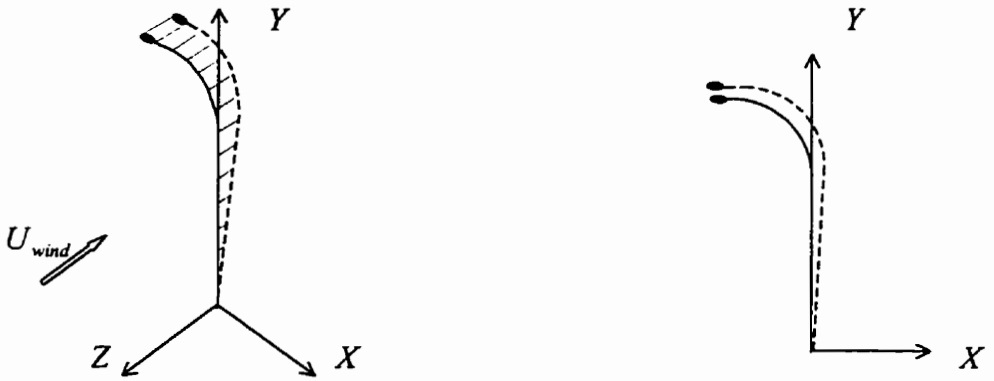

Out-of-plane In-plane

(b) $t = 20s$

Figure 4.22 Deformation history at the critical wind speed of the hexagonal light pole with a lamp when $\delta = 0$, $\bar{\varepsilon} = 0.5^{\circ}$ and $U_{wind} = 11\ m/s$.

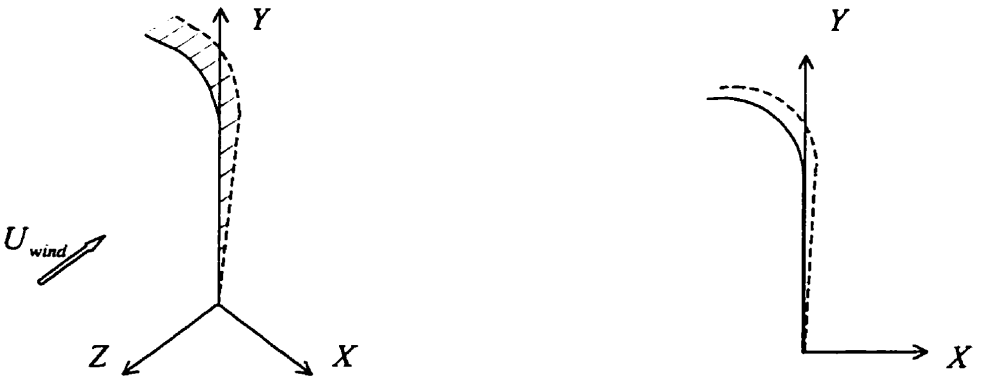

Out-of-plane In-plane

(a) $t = 2s$

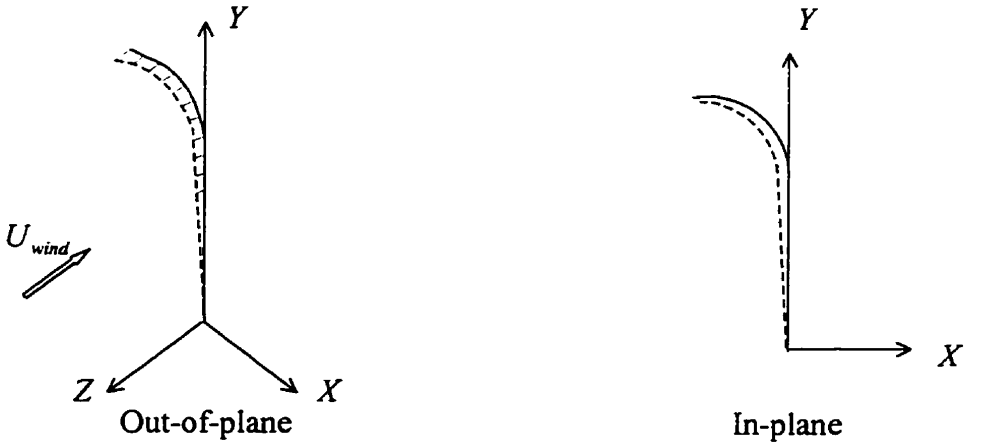

Out-of-plane In-plane

(b) $t = 20s$

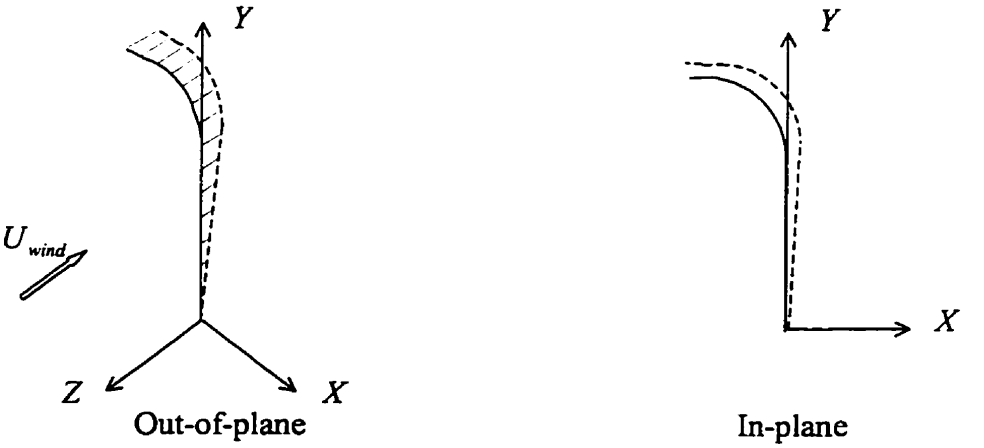

Out-of-plane In-plane

(c) $t = 22s$

Figure 4.23 Deformation history at the critical wind speed of the hexagonal light pole without a lamp when $\delta = 0$, $\bar{\varepsilon} = -0.5^{\circ}$ and $U_{wind} = 8.7\ m/s$.

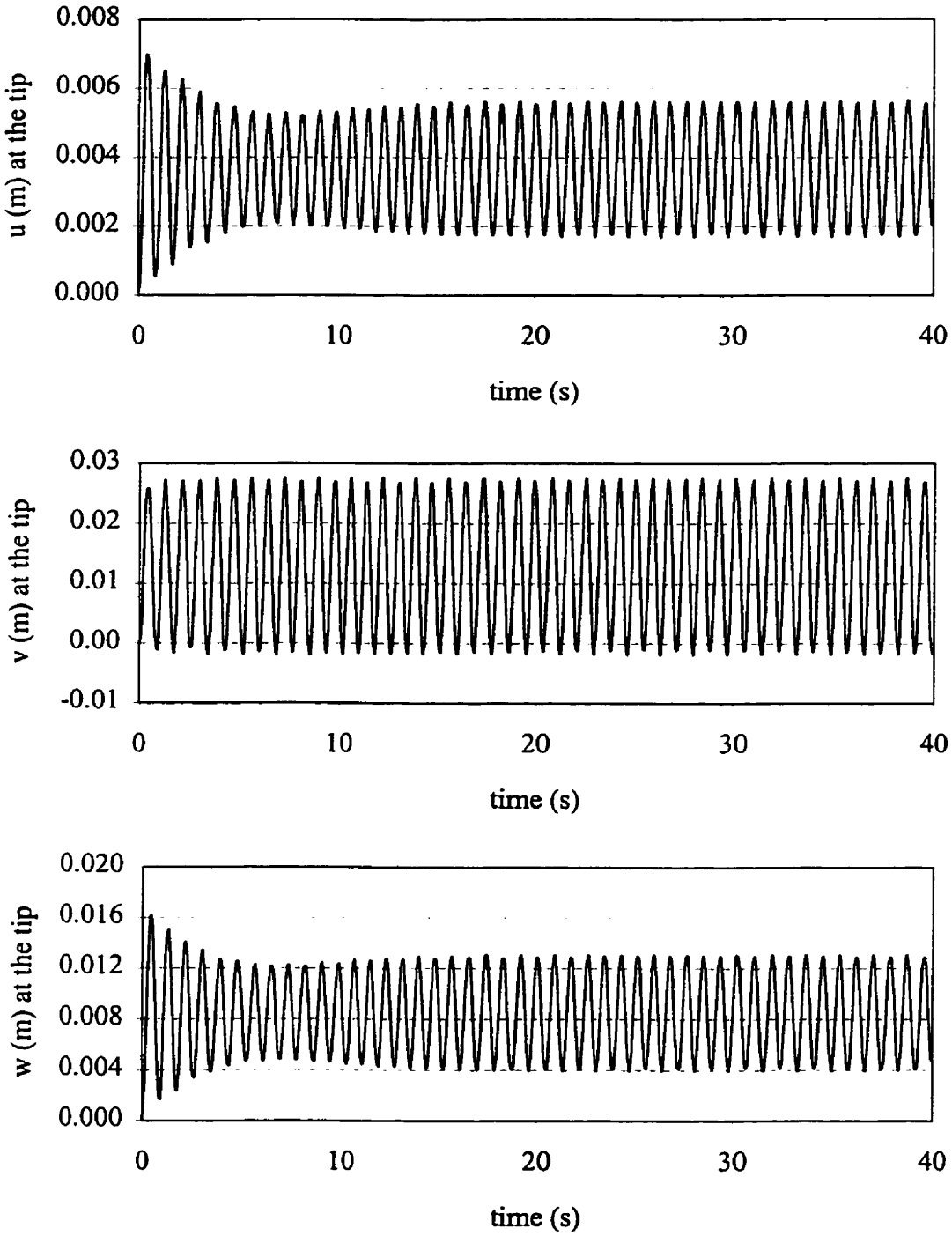

Figure 4.24 Dynamic response of the hexagonal light pole with a lamp when $\delta = 0$, $\bar{\varepsilon} = 0.5^{\circ}$ and $U_{wind} = 11\, m/s$.

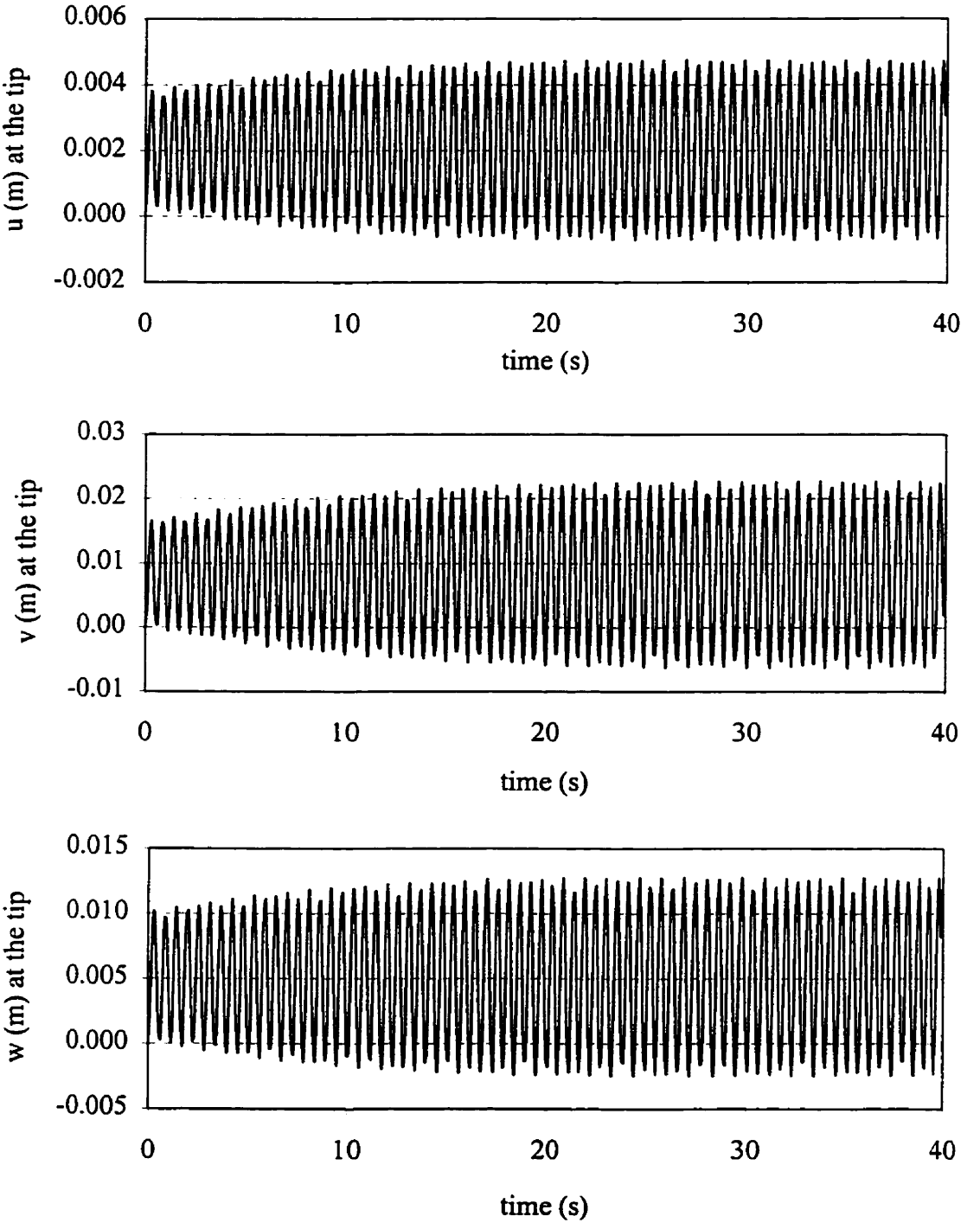

Figure 4.25 Dynamic response of the hexagonal light pole without a lamp when

$$\delta = 0,\ \bar{\varepsilon} = -0.5^{\circ} \text{ and } U_{wind} = 8.7\ m/s\ .$$

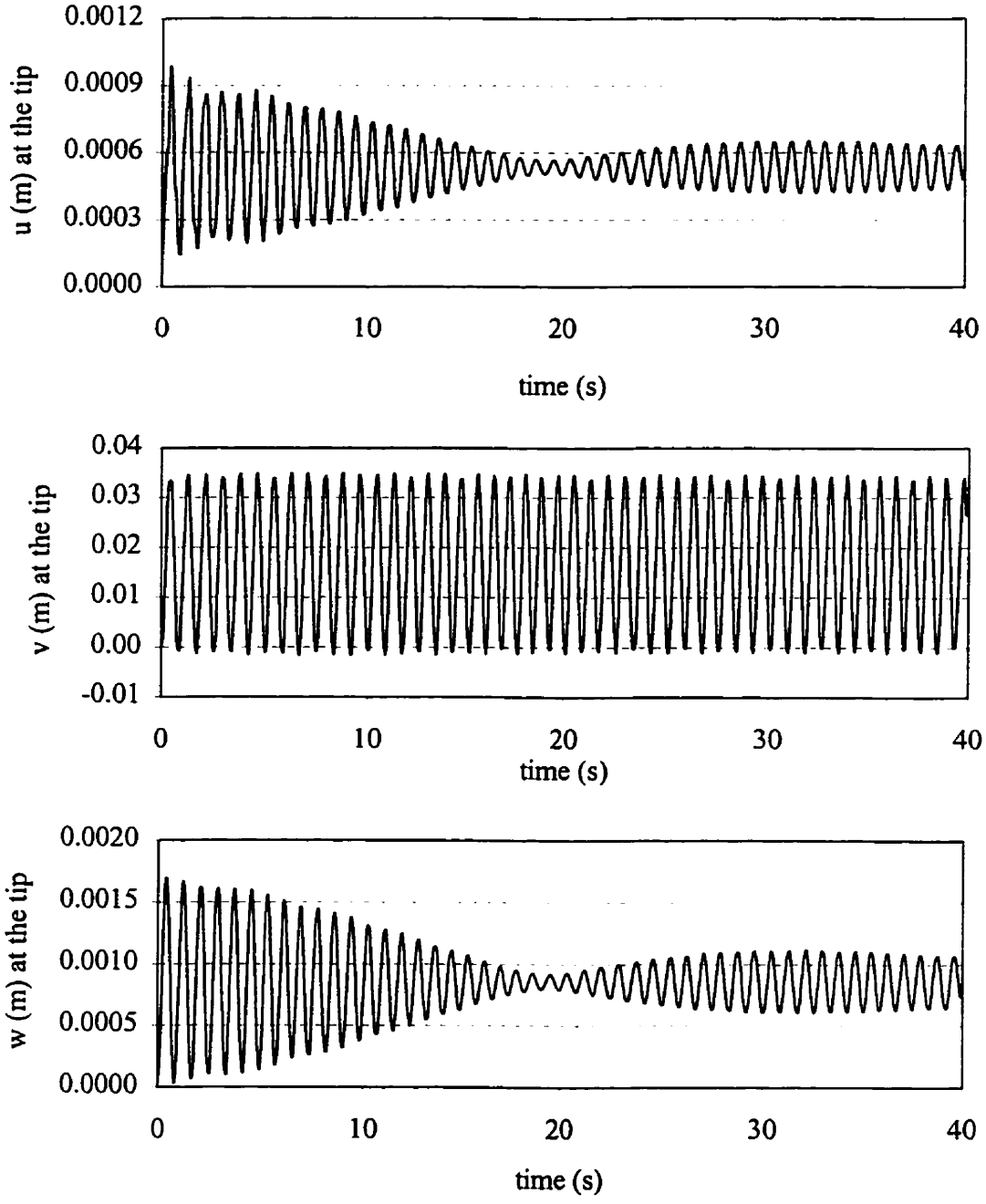

Figure 4.26 Dynamic response of the octagonal light pole with a lamp when $\delta = 0$, $\bar{\varepsilon} = 0.5^{\circ}$ and $U_{wind} = 11\ m/s$.

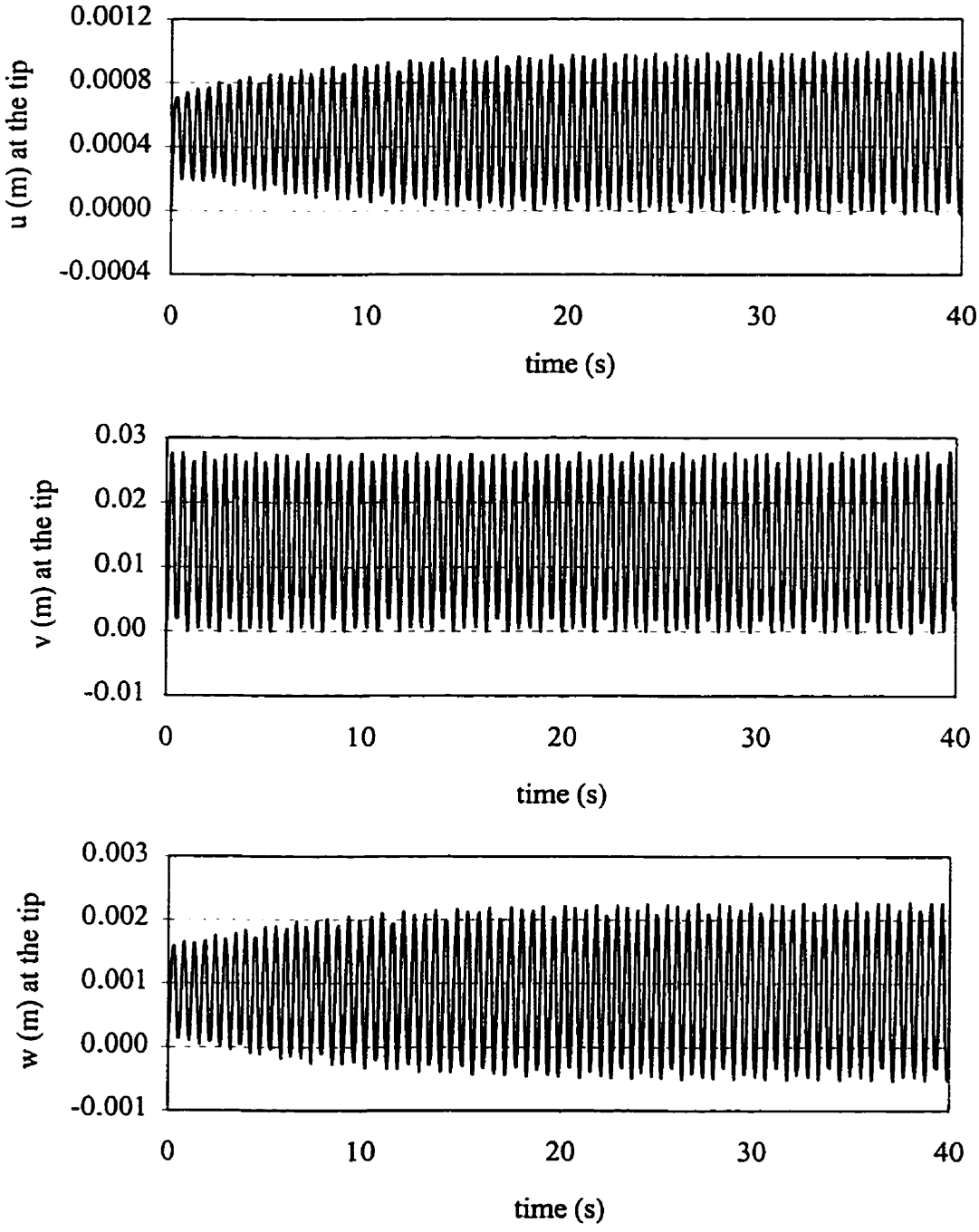

Figure 4.27 Dynamic response of the octagonal light pole without a lamp when $\delta = 0$, $\bar{\varepsilon} = 1^{\circ}$ and $U_{wind} = 10\ m/s$.

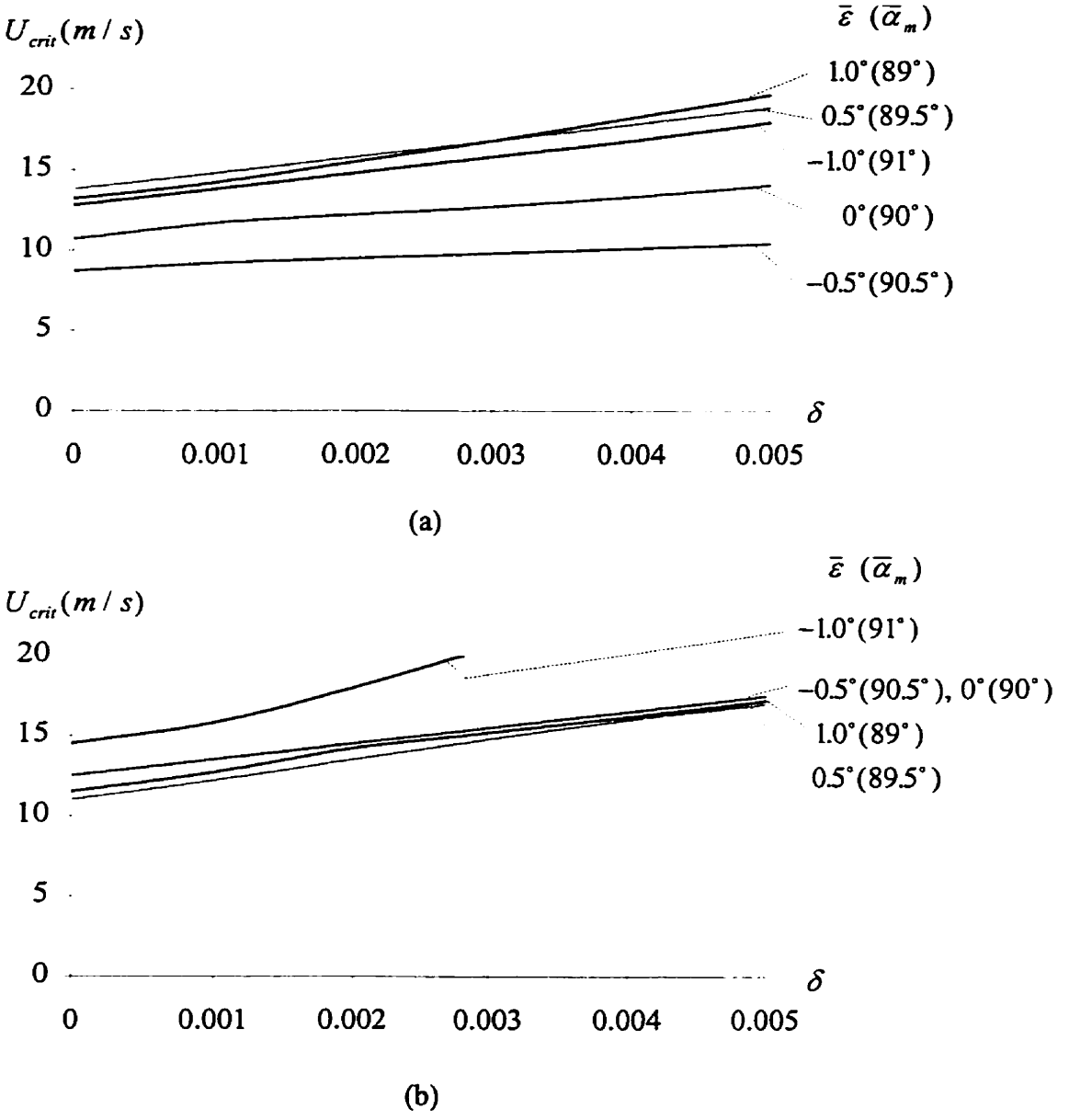

Figure 4.28 Critical wind speeds for a hexagonal light pole having different structural damping ratios, δ, and exposed to various wind directions, $\bar{\varepsilon}$. Showing (a) without a lamp and (b) with a lamp.

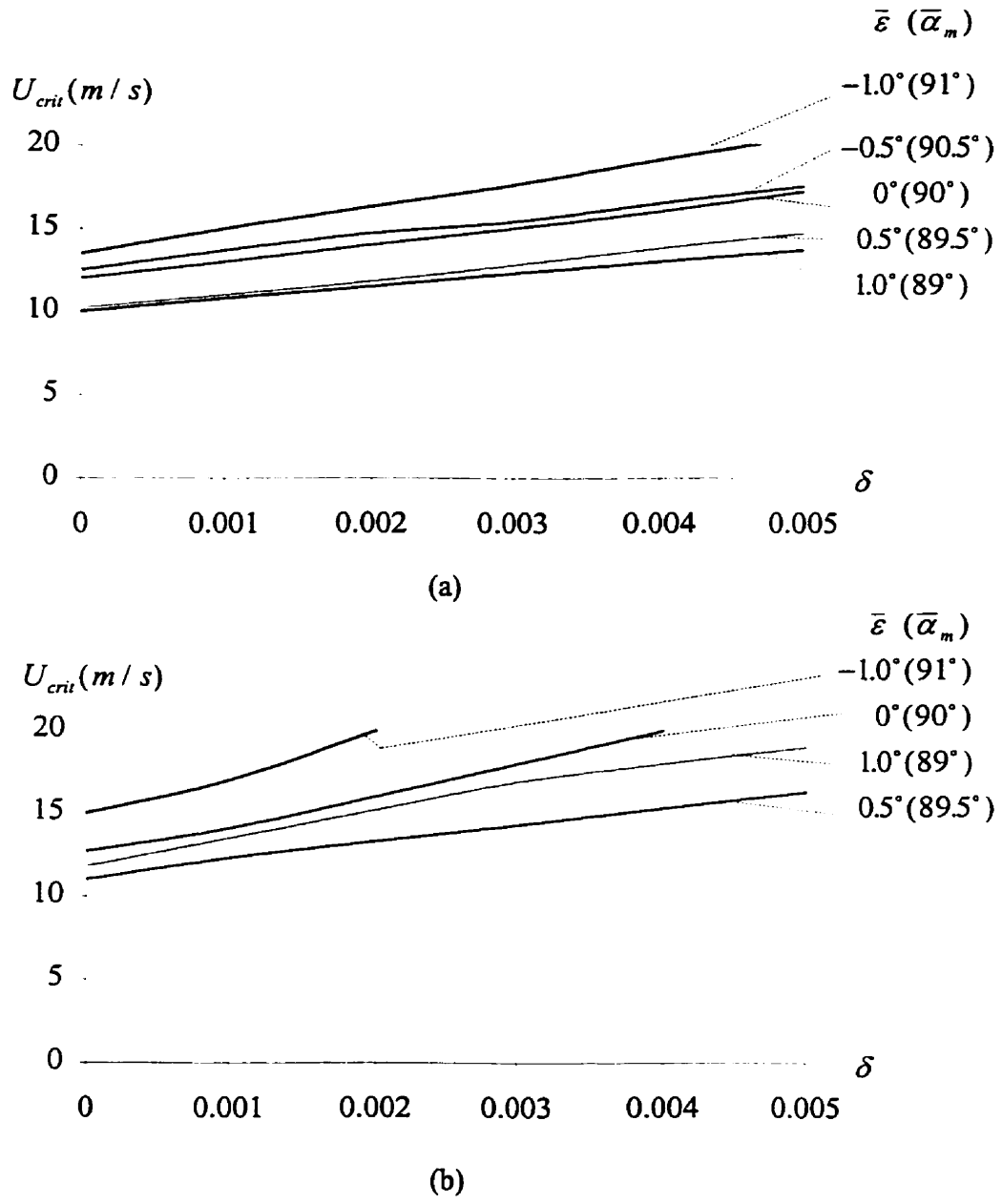

Figure 4.29 Critical wind speeds for an octagonal light pole having different structural damping ratios, δ, and exposed to various wind directions, $\bar{\varepsilon}$. Showing (a) without a lamp and (b) with a lamp.

Table 4.2 The effect of the wind direction for the hexagonal light pole with a lamp when $\delta = 0.002$ and $U_{wind} = 14.5\ m/s$

$\bar{\varepsilon}$ $(\overline{\alpha}_m)$	Stability
$-1.0°(91°)$	Stable
$-0.5°(90.5°)$	Critical
$0°(90°)$	Critical
$0.5°(89.5°)$	Unstable
$1.0°(89°)$	Unstable

4.12 Concluding Remarks

The proposed element is used to investigate the wind induced vibrations of traffic poles. The computational results show that the two lowest frequency modes, one of which is out-of-plane, the other is in-plane, dominate the dynamic deflections. The critical wind speed, which just initiates galloping, is sensitive to the wind's direction and, as expected, it increases with a larger structural damping ratio. These results are consistent with field observations [28]. Indeed, the computed critical wind speeds are in or above the 4.5 to 13.4 m/s range observed in the field [28]. The computed results also show that the critical wind speed usually increases when a lamp is introduced and the octagonal cross-section is somewhat more stable than the hexagonal one.

Chapter 5

Conclusions

5.1 Concluding Remarks

A three-node curved beam element has been developed that includes shear deformation and rotary inertia. Several static and free vibration problems are used to verify that the proposed element, in conjunction with reduced integration, avoids locking. The computed results agree well with exact solutions or results taken from the literature.

Wind induced vibrations of curved traffic poles are analyzed by using the element. Natural frequencies and mode shapes are computed and the formulae are derived for the aerodynamic loads. The method to obtain the aerodynamic coefficients is provided. Time integration is used to obtain the dynamic responses which are shown to be dominated by the two lowest frequency modes. One of these modes is predominantly out-of-plane and the other is in-plane. The critical wind speeds of curved poles having a hexagonal and octagonal cross-section are found for the initiation of galloping. It is shown that the critical wind speed is related to the wind's direction and the structural damping ratio. The octagonal pole is usually more stable than the hexagonal pole. In addition, the computed results suggest that the Den Hartog criterion can be normally used to indicate the initiation of galloping.

Suggestions are given next for future work.

5.2 Recommendations for Future Work

1. Further investigations about the galloping of curved poles could be performed. The coupling effect between the aerodynamic forces and moments on the critical wind speeds could be investigated further. An analytical condition to find the critical wind speed could be pursued. An investigation about the dynamic stability after the initiation of galloping could be undertaken.
2. Experiments to determine the dynamic response of curved poles under wind loads should be carried out to verify the programs and computed results.
3. The time integration of the equations of motion could be refined to reduce the computational effort, such as transforming to the principal coordinate system; using an expeditious method.

References

1. Wen, R. K. and Suhendro, B., Nonlinear curved-beam element for arch structures. *Journal of Structural Engineering, ASCE,* 1991, **117**(11), 3496-3515.
2. Day, R. A. and Potts, D. M., Curved Mindlin beam and axi-symmetric shell elements- a new approach. *International Journal for Numerical Methods in Engineering,* 1990, **30**, 1263-1274.
3. Dasgupta, S. and Sengupta, D., Horizontally curved isoparametric beam element with or without elastic foundation including effect of shear deformation. *Computers and Structures,* 1988, **29**(6), 967-973.
4. Mukhopadhyay, M. and Sheikh, A. H., Large amplitude vibration of horizontally curved beams: a finite element approach. *Journal of Sound and Vibration,* 1995, **180**(2), 239-251.
5. Surana, K. S. and Nguyen, S. H., Completely hierarchical two-dimensional curved beam element for dynamics. *Computers and Structures,* 1991, **40**(4), 957-967.
6. Koziey, B. L. and Mirza, F. A., Consistent curved beam element. *Computers and Structures,* 1994, **51**(6), 643-654.
7. Sengupta, D. and Dasgupta, S., Static and dynamic applications of a five noded horizontally curved beam element with shear deformation. *International Journal for Numerical Methods in Engineering,* 1997, **40**, 1801-1819.

8. Lee, P.-G. and Sin, H.-C., Locking-free curved beam element based on curvature. *International Journal for Numerical Methods in Engineering*, 1994, **37**, 989-1007.

9. Tessler, A. and Spiridigliozzi, L., Curved beam elements with penalty relaxation. *International Journal for Numerical Methods in Engineering*, 1986, **23**, 2245-2262.

10. Babu, C. R. and Prathap, G., A linear thick curved beam element. *International Journal for Numerical Methods in Engineering*, 1986, **23**, 1313-1328.

11. Issa, M. S., Wang, T. M. and Hsiao, B. T., Extensional vibrations of continuous circular curved beams with rotary inertia and shear deformation, I: free vibration. *Journal of Sound and Vibration*, 1987, **114**(2), 297-308.

12. Litewka, P. and Rakowski, J., An efficient curved beam finite element. *International Journal for Numerical Methods in Engineering*, 1997, **40**, 2629-2652.

13. Yang, S.-Y. and Sin, H.-C., Curvature-based beam elements for the analysis of Timoshenko and shear-deformable curved beams. *Journal of Sound and Vibration*, 1995, **187**(4), 569-584.

14. Saleeb, A. F. and Chang, T. Y., On the hybrid-mixed formation of C^0 curved beam elements. *Computer Methods in Applied Mechanics and Engineering*, 1987, **60**, 95-121.

15. Stolarski, H. and Belytschko, T., Shear and membrane locking in curved C^0 elements. *Computer Methods in Applied Mechanics and Engineering*, 1983, **41**, 279-296.

16. Bucalem, M.L. and Bathe, K.J., Locking behavior of isoparametric curved beam finite elements. *Applied Mechanics Review, ASME*, 1995, **48**(11), part 2, S25-S29.

17. Stolarski, H. and Belytschko, T., Membrane locking and reduced integration for curved elements. *Journal of Applied Mechanics,* 1982, **49**, 172-176.

18. Tokarz, F. J. and Sandhu, R. S., Lateral-torsional buckling of parabolic arches. *Journal of the Structural Division, ASCE,* 1972, **98**(ST5), 1161-1179.

19. Yang, Y. B., *Theory and Analysis of Nonlinear Framed Structures,* Prentice-Hall, 1994.

20. Bathe, K. J., *Finite Element Procedures in Engineering Analysis,* Prentice-Hall, 1982.

21. Saada, A. S., *Elasticity: Theory and Applications*, Pergamon Press Inc.,1974.

22. MATH/LIBRARY , *User's manual,* Version 1.0, IMSL Incorporation, 1987.

23. Friedman, I. and Kosmatka, J. B., An improved two-node Timoshenko beam finite element. *Computers and Structures,* 1993, **47**(3), 473-481.

24. Tessler, A. and Dong, S. B., On a hierarchy of conforming Timoshenko beam elements. *Computers and Structures,* 1981, **14**(3-4), 335-344.

25. Dong, S.B. and Wolf, J.A. Jr., Effect of transverse shear deformation on vibrations of planar structures composed of beam-type elements. *Journal of the Acoustical Society of America,* 1973, **53**(1), 120-127.

26. Tan, C. P. and Shore, S., Dynamic response of a horizontally curved bridge. *Journal of Structural Division, ASCE,* 1968, **94**(ST3), 761-781.

27. Kawakami, M., Sakiyama, T., Matsuda, H. and Morita, C., In-plane and out-of-plane free vibrations of curved beams with variable sections. *Journal of Sound and Vibration,* 1995, **187**(3), 381-401.

28. McDonald, J. R., Mehta, K. C., Oler, W. W. and Pulipaka, N., *Wind Load Effects on Signs, Luminaires and Traffic Signal Structures.* Texas Tech University, 1995.

29. Simiu, E. and Scanlan, R. H., *Wind Effects on Structures.* Second Ed., John Wiley and Sons, New York, 1986.

30. Mukhopadhyay, V., Wind excited vibration of a square section cantilever beam in smooth flow. *Journal of Sound and Vibration,* **45,** 329-339, 1976.

31. Chen, C. and Steve, W., Effects of dynamic wind loads on compliant towers, *Proceedings of the International Conference on Offshore Mechanics and Arctic Engineering,* OMAE, 1,143-151, 1994.

32. Allan, L., Generalized model for assessment of vortex-induced vibrations of flexible structures, *Journal of Wind Engineering and Industrial Aerodynamics,* **57,** 281-294, 1995.

33. Augusti, G., Bartoli, G., Borri, C., Gusella, V. and Spinelli, P., Wind load and response of broadcasting antennas, *Proceedings, 8th International Conference on Wind Engineering*, 2077-2088, 1991.

34. Blevins, R. D., *Flow-induced Vibration.* Second Ed.,Van Nostrand Reinhold, New York, 1990.

35. Flather, C. Wayne, *Wind Induced Vibrations of Pole Structures.* M.Sc. thesis, University of Manitoba, 1997.

36. Weaver, Jr., William and Paul R. Johnston, *Structural Dynamics by Finite Elements,* Englewood Cliffs, Prentice-Hall, 1987.

37. Clough, R. W., *Dynamics of Structures,* Second Ed., McGraw-Hill, New York, 1993.

38. Desai, Y. M., *Modelling of Planar Transmission Line Galloping,* Ph.D thesis, University of Manitoba, 1991.

39. Petyt, M. *Introduction to Finite Element Vibration Analysis,* Cambridge University Press, 1990.

40. K-J. Bathe and E.L. Wilson, *Numerical Methods in Finite Element Analysis,* Englewood Cliffs: Prentice-Hall, 1976.

41. Rao, S. S., *Mechanical Vibrations,* Addison-Wesley Publishing Company, 1986.

42. James, M. L., Smith, G. M., Wolford, J. C. and Whaley, P. W., *Vibration of Mechanical and Structural Systems with Microcomputer Applications,* Harper Collins, 1993.

43. Craig, R. Jr., *Structural Dynamics, An Introduction to Computer Methods,* John Wiley and Sons, New York, 1981.

Appendix A

Calculation of an Element's Radius of Curvature, R

Assume that the coordinates of the nodes 1, 2 and 3, with respect to the global coordinate system, are (X_1, Y_1), (X_2, Y_2), (X_3, Y_3), respectively. Node 2 is not necessarily at the element's center. See, for example, Figure A.1. For convenience, let

$$\bar{X} = X - X_1 \qquad \bar{Y} = Y - Y_1 \tag{A.1a}$$

then

$$\begin{aligned} \bar{X}_1 &= X_1 - X_1 = 0 & \bar{Y}_1 &= 0 \\ \bar{X}_2 &= X_2 - X_1 & \bar{Y}_2 &= Y_2 - Y_1 \\ \bar{X}_3 &= X_3 - X_1 & \bar{Y}_3 &= Y_3 - Y_1 . \end{aligned} \tag{A.1b}$$

To obtain the curvature of an element, use a sector of a circle to approximate the curve, i.e. assume that nodes 1, 2 and 3 are on a circle whose equation is:

$$\left(\bar{X} - \bar{a}\right)^2 + \left(\bar{Y} - \bar{b}\right)^2 = R^2 . \tag{A.2}$$

Constants $\bar{a}, \bar{b}$ and R can be determined from the following algebraic equations:

$$\begin{aligned} \left(\bar{X}_1 - \bar{a}\right)^2 + \left(\bar{Y}_1 - \bar{b}\right)^2 &= R^2 \\ \left(\bar{X}_2 - \bar{a}\right)^2 + \left(\bar{Y}_2 - \bar{b}\right)^2 &= R^2 \\ \left(\bar{X}_3 - \bar{a}\right)^2 + \left(\bar{Y}_3 - \bar{b}\right)^2 &= R^2 . \end{aligned} \tag{A.3}$$

By straightforwardly solving these equations, it can be shown that:

$$\bar{a} = \frac{-\bar{Y}_3 \bar{X}_2^{\,2} + \bar{Y}_2 \bar{X}_3^{\,2} - \bar{Y}_2^{\,2} \bar{Y}_3 + \bar{Y}_3^{\,2} \bar{Y}_2}{2(\bar{Y}_2 \bar{X}_3 - \bar{Y}_3 \bar{X}_2)} \tag{A.4a}$$

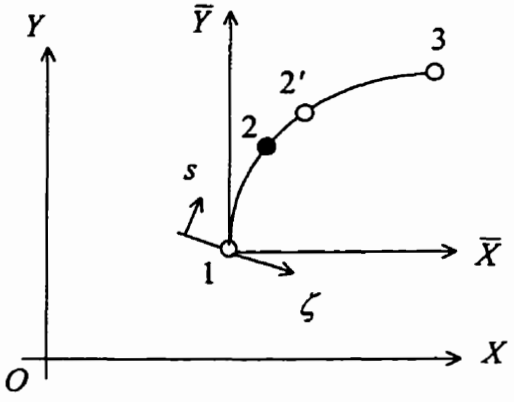

Figure A.1 Coordinate systems.

and

$$\bar{b} = \frac{\bar{X}_3\bar{X}_2^{\,2} - \bar{X}_2\bar{X}_3^{\,2} + \bar{Y}_2^{\,2}\bar{X}_3 - \bar{Y}_3^{\,2}\bar{X}_2}{2(\bar{Y}_2\bar{X}_3 - \bar{Y}_3\bar{X}_2)} \quad . \tag{A.4b}$$

R can be found by substituting equations (A.4a) and (A.4b) into:

$$R = \sqrt{\bar{a}^2 + \bar{b}^2} \quad . \tag{A.4c}$$

To simplify the computations when the given node 2 is not at the center of the element, which is shown as 2′ in Figure A.1, use 2′ to do the static or dynamic calculations. Then interpolate the results from 1, 2′ and 3 to the original node 2. The calculation of the coordinates ($\bar{X}_{2'}, \bar{Y}_{2'}$) of point 2′ is given next.

Let:

$$\bar{X}' = \bar{X} - \bar{a} \quad \text{and} \quad \bar{Y}' = \bar{Y} - \bar{b} \, . \tag{A.5}$$

From equation (A.2):

$$(\bar{X}')^2 + (\bar{Y}')^2 = R^2 \tag{A.6}$$

and, from equation (A.5),

$$\begin{cases} \bar{X}_i' = \bar{X}_i - \bar{a} \\ \bar{Y}_i' = \bar{Y}_i - \bar{b} \end{cases} \qquad (i = 1, 2, 3) \tag{A.7}$$

because $R \neq 0$ so that $\bar{X}'$ and $\bar{Y}'$ cannot be both zero. Subscript i designates a node. For convenience, define the angle from the $\bar{X}'$ axis to the ith node as θ_i. (Figure A.2, for example, illustrates the situation when θ_i corresponds to θ_2.) Then

$$tg\theta_i = \frac{\bar{Y}_i'}{\bar{X}_i'} \qquad (i = 1, 2, 3). \tag{A.8}$$

θ_i can be obtained from $\bar{X}_i'$ and $\bar{Y}_i'$ in the following way:

$$\bar{X}_i' = 0, \begin{cases} \bar{Y}_i' > 0, \ \theta_i = \pi / 2 \\ \bar{Y}_i' < 0, \ \theta_i = -\pi / 2 \end{cases} \tag{A.9}$$

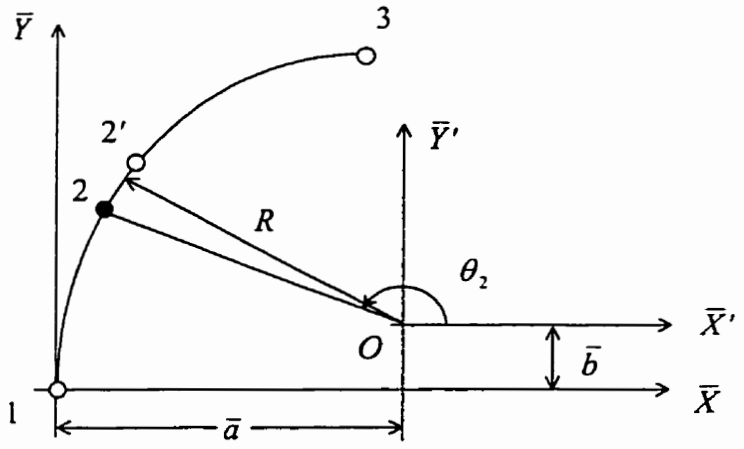

Figure A.2 Coordinate transformation.

and

$$\bar{Y}_i' = 0, \begin{cases} \bar{X}_i' > 0, & \theta_i = 0 \\ \bar{X}_i' < 0, & \theta_i = \pi \end{cases}. \tag{A.10}$$

For $\bar{X}_i' \neq 0$ and $\bar{Y}_i' \neq 0$, let

$$\bar{\theta}_i = arctg\left|\frac{\bar{Y}_i'}{\bar{X}_i'}\right| \tag{A.11}$$

so that

$$\bar{X}_i' > 0, \begin{cases} \bar{Y}_i' > 0, & \theta_i = \bar{\theta}_i \\ \bar{Y}_i' < 0, & \theta_i = -\bar{\theta}_i \end{cases} \tag{A.12}$$

and

$$\bar{X}_i' < 0, \begin{cases} \bar{Y}_i' > 0, & \theta_i = \pi - \bar{\theta}_i \\ \bar{Y}_i' < 0, & \theta_i = \pi + \bar{\theta}_i \end{cases}. \tag{A.13}$$

θ_1 and θ_3 can be found from $(\bar{X}_1', \bar{Y}_1')$ and $(\bar{X}_3', \bar{Y}_3')$. Then, at point 2',

$$\theta_{2'} = \frac{\theta_1 + \theta_3}{2} \qquad \bar{X}_{2'}' = R\cos\theta_{2'} \quad \text{and} \quad \bar{Y}_{2'}' = R\sin\theta_{2'}$$

so that

$$\begin{aligned} \bar{X}_{2'} &= \bar{X}_{2'}' + \bar{a} = R\cos\theta_{2'} + \bar{a} \\ \bar{Y}_{2'} &= \bar{Y}_{2'}' + \bar{b} = R\sin\theta_{2'} + \bar{b} \end{aligned} \tag{A.14a}$$

and

$$\begin{aligned} X_{2'} &= X_1 + \bar{X}_{2'} \\ Y_{2'} &= Y_1 + \bar{Y}_{2'} \end{aligned}. \tag{A.14b}$$

Therefore, the coordinates of point 2' are obtained. Moreover,

$$s_3 \equiv L_e = |\theta_3 - \theta_1| R. \tag{A.15}$$

Furthermore, having found θ_2 from $(\bar{X}_2', \bar{Y}_2')$, then

$$s_2 = |\theta_2 - \theta_1| R \ .$$

As explained in Section 2.2,

$$s = \frac{L_e}{2}(1+\xi)$$

so that, from s_2,

$$\xi_2 = \frac{2s_2}{L_e} - 1 \ . \tag{A.16}$$

Therefore, the displacements at the original node 2 can be obtained from the above ξ_2 by using equation (2.1) in the main text. The following diagram gives the flowchart which is based upon the above methodology.

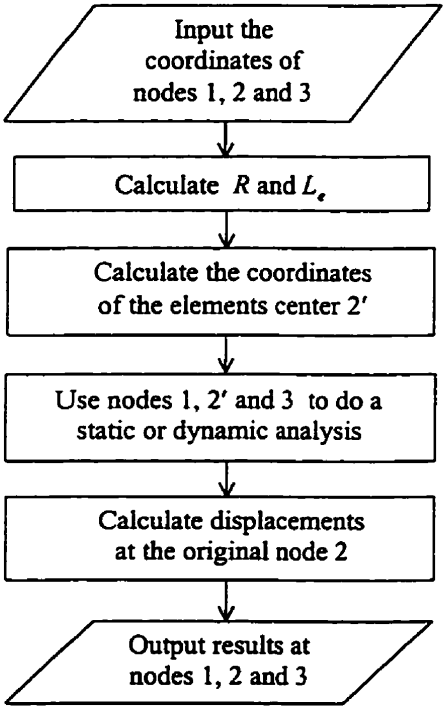

Figure A.3 Flowchart

Appendix B

Details of $[B]_\varepsilon, [B]_{\gamma\zeta}, [B]_{\gamma\eta}, [B]_t$ and $[m]$

B.1 General Formulae

Details are given here of the curved element's mass and stiffness matrices whose development is outlined in Chapter 2. The element's strain matrices are:

$$[B]_\varepsilon = [B_{\varepsilon 1}\ B_{\varepsilon 2}\ B_{\varepsilon 3}] \tag{B.1}$$

where

$$[B]_{\varepsilon i} = \left[\frac{-N_i}{R} \quad \frac{2}{L_e}\eta N'_{i\xi} \quad 0 \quad \frac{-2}{L_e}\zeta N'_{i\xi} \quad \frac{2}{L_e}N'_{i\xi} \quad \eta\frac{N_i}{R}\right] \quad \text{for } i = 1, 2, 3$$

and a prime superscript denotes differentiation with respect to ξ. On the other hand,

$$[B]_{\gamma\zeta} = [B_{\gamma\zeta 1}\ B_{\gamma\zeta 2}\ B_{\gamma\zeta 3}] \tag{B.2}$$

and

$$[B]_{\gamma\zeta i} = \left[\frac{2}{L_e}N'_{i\zeta} \quad 0 \quad 0 \quad -N_i \quad \frac{N_i}{R} \quad 0\right] \quad \text{for } i = 1, 2, 3.$$

Furthermore

$$[B]_{\gamma\eta} = [B_{\gamma\eta 1}\ B_{\gamma\eta 2}\ B_{\gamma\eta 3}] \tag{B.3}$$

in which

$$[B]_{\gamma\eta i} = \left[0 \quad N_i \quad \frac{2}{L_e}N'_{i\xi} \quad 0 \quad 0 \quad 0\right] \qquad \text{for } i = 1, 2, 3.$$

and

$$[B]_t = [B_{t1}\ B_{t2}\ B_{t3}] \tag{B.4}$$

where

$$[B]_{ti} = \begin{bmatrix} 0 & \dfrac{-N_i}{R} & 0 & 0 & 0 & \dfrac{2}{L_e} N'_{i\xi} \end{bmatrix} \qquad \text{for } i = 1, 2, 3.$$

Next, u, v and w can be written in the form:

$$u = [N_u]\{q\} \tag{B.5a}$$

where

$$[N_u] = [N_{u1}\ N_{u2}\ N_{u3}] \tag{B.5b}$$

$$[N_{ui}] = [N_i\ 0\ 0\ 0\ 0\ 0] \qquad \text{for } i = 1, 2, 3. \tag{B.5c}$$

Furthermore,

$$v = [N_v]\{q\} \tag{B.6a}$$

where

$$[N_v] = [N_{v1}\ N_{v2}\ N_{v3}] \tag{B.6b}$$

$$[N_{vi}] = [0\ 0\ N_i\ 0\ 0\ 0] \qquad \text{for } i = 1, 2, 3. \tag{B.6c}$$

and

$$w = [N_w]\{q\} \tag{B.7a}$$

where

$$[N_w] = [N_{w1}\ N_{w2}\ N_{w3}] \tag{B.7b}$$

and

$$[N_{wi}] = [0 \;\; 0 \;\; 0 \;\; 0 \;\; N_i \;\; 0] \qquad \text{for} \;\; i = 1, 2, 3. \tag{B.7c}$$

Similarly,

$$\theta_{\zeta} = [N_{\theta_{\zeta}}]\{q\} \tag{B.8a}$$

where

$$[N_{\theta_{\zeta}}] = [N_{\theta_{\zeta}1} \; N_{\theta_{\zeta}2} \; N_{\theta_{\zeta}3}] \tag{B.8b}$$

and

$$[N_{\theta_{\zeta}i}] = [0 \;\; N_i \; 0 \;\; 0 \;\; 0 \;\; 0] \qquad \text{for} \;\; i = 1, 2, 3. \tag{B.8c}$$

Moreover,

$$\theta_{\eta} = [N_{\theta_{\eta}}]\{q\} \tag{B.9a}$$

where

$$[N_{\theta_{\eta}}] = [N_{\theta_{\eta}1} \; N_{\theta_{\eta}2} \; N_{\theta_{\eta}3}] \tag{B.9b}$$

$$[N_{\theta_{\eta}i}] = [0 \;\; 0 \;\; 0 \;\; N_i \; 0 \;\; 0] \qquad \text{for} \;\; i = 1, 2, 3 \tag{B.9c}$$

and

$$\theta_{x} = [N_{\theta_{x}}]\{q\} \tag{B.10a}$$

whilst

$$[N_{\theta_{x}}] = [N_{\theta_{x}1} \; N_{\theta_{x}2} \; N_{\theta_{x}3}] \tag{B.10b}$$

and

$$[N_{\theta_{x}i}] = [0 \;\; 0 \;\; 0 \;\; 0 \;\; 0 \;\; N_i] \qquad \text{for} \;\; i = 1, 2, 3. \tag{B.10c}$$

Then

$$\dot{u} = [N_u]\{\dot{q}\} = \{\dot{q}\}^T[N_u]^T \qquad \dot{v} = [N_v]\{\dot{q}\} = \{\dot{q}\}^T[N_v]^T$$

$$\dot{w} = [N_w]\{\dot{q}\} = \{\dot{q}\}^T[N_w]^T \qquad \dot{\theta}_\zeta = \left[N_{\theta_\zeta}\right]\{\dot{q}\} = \{\dot{q}\}^T\left[N_{\theta_\zeta}\right]^T$$

$$\dot{\theta}_\eta = \left[N_{\theta_\eta}\right]\{\dot{q}\} = \{\dot{q}\}^T\left[N_{\theta_\eta}\right]^T \qquad \dot{\theta}_x = \left[N_{\theta_x}\right]\{\dot{q}\} = \{\dot{q}\}^T\left[N_{\theta_x}\right]^T.$$

Now

$$\begin{aligned} T_{\mathrm{I}} &= \frac{1}{2}\int_{L_e} \rho A\left[(\dot{u})^2 + (\dot{v})^2 + (\dot{w})^2\right] ds \\ &= \frac{1}{2}\int_{L_e} \rho A\left(\{\dot{q}\}^T[N_u]^T[N_u]\{\dot{q}\} + \{\dot{q}\}^T[N_v]^T[N_v]\{\dot{q}\} + \{\dot{q}\}^T[N_w]^T[N_w]\{\dot{q}\}\right) ds \\ &= \frac{1}{2}\{\dot{q}\}^T[m]_{\mathrm{I}}\{\dot{q}\} \end{aligned}$$

where

$$[m]_{\mathrm{I}} = \int_{L_e} \rho A\left([N_u]^T[N_u] + [N_v]^T[N_v] + [N_w]^T[N_w]\right) ds \tag{B.11a}$$

and

$$m_{\mathrm{I}ij} = \int_{L_e} \rho A\left(N_{ui}N_{uj} + N_{vi}N_{vj} + N_{wi}N_{wj}\right) ds \qquad i, j = 1, 2, \cdots 18. \tag{B.11b}$$

Similarly,

$$T_{\mathrm{II}} = \frac{1}{2}\int_{L_e} \rho\left[I_\eta\left(\dot{\theta}_\eta\right)^2 + I_\zeta\left(\dot{\theta}_\zeta\right)^2\right] ds = \frac{1}{2}\{\dot{q}\}^T[m]_{\mathrm{II}}\{\dot{q}\}$$

where

$$[m]_{\mathrm{II}} = \int_{L_e} \rho\left(I_\eta\left[N_{\theta_\eta}\right]^T\left[N_{\theta_\eta}\right] + I_\zeta\left[N_{\theta_\zeta}\right]^T\left[N_{\theta_\zeta}\right]\right) ds \tag{B.12a}$$

and

$$m_{\text{III}ij} = \int_{L_e} \rho\left(I_\eta N_{\theta_\eta i} N_{\theta_\eta j} + I_\zeta N_{\theta_\zeta i} N_{\theta_\zeta j}\right) ds \qquad i, j = 1, 2, \cdots 18 . \tag{B.12b}$$

Next,

$$\frac{d\phi_t}{ds} = \frac{d\theta_x}{ds} - \frac{\theta_\zeta}{R}$$

so that

$$\int_0^s d\phi_t = \int_0^s d\theta_x - \int_0^s \frac{\theta_\zeta}{R} ds$$

and

$$\phi_t = \theta_x - \frac{1}{R}\int_0^s \theta_\zeta ds = \theta_x - \frac{L_e}{2R}\int_{-1}^{\xi}\left(N_1\theta_{\zeta 1} + N_2\theta_{\zeta 2} + N_3\theta_{\zeta 3}\right) d\xi = \left[N_{\theta_t}\right]\{q\} + \left[N_\phi\right]\{q\} \tag{B.13}$$

where

$$\left[N_\phi\right] = \left[N_{\phi 1} N_{\phi 2} N_{\phi 3} N_{\phi 4} N_{\phi 5} N_{\phi 6} N_{\phi 7} N_{\phi 8} N_{\phi 9} N_{\phi 10} N_{\phi 11} N_{\phi 12} N_{\phi 13} N_{\phi 14} N_{\phi 15} N_{\phi 16} N_{\phi 17} N_{\phi 18}\right] \tag{B.14a}$$

$$N_{\phi 2} = \frac{-L_e}{4R}\left(-\frac{\xi^2}{2} + \frac{\xi^3}{3} + \frac{5}{6}\right)$$

$$N_{\phi 8} = \frac{-L_e}{2R}\left(\xi - \frac{\xi^3}{3} + \frac{2}{3}\right)$$

$$N_{\phi 14} = \frac{-L_e}{4R}\left(\frac{\xi^2}{2} + \frac{\xi^3}{3} - \frac{1}{6}\right).$$

The remaining

$$N_{\phi i} = 0 \qquad i \neq 2, 8, 14 . \tag{B.14b}$$

Then

$$T_{\text{III}} = \frac{1}{2}\int_{L_e} \rho K_t \left(\dot{\phi}_t\right)^2 ds = \frac{1}{2}\{\dot{q}\}^T [m]_{\text{III}} \{\dot{q}\}$$

where

$$[m]_{\text{III}} = \int_{L_e} \rho K_t \left(\left[N_{\theta_x}\right]^T + \left[N_\phi\right]^T \right) \left(\left[N_{\theta_x}\right] + \left[N_\phi\right] \right) ds \tag{B.15a}$$

and

$$m_{\text{III}ij} = \int_{L_e} \rho K_t \left(N_{\theta_x i} + N_{\phi i}\right)\left(N_{\theta_x j} + N_{\phi j}\right) ds \qquad i, j = 1, 2, \cdots 18 . \tag{B.15b}$$

Finally,

$$[m] = [m]_{\text{I}} + [m]_{\text{II}} + [m]_{\text{III}} . \tag{B.16}$$

B.2 Formulae for a Planar Problem

For a planar problem, the above general formulae reduce to:

$$[B]_\varepsilon = \left[B_{\varepsilon 1}\ B_{\varepsilon 2}\ B_{\varepsilon 3}\right] \tag{B.17}$$

where

$$[B]_{\varepsilon i} = \left[-\frac{N_i}{R} \quad -\frac{2}{L_e}\zeta N'_{i\xi} \quad \frac{2}{L_e} N'_{i\xi} \right] \qquad \text{for } i = 1, 2, 3.$$

and

$$[B]_{\gamma\zeta} = \left[B_{\gamma\zeta 1}\ B_{\gamma\zeta 2}\ B_{\gamma\zeta 3}\right] \tag{B.18}$$

$$\left[B_{\gamma\zeta i}\right] = \left[\frac{2}{L_e} N'_{i\xi} \quad -N_i \quad \frac{N_i}{R} \right] \qquad \text{for } i = 1, 2, 3.$$

Next,

$$\dot{u} = [N_u]\{\dot{q}\}$$

where

$$[N_u] = [N_1\ 0\ 0\ N_2\ 0\ 0\ N_3\ 0\ 0]. \tag{B.19}$$

Also

$$\dot{w} = [N_w]\{\dot{q}\}$$

where

$$[N_w] = [\,0\ \ 0\ \ N_1\ 0\ \ 0\ \ N_2\ 0\ \ 0\ \ N_3] \tag{B.20}$$

and

$$\dot{\theta}_\eta = \left[N_{\theta_\eta}\right]\{\dot{q}\}$$

$$\left[N_{\theta_\eta}\right] = [\,0\ \ N_1\ 0\ 0\ \ N_2\ 0\ 0\ \ N_3\ 0\,]. \tag{B.21}$$

Then

$$[m] = [m]_I + [m]_{II} \tag{B.22}$$

where

$$[m]_1 = \int_{L_e} \rho A\left([N_u]^T[N_u] + [N_w]^T[N_w]\right) ds \tag{B.23a}$$

and

$$\begin{aligned} m_{1ij} &= \int_{L_e} \rho A\left(N_{ui}N_{uj} + N_{wi}N_{wj}\right)ds \\ &= \frac{\rho A L_e}{2}\int_{-1}^{1}\left(N_{ui}N_{uj} + N_{wi}N_{wj}\right)d\xi \qquad i,j = 1, 2, \cdots 9\,. \end{aligned} \tag{B.23b}$$

Moreover

$$[m]_{\text{II}} = \int_{L_e} \rho I_\eta \left[N_{\theta_\eta}\right]^T \left[N_{\theta_\eta}\right] ds \tag{B.24a}$$

and

$$m_{\text{II}ij} = \int_{L_e} \rho I_\eta N_{\theta_\eta i} N_{\theta_\eta j} ds = \frac{\rho I_\eta L_e}{2} \int_{-1}^{1} N_{\theta_\eta i} N_{\theta_\eta j} d\xi \qquad i, j = 1, 2, \cdots 9 \,. \tag{B.24b}$$

Appendix C

Implementation of Computer Programs

The computer program STATIC is used for the static analysis of curved beams. On the other hand, FREEVIB is used to obtain the natural frequencies and mode shapes of a curved beam. DYNA finds the dynamic response. All three programs are written in FORTRAN 77. Figures C.1 through C.3 present the corresponding flowcharts. Then the three programs are given. Subroutines DLSASF (to solve linear equations) and DGVCSP (to solve eigenvalues and eigenvectors) in the International Math and Statistical Library (IMSL) [22] are utilized. These programs are run in the Unix system.

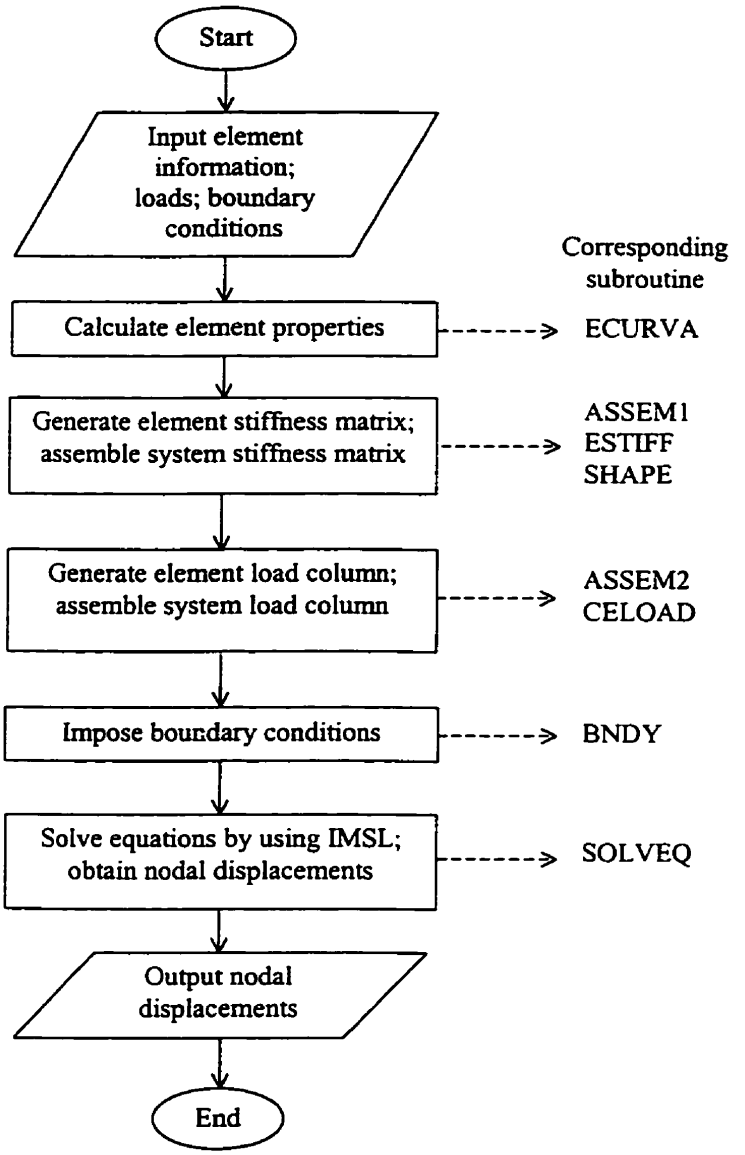

Figure C.1 Flowchart for STATIC.

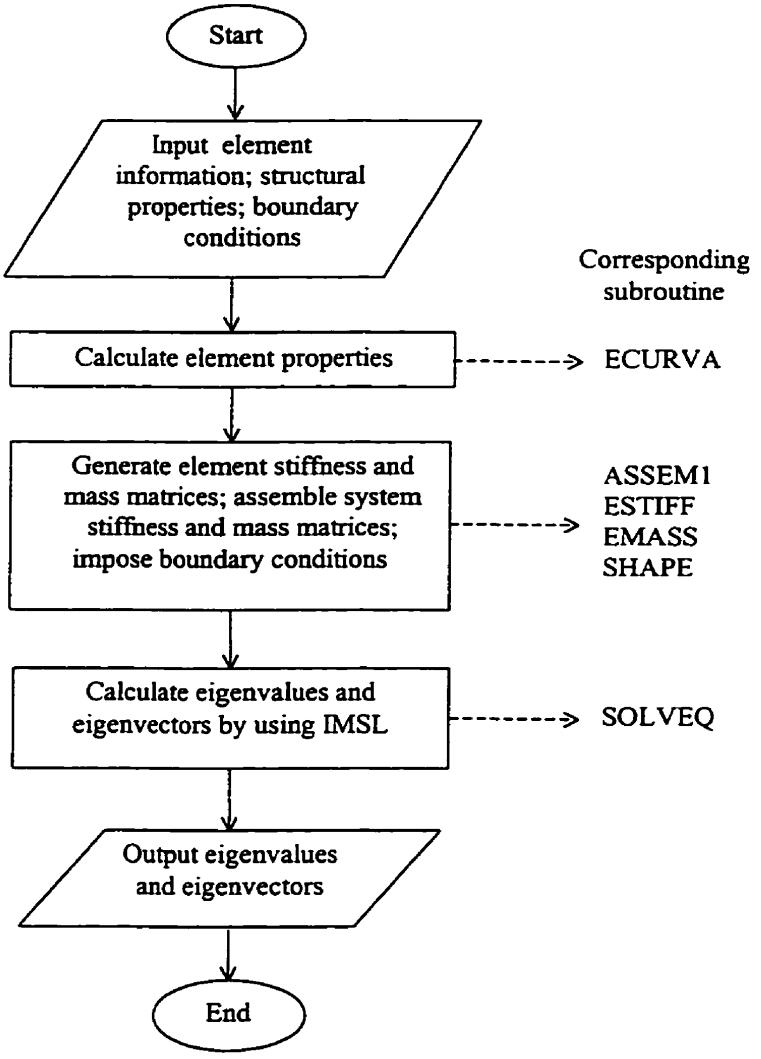

Figure C.2 Flowchart for FREEVIB.

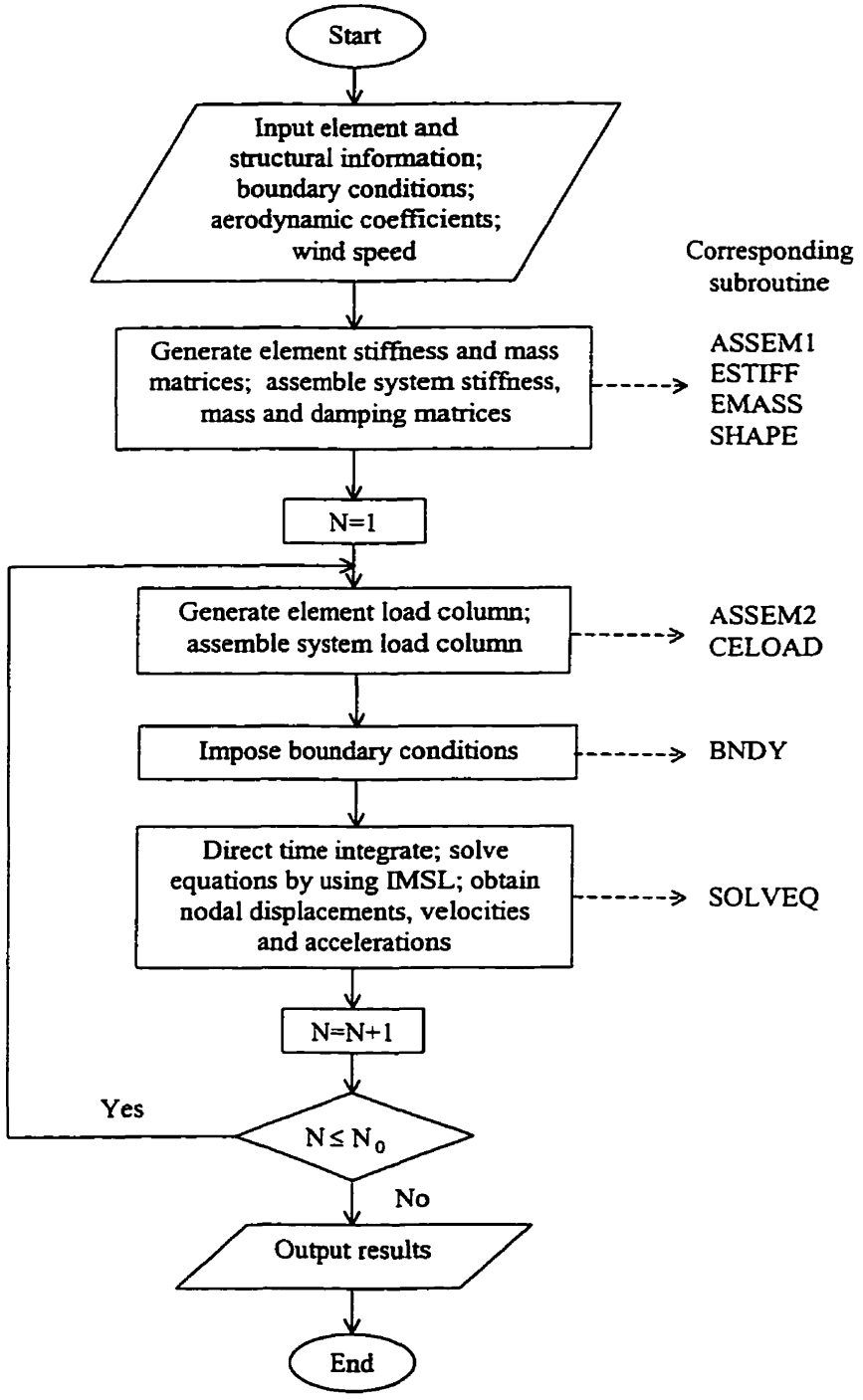

Figure C.3 Flowchart for DYNA.

```
C  ***************************************************************
C  *                                                             *
C  *          Program Name: STATIC                               *
C  *          Description:  static analysis of beams by using    *
C  *                        3-node curved beam element(6-DOF)    *
C  *                        (including shear deformation         *
C  *                          and rotary inertia)                *
C  *                                                             *
C  ***************************************************************
C
C  Definition
C
C        NE----------number of elements
C        NN----------total number of nodes
C        ND----------total number of degrees of freedom
C        NP1~NP3-----the number of Gauss integral points
C        E,G---------modulus of elasticity
C        SK----------shear correction factor
C        ELEN--------beam element length
C        EAREA-------beam element cross-sectional area
C        EIN,
C        EIZ,EIT-----element cross-sectional moments of inertia
C        SSTIFF------system stiffness matrix
C        SLOAD-------system load column
C        SDISP-------system displacement column
C        DISTP(I,J)--uniformly distributed load Pu,Pv and Pw
C                    of ith element
C        EK----------element stiffness matrix
C        X1----------local coordinate
C        CUR(I)------curvature(1/R) of Ith element
C        NOD(I,J)----global node number of Ith element
C        ID(I,J)-----global freedom number corresponding to Ith element
C        IDE---------number of degrees of freedom of each node
C        INOD--------number of nodes of each element
C        NNE=INOD*IDE
C        unknown displacement: input 500.0
C
C     subroutine name                  function
C
C
C       ESTIFF              calculate element stiffness
C
C       CELOAD              calculate element equivalent load
C
C       SHAPE               evaluation of the interpolation function
C                           and the derivatives at the Gauss points
C
C       ASSEM1              assemble system stiffness
C
C       ASSEM2              assemble system load
C
C       BNDY                impose boundary conditions
C
C       SOLVEQ              solve linear equations by using IMSL
```

```
C
C       ECURVA                calculate element curvature etc.
C-----------------------------------------------------------------
C
        COMMON/SDATA/SSTIFF(500,500),SLOAD(500),SDISP(500)
        COMMON/FDATA1/ELEN(50),EAREA(50),EIN(50),EIZ(50),EIT(50),
     &CUR(50),E,G,SK
        COMMON/FDATA2/NE,NN,ND,IDE,INOD,NOD(50,3),ID(50,18)
        COMMON/FDATA3/NP1,NP2,NPB,NPT
        COMMON/FDATA4/X(100),Y(100),XN(100),YN(100)
        COMMON/EDATA/EK(18,18)
        COMMON/SHP/SN(3),DSN(3),SNU(18),SNV(18),SNW(18),SNTHN(18),
     &SNTHZ(18),SNTHX(18),SNF(18)
        DIMENSION DISTP(50,6),TK1(250000),CX2(50),SNN(3)
        IMPLICIT DOUBLE PRECISION (A-H,O-Z)
        OPEN(UNIT=10,FILE='static.dat')
        OPEN(UNIT=20,FILE='static.out')
C
C       read general data and initialize variables
C
        IDE=6
        INOD=3
        WRITE(20,10)
10      FORMAT(1X,'input data')
        NP1=2
        NP2=2
        NPB=3
        NPT=3
        WRITE(20,8) NP1,NP2,NPB,NPT
8       FORMAT(1X,'NP1=',I3,2X,'NP2=',I3,2X,'NPB=',I3,2X,'NPT='I3)
        READ(10,*) NE,NN,E,G,SK,M0
        WRITE(20,20) NE,NN,E,G,SK,M0
20      FORMAT(1X,'NE=',I5,2X,'NN=',I5,2X,'E=',E15.6,2X,'G=',
     &E15.6,2X,'SK=',F10.6,2X,'M0=',I2)
        READ(10,*) (EAREA(I),EIN(I),EIZ(I),EIT(I),I=1,NE)
        WRITE(20,12) (I,EAREA(I),I=1,NE)
12      FORMAT(1X,'I=',I3,2X,'EAREA=',E15.6)
        WRITE(20,13) (I,EIN(I),EIZ(I),EIT(I),I=1,NE)
13      FORMAT(1X,'I=',I3,2X,'EIN=',E14.6,2X,'EIZ=',E14.6,2X,
     &'EIT=',E14.6)
        READ(10,*) ((NOD(I,J),J=1,INOD),I=1,NE)
        WRITE(20,25)
25      FORMAT(1X,'NOD=')
        WRITE(20,*) ((NOD(I,J),J=1,INOD),I=1,NE)
C
        IF(M0.EQ.1) GOTO 11
C
        READ(10,*) (X(I),Y(I),I=1,NN)
        WRITE(20,16) (I,X(I),Y(I),I=1,NN)
16      FORMAT(1X,'NODE',I3,2X,'X=',F10.4,2X,'Y=',F10.4)
C
        CALL ECURVA(CUR,ELEN,CX2)
C
        GOTO 15
```

```
11      READ(10,*) (ELEN(I),I=1,NE)
        READ(10,*) (CUR(I),I=1,NE)
15      WRITE(20,14) (I,ELEN(I),CUR(I),CX2(I),I=1,NE)
14      FORMAT(1X,'I=',I3,2X,'ELEN=',E15.6,2X,'CUR=',E15.6,
     &2X,'CX2=',E15.6)
C
        ND=IDE*NN
C
        READ(10,*) (SDISP(I),I=1,ND)
        WRITE(20,30)
30      FORMAT(1X,'SDISP=')
        WRITE(20,*) (SDISP(I),I=1,ND)
        READ(10,*) (SLOAD(I),I=1,ND)
        WRITE(20,40)
40      FORMAT(1X,'SLOAD=')
        WRITE(20,*) (SLOAD(I),I=1,ND)
        READ(10,*) ((DISTP(I,J),J=1,6),I=1,NE)
        WRITE(20,45)
45      FORMAT(1X,'DISTP=')
        WRITE(20,*) ((DISTP(I,J),J=1,6),I=1,NE)
C
        DO 50 I=1,ND
        DO 60 J=1,ND
60      SSTIFF(I,J)=0.0D0
50      CONTINUE
C
C       generate ID according to NOD
C
        DO 70 I=1,NE
        DO 80 J=1,INOD
        I0=(NOD(I,J)-1)*IDE
        IE0=(J-1)*IDE
        DO 90 II=1,IDE
        ID(I,IE0+II)=I0+II
90      CONTINUE
80      CONTINUE
70      CONTINUE
C
        WRITE(20,85)
85      FORMAT(1X,'ID=')
        WRITE(20,88) ((ID(I,J),J=1,18),I=1,NE)
88      FORMAT(1X,9I5)
C
        CALL ASSEM1
C
        CALL ASSEM2(DISTP,ELEN,SLOAD)
C
        CALL BNDY(ND)
C
         WRITE(20,130)
130     FORMAT(1X,'SLOAD=')
        WRITE(20,*) (SLOAD(I),I=1,ND)
C
        DO 600 J=1,ND
```

```
      DO 600 I=1,ND
600   TK1(ND*(J-1)+I)=SSTIFF(I,J)
C
      CALL SOLVEQ(ND,TK1,SLOAD,SDISP)
C
      IF(M0.EQ.1) GOTO 211
      DO 700 I=2,NN-1,2
      XX1=CX2(I/2)
      SNN(1)=-0.5D0*XX1*(1.0D0-XX1)
      SNN(2)=1.0D0-XX1**2
      SNN(3)=0.5D0*XX1*(1.0D0+XX1)
      DO 710 J=5,0,-1
      SDISP(6*I-J)=SNN(1)*SDISP(6*(I-1)-J)
     &+SNN(2)*SDISP(6*I-J)
     &+SNN(3)*SDISP(6*(I+1)-J)
710   CONTINUE
700   CONTINUE
C
C     print solutions
C
211   WRITE(20,200)
200   FORMAT( )
      WRITE(20,205)
205   FORMAT(1X,'output data')
      WRITE(20,210)
210   FORMAT(1X,'Nodal Displacements:')
      DO 220 I=1,NN
      WRITE(20,300) I
300   FORMAT(1X,'Node',I3)
      WRITE(20,310) SDISP(6*I-5),SDISP(6*I-4),SDISP(6*I-3)
      WRITE(20,320) SDISP(6*I-2),SDISP(6*I-1),SDISP(6*I)
310   FORMAT(1X,'U=',D17.10,2X,'THZ=',D17.10,2X,'V=',D17.10)
320   FORMAT(1X,'THN=',D17.10,2X,'W=',D17.10,2X,'THX=',D17.10)
220   CONTINUE
500   END
C-----------------------------------------------------------------------
      SUBROUTINE ESTIFF(K)
C
C     SN------------------element shape functions N
C     DSN-----------------first derivative of N
C     GAUSS---------------matrix of Gauss points
C     WT------------------Gauss weights corresponding to
C                         the Gauss points
C     B,C,D---------------element matrices needed to calculate EK
C
      COMMON/FDATA1/ELEN(50),EAREA(50),EIN(50),EIZ(50),EIT(50),
     &CUR(50),E,G,SK
      COMMON/FDATA3/NP1,NP2,NPB,NPT
      COMMON/EDATA/EK(18,18)
      COMMON/SHP/SN(3),DSN(3),SNU(18),SNV(18),SNW(18),SNTHN(18),
     &SNTHZ(18),SNTHX(18),SNF(18)
      DIMENSION GAUSS(4,4),WT(4,4),B(18,18),C(18,18),BZ(18),
     &BN(18),BT(18),D(18,18)
      IMPLICIT DOUBLE PRECISION (A-H,O-Z)
```

```
C
      DATA GAUSS/4*0.0D0,0.5773502692D0,-0.5773502692D0,2*0.0D0,
     &0.0D0,0.7745966692D0,-0.7745966692D0,0.0D0,
     &0.3399810436D0,-0.3399810436D0,0.8611363116D0,-0.8611363116D0/
      DATA WT/2.0D0,3*0.0D0,2*1.0D0,2*0.0D0,0.8888888889D0,
     &2*0.5555555556D0,0.0D0,2*0.6521451549D0,2*0.3478548451D0/
C
      DO 10 I=1,18
      BZ(I)=0.0D0
      BN(I)=0.0D0
      BT(I)=0.0D0
      DO 10 J=1,18
      B(I,J)=0.0D0
      C(I,J)=0.0D0
      D(I,J)=0.0D0
      EK(I,J)=0.0D0
10    CONTINUE
C
      B1=0.5D0*E*EAREA(K)*ELEN(K)*CUR(K)**2
      B2=2.0D0*E*EIN(K)/ELEN(K)
      B3=-E*EAREA(K)*CUR(K)
      B4=2.0D0*E*EAREA(K)/ELEN(K)
      B5=2.0D0*E*EIZ(K)/ELEN(K)
      B6=E*EIZ(K)*CUR(K)
      B7=0.5D0*E*ELEN(K)*EIZ(K)*CUR(K)**2
C
      DO 20 N1=1,NP1
      X1=GAUSS(N1,NP1)
C
C     call SUBROUTINE SHAPE to evaluate the interpolation
C     functions and their derivatives at Gauss point X1
C
      CALL SHAPE(X1,K)
C
      B(1,1)=WT(N1,NP1)*SN(1)**2*B1+B(1,1)
      B(5,1)=WT(N1,NP1)*DSN(1)*SN(1)*B3+B(5,1)
      B(5,5)=WT(N1,NP1)*DSN(1)**2*B4+B(5,5)
      B(7,1)=WT(N1,NP1)*SN(1)*SN(2)*B1+B(7,1)
      B(7,5)=WT(N1,NP1)*SN(2)*DSN(1)*B3+B(7,5)
      B(7,7)=WT(N1,NP1)*SN(2)**2*B1+B(7,7)
      B(11,1)=WT(N1,NP1)*SN(1)*DSN(2)*B3+B(11,1)
      B(11,5)=WT(N1,NP1)*DSN(1)*DSN(2)*B4+B(11,5)
      B(11,7)=WT(N1,NP1)*SN(2)*DSN(2)*B3+B(11,7)
      B(11,11)=WT(N1,NP1)*DSN(2)**2*B4+B(11,11)
      B(13,1)=WT(N1,NP1)*SN(1)*SN(3)*B1+B(13,1)
      B(13,5)=WT(N1,NP1)*SN(3)*DSN(1)*B3+B(13,5)
      B(13,7)=WT(N1,NP1)*SN(2)*SN(3)*B1+B(13,7)
      B(13,11)=WT(N1,NP1)*SN(3)*DSN(2)*B3+B(13,11)
      B(13,13)=WT(N1,NP1)*SN(3)**2*B1+B(13,13)
      B(17,1)=WT(N1,NP1)*SN(1)*DSN(3)*B3+B(17,1)
      B(17,5)=WT(N1,NP1)*DSN(1)*DSN(3)*B4+B(17,5)
      B(17,7)=WT(N1,NP1)*SN(2)*DSN(3)*B3+B(17,7)
      B(17,11)=WT(N1,NP1)*DSN(2)*DSN(3)*B4+B(17,11)
      B(17,13)=WT(N1,NP1)*SN(3)*DSN(3)*B3+B(17,13)
```

```
      B(17,17)=WT(N1,NP1)*DSN(3)**2*B4+B(17,17)
20    CONTINUE
C
      DO 25 N1=1,NPB
      X1=GAUSS(N1,NPB)
C
      CALL SHAPE(X1,K)
C
      B(4,4)=WT(N1,NPB)*DSN(1)**2*B2+B(4,4)
      B(2,2)=WT(N1,NPB)*DSN(1)**2*B5+B(2,2)
      B(6,2)=WT(N1,NPB)*SN(1)*DSN(1)*B6+B(6,2)
      B(6,6)=WT(N1,NPB)*SN(1)**2*B7+B(6,6)
      B(10,4)=WT(N1,NPB)*DSN(1)*DSN(2)*B2+B(10,4)
      B(10,10)=WT(N1,NPB)*DSN(2)**2*B2+B(10,10)
      B(8,2)=WT(N1,NPB)*DSN(1)*DSN(2)*B5+B(8,2)
      B(8,6)=WT(N1,NPB)*SN(1)*DSN(2)*B6+B(8,6)
      B(8,8)=WT(N1,NPB)*DSN(2)**2*B5+B(8,8)
      B(12,2)=WT(N1,NPB)*SN(2)*DSN(1)*B6+B(12,2)
      B(12,6)=WT(N1,NPB)*SN(1)*SN(2)*B7+B(12,6)
      B(12,8)=WT(N1,NPB)*SN(2)*DSN(2)*B6+B(12,8)
      B(12,12)=WT(N1,NPB)*SN(2)**2*B7+B(12,12)
      B(16,4)=WT(N1,NPB)*DSN(1)*DSN(3)*B2+B(16,4)
      B(16,10)=WT(N1,NPB)*DSN(2)*DSN(3)*B2+B(16,10)
      B(16,16)=WT(N1,NPB)*DSN(3)**2*B2+B(16,16)
      B(14,2)=WT(N1,NPB)*DSN(1)*DSN(3)*B5+B(14,2)
      B(14,6)=WT(N1,NPB)*SN(1)*DSN(3)*B6+B(14,6)
      B(14,8)=WT(N1,NPB)*DSN(2)*DSN(3)*B5+B(14,8)
      B(14,12)=WT(N1,NPB)*SN(2)*DSN(3)*B6+B(14,12)
      B(14,14)=WT(N1,NPB)*DSN(3)**2*B5+B(14,14)
      B(18,2)=WT(N1,NPB)*SN(3)*DSN(1)*B6+B(18,2)
      B(18,6)=WT(N1,NPB)*SN(1)*SN(3)*B7+B(18,6)
      B(18,8)=WT(N1,NPB)*SN(3)*DSN(2)*B6+B(18,8)
      B(18,12)=WT(N1,NPB)*SN(2)*SN(3)*B7+B(18,12)
      B(18,14)=WT(N1,NPB)*SN(3)*DSN(3)*B6+B(18,14)
      B(18,18)=WT(N1,NPB)*SN(3)**2*B7+B(18,18)
25    CONTINUE
C
      DO 30 N1=1,NP2
      X1=GAUSS(N1,NP2)
C
      CALL SHAPE(X1,K)
C
      BZ(1)=2.0D0*DSN(1)/ELEN(K)
      BZ(4)=-SN(1)
      BZ(5)=SN(1)*CUR(K)
      BZ(7)=2.0D0*DSN(2)/ELEN(K)
      BZ(10)=-SN(2)
      BZ(11)=SN(2)*CUR(K)
      BZ(13)=2.0D0*DSN(3)/ELEN(K)
      BZ(16)=-SN(3)
      BZ(17)=SN(3)*CUR(K)
C
      BN(3)=2.0D0*DSN(1)/ELEN(K)
      BN(2)=SN(1)
```

```
        BN(9)=2.0D0*DSN(2)/ELEN(K)
        BN(8)=SN(2)
        BN(15)=2.0D0*DSN(3)/ELEN(K)
        BN(14)=SN(3)
C
        DO 32 I=1,18
        DO 34 J=1,I
        C(I,J)=0.5D0*SK*EAREA(K)*G*ELEN(K)*(BZ(I)*BZ(J)+BN(I)*BN(J))
     &*WT(N1,NP2)+C(I,J)
 34     CONTINUE
 32     CONTINUE
C
30      CONTINUE
C
        DO 40 N1=1,NPT
        X1=GAUSS(N1,NPT)
C
        CALL SHAPE(X1,K)
C
        BT(2)=-SN(1)*CUR(K)
        BT(6)=2.0D0*DSN(1)/ELEN(K)
        BT(8)=-SN(2)*CUR(K)
        BT(12)=2.0D0*DSN(2)/ELEN(K)
        BT(14)=-SN(3)*CUR(K)
        BT(18)=2.0D0*DSN(3)/ELEN(K)
C
        DO 42 I=1,18
        DO 44 J=1,I
        D(I,J)=0.5D0*G*EIT(K)*ELEN(K)*BT(I)*BT(J)*WT(N1,NPT)+D(I,J)
 44     CONTINUE
 42     CONTINUE
C
40      CONTINUE
C
        DO 60 I=1,18
        DO 60 J=1,I
        EK(I,J)=B(I,J)+C(I,J)+D(I,J)
60      CONTINUE
C
        DO 65 I=1,18
        DO 65 J=I+1,18
        EK(I,J)=EK(J,I)
65      CONTINUE
100     RETURN
        END
C-----------------------------------------------------------------------
        SUBROUTINE SHAPE(X1,K)
C
C       SN--------------element shape functions N at X1
C
C       DSN-----------------first derivative of N at X1
C
        COMMON/FDATA1/ELEN(50),EAREA(50),EIN(50),EIZ(50),EIT(50),
     &CUR(50),E,G,SK
```

```
      COMMON/SHP/SN(3),DSN(3),SNU(18),SNV(18),SNW(18),SNTHN(18),
     &SNTHZ(18),SNTHX(18),SNF(18)
      IMPLICIT DOUBLE PRECISION (A-H,O-Z)
C
      DO 10 I=1,3
      SN(I)=0.0D0
      DSN(I)=0.0D0
10    CONTINUE
C
      DO 20 I=1,18
      SNU(I)=0.0D0
      SNV(I)=0.0D0
      SNW(I)=0.0D0
      SNTHN(I)=0.0D0
      SNTHZ(I)=0.0D0
      SNTHX(I)=0.0D0
      SNF(I)=0.0D0
20    CONTINUE
C
      SN(1)=-0.5D0*X1*(1.0D0-X1)
      SN(2)=1.0D0-X1**2
      SN(3)=0.5D0*X1*(1.0D0+X1)
C
      DSN(1)=X1-0.5D0
      DSN(2)=-2.0D0*X1
      DSN(3)=X1+0.5D0
C
      SNU(1)=SN(1)
      SNU(7)=SN(2)
      SNU(13)=SN(3)
C
      SNV(3)=SN(1)
      SNV(9)=SN(2)
      SNV(15)=SN(3)
C
      SNW(5)=SN(1)
      SNW(11)=SN(2)
      SNW(17)=SN(3)
C
      SNTHN(4)=SN(1)
      SNTHN(10)=SN(2)
      SNTHN(16)=SN(3)
C
      SNTHZ(2)=SN(1)
      SNTHZ(8)=SN(2)
      SNTHZ(14)=SN(3)
C
      SNTHX(6)=SN(1)
      SNTHX(12)=SN(2)
      SNTHX(18)=SN(3)
C
      SNF(2)=-0.25D0*ELEN(K)*CUR(K)*(-0.5D0*X1**2+(X1**3)/3.0D0
     &+5.0D0/6.0D0)
      SNF(8)=-0.5D0*ELEN(K)*CUR(K)*(X1-(X1**3)/3.0D0+2.0D0/3.0D0)
```

```
        SNF(14)=-0.25D0*ELEN(K)*CUR(K)*(0.5D0*X1**2+(X1**3)/3.0D0
     &-1.0D0/6.0D0)
C
        RETURN
        END
C-----------------------------------------------------------------
        SUBROUTINE ASSEM1
        COMMON/EDATA/EK(18,18)
        COMMON/SDATA/SSTIFF(500,500)
        COMMON/FDATA2/NE,NN,ND,IDE,INOD,NOD(50,3),ID(50,18)
        IMPLICIT DOUBLE PRECISION (A-H,O-Z)
C
        NNE=INOD*IDE
        DO 40 I=1,NE
C
C       for element I,generate element stiffness matrix EK
C
        CALL ESTIFF(I)
C
        DO 35 J=1,NNE
        IJ=ID(I,J)
        DO 30 K=1,NNE
        IK=ID(I,K)
        SSTIFF(IJ,IK)=SSTIFF(IJ,IK)+EK(J,K)
30      CONTINUE
35      CONTINUE
40      CONTINUE
        RETURN
        END
C-----------------------------------------------------------------
        SUBROUTINE BNDY(ND)
        COMMON/SDATA/SSTIFF(500,500),SLOAD(500),SDISP(500)
        IMPLICIT DOUBLE PRECISION (A-H,O-Z)
C
        DO 70 I=1,ND
        IF(SDISP(I).GT.400.0) GOTO 70
        DO 40 J=1,ND
        IF(J.EQ.I) GOTO 40
        SLOAD(J)=SLOAD(J)-SSTIFF(J,I)*SDISP(I)
        SSTIFF(I,J)=0.0D0
        SSTIFF(J,I)=0.0D0
40      CONTINUE
        SSTIFF(I,I)=1.0D0
        SLOAD(I)=SDISP(I)
70      CONTINUE
        RETURN
        END
C-----------------------------------------------------------------
        SUBROUTINE ASSEM2(DISTP,ELEN,SLOAD)
        COMMON/FDATA2/NE,NN,ND,IDE,INOD,NOD(50,3),ID(50,18)
        DIMENSION DISTP(50,6),ELOAD(18),SLOAD(500),ELEN(50)
        IMPLICIT DOUBLE PRECISION (A-H,O-Z)
C
        NNE=INOD*IDE
```

```
      DO 30 I=1,NE
C
C     generate element load matrix ELOAD
C
      CALL CELOAD(DISTP(I,1),DISTP(I,2),DISTP(I,3),DISTP(I,4),
     &DISTP(I,5),DISTP(I,6),ELEN(I),ELOAD)
C
C     for element I
C
      DO 40 J=1,NNE
      IJ=ID(I,J)
      SLOAD(IJ)=SLOAD(IJ)+ELOAD(J)
40    CONTINUE
30    CONTINUE
      RETURN
      END
C-----------------------------------------------------------------------
      SUBROUTINE ECURVA(CUR,ELEN,CX2)
      COMMON/FDATA2/NE,NN,ND,IDE,INOD,NOD(50,3),ID(50,18)
      COMMON/FDATA4/X(100),Y(100),XN(100),YN(100)
      DIMENSION CUR(50),ELEN(50),TH(3),XP(3),YP(3),CX2(50)
      IMPLICIT DOUBLE PRECISION (A-H,O-Z)
C
      DO 5 I=1,NN
      XN(I)=X(I)
5     YN(I)=Y(I)
      PI=3.1415926D0
      DO 10 I=1,NE
      X2=XN(NOD(I,2))-XN(NOD(I,1))
      X3=XN(NOD(I,3))-XN(NOD(I,1))
      Y2=YN(NOD(I,2))-YN(NOD(I,1))
      Y3=YN(NOD(I,3))-YN(NOD(I,1))
      C=2.0D0*(Y2*X3-Y3*X2)
      A=(-Y3*X2**2+Y2*X3**2-Y2**2*Y3+Y3**2*Y2)/C
      B=(X3*X2**2-X2*X3**2+Y2**2*X3-Y3**2*X2)/C
      R=DSQRT(A**2+B**2)
      CUR(I)=1.0D0/R
C
      XP(1)=-A
      YP(1)=-B
      XP(2)=X2-A
      YP(2)=Y2-B
      XP(3)=X3-A
      YP(3)=Y3-B
C
      DO 30 I1=1,3
      THT=DATAN(DABS(YP(I1)/XP(I1)))
      IF(XP(I1).EQ.0) GOTO 40
      IF(XP(I1).GT.0) GOTO 50
      IF(XP(I1).LT.0) GOTO 60
C
40    IF(YP(I1).GT.0) TH(I1)=PI/2.0D0
      IF(YP(I1).LT.0) TH(I1)=-PI/2.0D0
C
```

```
50      IF(YP(I1).GT.0) TH(I1)=THT
        IF(YP(I1).LT.0) TH(I1)=-THT
        IF(YP(I1).EQ.0) TH(I1)=0.0D0
C
60      IF(YP(I1).GT.0) TH(I1)=PI-THT
        IF(YP(I1).LT.0) TH(I1)=PI+THT
        IF(YP(I1).EQ.0) TH(I1)=PI
30      CONTINUE
        THN2=(TH(1)+TH(3))/2.0D0
        XPN2=R*DCOS(THN2)
        YPN2=R*DSIN(THN2)
        X2N=XPN2+A
        Y2N=YPN2+B
        XN(NOD(I,2))=XN(NOD(I,1))+X2N
        YN(NOD(I,2))=YN(NOD(I,1))+Y2N
        ELEN(I)=(DABS(TH(3)-TH(1)))*R
        S2=(DABS(TH(2)-TH(1)))*R
        CX2(I)=2.0D0*S2/ELEN(I)-1.0D0
10      CONTINUE
C
        WRITE(20,80)  (I,XN(I),YN(I),I=1,NN)
80      FORMAT(1X,'NODE',I3,2X,'XN=',F10.4,2X,'YN=',F10.4)
        RETURN
        END
C-----------------------------------------------------------------
        SUBROUTINE CELOAD(PZ,PMZ,PN,PMN,PX,PMX,ELEN,ELOAD)
        COMMON/SHP/SN(3),DSN(3),SNU(18),SNV(18),SNW(18),SNTHN(18),
     &SNTHZ(18),SNTHX(18),SNF(18)
        DIMENSION ELOAD(18)
        IMPLICIT DOUBLE PRECISION (A-H,O-Z)
C
        C1=ELEN/4.0D0
C
        DO 10 I=1,18
10      ELOAD(I)=0.0D0
C
        ELOAD(1)=PZ
        ELOAD(2)=PMZ
        ELOAD(3)=PN
        ELOAD(4)=PMN
        ELOAD(5)=PX
        ELOAD(6)=PMX
        ELOAD(7)=2.0D0*PZ
        ELOAD(8)=2.0D0*PMZ
        ELOAD(9)=2.0D0*PN
        ELOAD(10)=2.0D0*PMN
        ELOAD(11)=2.0D0*PX
        ELOAD(12)=2.0D0*PMX
        ELOAD(13)=PZ
        ELOAD(14)=PMZ
        ELOAD(15)=PN
        ELOAD(16)=PMN
        ELOAD(17)=PX
        ELOAD(18)=PMX
```

```
C
      DO 30 I=1,18
30    ELOAD(I)=C1*ELOAD(I)
      RETURN
      END
C-----------------------------------------------------------------------
      SUBROUTINE SOLVEQ(N,A,B,X)
      DIMENSION A(N,N),B(N),X(N)
      IMPLICIT DOUBLE PRECISION (A-H,O-Z)
C
      CALL DLSASF(N,A,N,B,X)
C
      RETURN
      END
```

```
C  ************************************************************
C  *                                                          *
C  *         Program Name:  FREEVIB                           *
C  *         Description:  free vibration of beams            *
C  *                       by using 3-node curved beam        *
C  *                       element(6-DOF)                     *
C  *                       (including shear deformation       *
C  *                        and rotary inertia)               *
C  *                                                          *
C  ************************************************************
C
C  Definition
C
C        NE--------number of elements
C        NN--------total number of nodes
C        ND--------total number of degrees of freedom
C        NP1~NP3---the number of Gauss integral points
C        NC--------the number of constrained DOF
C        NDA-------the number of active DOF
C        NDA=ND-NC
C        E,G-------modulus of elasticity
C        SK--------shear correction factor
C        ELEN------beam element length
C        EAREA-----beam element cross-sectional area
C        EIN,EIZ,
C        EIT-------element cross-sectional moments of inertia
C        ERO-------ro, beam element mass per unit of volume
C        SSTIFF----system stiffness matrix
C        SMASS-----system mass matrix
C        EK--------local element stiffness matrix
C        EM--------local element mass matrix
C        X1--------local coordinate
C        CUR(I)----curvature(1/R) of Ith element
C        NOD(I,J)--global node number of Ith element
C        ID(I,J)---global freedom number corresponding to Ith element
C        IDE-------number of degrees of freedom of each node
C        INOD------number of nodes of each element
C        EVAL------eigenvalue(OMEGA**2)
C        OMEGA-----natural frequency
C        EVEC------eigenvector
C        NNE=INOD*IDE
C
C     subroutine name                 function
C
C
C       ESTIFF                 calculate element stiffness
C
C       EMASS                  calculate element mass
C
C       SHAPE                  evaluation of the interpolation function
C                              and the derivatives at the Gauss points
C
C       ASSEM1                 assemble system stiffness and mass
C
```

```
C       SOLVEQ                  calculate eigenvalues and eigenvectors
C                               by using IMSL
C
C       ECURVA                  calculate element curvature etc.
C-----------------------------------------------------------------------
C
        COMMON/SDATA/SSTIFF(500,500),SMASS(500,500)
        COMMON/FDATA1/ELEN(50),EAREA(50),EIN(50),EIZ(50),EIT(50),
     &CUR(50),E,G,SK
        COMMON/FDATA2/NE,NN,ND,IDE,INOD,NOD(50,3),ID(50,18)
        COMMON/FDATA3/NP1,NP2,NPM,NPB,NPT,NP4
        COMMON/FDATA4/X(100),Y(100),XN(100),YN(100)
        COMMON/EDATA/EK(18,18),EM(18,18)
        COMMON/SHP/SN(3),DSN(3),SNU(18),SNV(18),SNW(18),SNTHN(18),
     &SNTHZ(18),SNBT(18),SNF(18)
        DIMENSION EVAL(500),EVEC(500,500),OMEGA(500),
     &TK1(250000),TM1(250000),TEV1(250000)
        IMPLICIT DOUBLE PRECISION (A-H,O-Z)
        OPEN(UNIT=10,FILE='freevib.dat')
        OPEN(UNIT=20,FILE='freevib.out')
C
C       read general data and initialize variables
C
        IDE=6
        INOD=3
        WRITE(20,10)
10      FORMAT(1X,'input data')
        NP1=2
        NP2=2
        NPM=3
        NPB=3
        NPT=3
        NP4=4
        WRITE(20,8) NP1,NP2,NPM,NPB,NPT,NP4
8       FORMAT(1X,'NP1=',I3,2X,'NP2=',I3,2X,'NPM=',I3,2X,'NPB=',I3,
     &2X,'NPT=',I3,2X,'NP4=',I3)
        READ(10,*) NE,NN,NC,ERO,E,G,SK,M0
        WRITE(20,20) NE,NN,NC,ERO,E,G,SK,M0
20      FORMAT(1X,'NE=',I5,2X,'NN=',I5,2X,'NC='I3,2X,'ERO=',E15.6,
     &2X,'E=',E15.6,2X,'G=',E15.6,2X,'SK=',F10.6,2X,'M0=',I2)
C
        READ(10,*) (EAREA(I),EIN(I),EIZ(I),EIT(I),I=1,NE)
        WRITE(20,12) (I,EAREA(I),I=1,NE)
12      FORMAT(1X,'I=',I3,2X,'EAREA=',E14.6)
        WRITE(20,13) (I,EIN(I),EIZ(I),EIT(I),I=1,NE)
13      FORMAT(1X,'I=',I3,2X,'EIN=',E14.6,2X,'EIZ=',E14.6,2X,
     &'EIT=',E14.6)
C
        READ(10,*) ((NOD(I,J),J=1,INOD),I=1,NE)
        WRITE(20,25)
25      FORMAT(1X,'NOD=')
        WRITE(20,*) ((NOD(I,J),J=1,INOD),I=1,NE)
        IF(M0.EQ.1) GOTO 11
        READ(10,*) (X(I),Y(I),I=1,NN)
```

```
      WRITE(20,27) (I,X(I),Y(I),I=1,NN)
27    FORMAT(1X,'NODE',I3,2X,'X=',F10.4,2X,'Y=',F10.4)
C
      CALL ECURVA(CUR,ELEN)
C
      GOTO 15
11    READ(10,*) (ELEN(I),I=1,NE)
      READ(10,*) (CUR(I),I=1,NE)
15    WRITE(20,14) (I,ELEN(I),CUR(I),I=1,NE)
14    FORMAT(1X,'I=',I3,2X,'ELEN=',E15.6,2X,'CUR=',E15.6)
C
      ND=IDE*NN
      NDA=ND-NC
      WRITE(20,16) ND,NDA
16    FORMAT(1X,'ND=',I3,2X,'NDA=',I3)
C
      READ(10,*) ((ID(I,J),J=1,18),I=1,NE)
      WRITE(20,30)
30    FORMAT(1X,'ID=')
      WRITE(20,40) ((ID(I,J),J=1,18),I=1,NE)
40    FORMAT(1X,9I5)
C
      DO 50 I=1,NDA
      DO 60 J=1,NDA
      SMASS(I,J)=0.0D0
60    SSTIFF(I,J)=0.0D0
50    CONTINUE
C
      CALL ASSEM1(NDA,ERO)
C
      DO 440 J=1,NDA
      DO 440 I=1,NDA
      TK1(NDA*(J-1)+I)=SSTIFF(I,J)
440   TM1(NDA*(J-1)+I)=SMASS(I,J)
C
      CALL SOLVEQ(NDA,TK1,TM1,EVAL,TEV1)
C
      DO 460 J=1,NDA
      DO 460 I=1,NDA
460   EVEC(I,J)=TEV1(NDA*(J-1)+I)
      WRITE(20,910)
910   FORMAT(1X,'EVEC=')
      DO 900 J=NDA-6,NDA
      WRITE(20,920) J
920   FORMAT(1X,'J=',I3)
      WRITE(20,930) (EVEC(I,J),I=1,NDA)
900   CONTINUE
930   FORMAT(1X,3D23.14)
      DO 210 I=1,NDA
210   OMEGA(I)=DSQRT(EVAL(I))
C
C     print solutions
C
      WRITE(20,205)
```

```
205     FORMAT( )
        WRITE(20,220)
220     FORMAT(1X,'output data')
        WRITE(20,230)
230     FORMAT( )
        WRITE(20,200)
200     FORMAT(1X,'EVAL=')
        WRITE(20,*) (EVAL(I),I=1,NDA)
        WRITE(20,300)
300     FORMAT(1X,'OMEGA=')
        WRITE(20,*) (OMEGA(I),I=1,NDA)
900     END
C-----------------------------------------------------------------------
        SUBROUTINE ESTIFF(K)
C
C       SN------------------element shape functions N
C       DSN-----------------first derivative of N
C       GAUSS---------------matrix of Gauss points
C       WT------------------Gauss weights corresponding to
C                           the Gauss points
C       B,C,D---------------element matrices needed to calculate EK
C
        COMMON/FDATA1/ELEN(50),EAREA(50),EIN(50),EIZ(50),EIT(50),
     &CUR(50),E,G,SK
        COMMON/FDATA3/NP1,NP2,NPM,NPB,NPT,NP4
        COMMON/EDATA/EK(18,18),EM(18,18)
        COMMON/SHP/SN(3),DSN(3),SNU(18),SNV(18),SNW(18),SNTHN(18),
     &SNTHZ(18),SNBT(18),SNF(18)
        DIMENSION GAUSS(4,4),WT(4,4),B(18,18),C(18,18),BZ(18),
     &BN(18),BT(18),D(18,18)
        IMPLICIT DOUBLE PRECISION (A-H,O-Z)
C
        DATA GAUSS/4*0.0D0,0.5773502692D0,-0.5773502692D0,2*0.0D0,
     &0.0D0,0.7745966692D0,-0.7745966692D0,0.0D0,
     &0.3399810436D0,-0.3399810436D0,0.8611363116D0,-0.8611363116D0/
        DATA WT/2.0D0,3*0.0D0,2*1.0D0,2*0.0D0,0.8888888889D0,
     &2*0.5555555556D0,0.0D0,2*0.6521451549D0,2*0.3478548451D0/
C
        DO 10 I=1,18
        BZ(I)=0.0D0
        BN(I)=0.0D0
        BT(I)=0.0D0
        DO 10 J=1,18
        B(I,J)=0.0D0
        C(I,J)=0.0D0
        D(I,J)=0.0D0
        EK(I,J)=0.0D0
10      CONTINUE
C
        B1=0.5D0*E*EAREA(K)*ELEN(K)*CUR(K)**2
        B2=2.0D0*E*EIN(K)/ELEN(K)
        B3=-E*EAREA(K)*CUR(K)
        B4=2.0D0*E*EAREA(K)/ELEN(K)
        B5=2.0D0*E*EIZ(K)/ELEN(K)
```

```
      B6=E*EIZ(K)*CUR(K)
      B7=0.5D0*E*ELEN(K)*EIZ(K)*CUR(K)**2
C
      DO 20 N1=1,NP1
      X1=GAUSS(N1,NP1)
C
C     call SUBROUTINE SHAPE to evaluate the interpolation
C     functions and their derivatives at Gauss point X1
C
      CALL SHAPE(X1,K)
C
      B(1,1)=WT(N1,NP1)*SN(1)**2*B1+B(1,1)
      B(5,1)=WT(N1,NP1)*DSN(1)*SN(1)*B3+B(5,1)
      B(5,5)=WT(N1,NP1)*DSN(1)**2*B4+B(5,5)
      B(7,1)=WT(N1,NP1)*SN(1)*SN(2)*B1+B(7,1)
      B(7,5)=WT(N1,NP1)*SN(2)*DSN(1)*B3+B(7,5)
      B(7,7)=WT(N1,NP1)*SN(2)**2*B1+B(7,7)
      B(11,1)=WT(N1,NP1)*SN(1)*DSN(2)*B3+B(11,1)
      B(11,5)=WT(N1,NP1)*DSN(1)*DSN(2)*B4+B(11,5)
      B(11,7)=WT(N1,NP1)*SN(2)*DSN(2)*B3+B(11,7)
      B(11,11)=WT(N1,NP1)*DSN(2)**2*B4+B(11,11)
      B(13,1)=WT(N1,NP1)*SN(1)*SN(3)*B1+B(13,1)
      B(13,5)=WT(N1,NP1)*SN(3)*DSN(1)*B3+B(13,5)
      B(13,7)=WT(N1,NP1)*SN(2)*SN(3)*B1+B(13,7)
      B(13,11)=WT(N1,NP1)*SN(3)*DSN(2)*B3+B(13,11)
      B(13,13)=WT(N1,NP1)*SN(3)**2*B1+B(13,13)
      B(17,1)=WT(N1,NP1)*SN(1)*DSN(3)*B3+B(17,1)
      B(17,5)=WT(N1,NP1)*DSN(1)*DSN(3)*B4+B(17,5)
      B(17,7)=WT(N1,NP1)*SN(2)*DSN(3)*B3+B(17,7)
      B(17,11)=WT(N1,NP1)*DSN(2)*DSN(3)*B4+B(17,11)
      B(17,13)=WT(N1,NP1)*SN(3)*DSN(3)*B3+B(17,13)
      B(17,17)=WT(N1,NP1)*DSN(3)**2*B4+B(17,17)
20    CONTINUE
C
      DO 25 N1=1,NPB
      X1=GAUSS(N1,NPB)
C
      CALL SHAPE(X1,K)
C
      B(4,4)=WT(N1,NPB)*DSN(1)**2*B2+B(4,4)
      B(2,2)=WT(N1,NPB)*DSN(1)**2*B5+B(2,2)
      B(6,2)=WT(N1,NPB)*SN(1)*DSN(1)*B6+B(6,2)
      B(6,6)=WT(N1,NPB)*SN(1)**2*B7+B(6,6)
      B(10,4)=WT(N1,NPB)*DSN(1)*DSN(2)*B2+B(10,4)
      B(10,10)=WT(N1,NPB)*DSN(2)**2*B2+B(10,10)
      B(8,2)=WT(N1,NPB)*DSN(1)*DSN(2)*B5+B(8,2)
      B(8,6)=WT(N1,NPB)*SN(1)*DSN(2)*B6+B(8,6)
      B(8,8)=WT(N1,NPB)*DSN(2)**2*B5+B(8,8)
      B(12,2)=WT(N1,NPB)*SN(2)*DSN(1)*B6+B(12,2)
      B(12,6)=WT(N1,NPB)*SN(1)*SN(2)*B7+B(12,6)
      B(12,8)=WT(N1,NPB)*SN(2)*DSN(2)*B6+B(12,8)
      B(12,12)=WT(N1,NPB)*SN(2)**2*B7+B(12,12)
      B(16,4)=WT(N1,NPB)*DSN(1)*DSN(3)*B2+B(16,4)
      B(16,10)=WT(N1,NPB)*DSN(2)*DSN(3)*B2+B(16,10)
```

```
      B(16,16)=WT(N1,NPB)*DSN(3)**2*B2+B(16,16)
      B(14,2)=WT(N1,NPB)*DSN(1)*DSN(3)*B5+B(14,2)
      B(14,6)=WT(N1,NPB)*SN(1)*DSN(3)*B6+B(14,6)
      B(14,8)=WT(N1,NPB)*DSN(2)*DSN(3)*B5+B(14,8)
      B(14,12)=WT(N1,NPB)*SN(2)*DSN(3)*B6+B(14,12)
      B(14,14)=WT(N1,NPB)*DSN(3)**2*B5+B(14,14)
      B(18,2)=WT(N1,NPB)*SN(3)*DSN(1)*B6+B(18,2)
      B(18,6)=WT(N1,NPB)*SN(1)*SN(3)*B7+B(18,6)
      B(18,8)=WT(N1,NPB)*SN(3)*DSN(2)*B6+B(18,8)
      B(18,12)=WT(N1,NPB)*SN(2)*SN(3)*B7+B(18,12)
      B(18,14)=WT(N1,NPB)*SN(3)*DSN(3)*B6+B(18,14)
      B(18,18)=WT(N1,NPB)*SN(3)**2*B7+B(18,18)
25    CONTINUE
C
      DO 30 N1=1,NP2
      X1=GAUSS(N1,NP2)
C
      CALL SHAPE(X1,K)
C
      BZ(1)=2.0D0*DSN(1)/ELEN(K)
      BZ(4)=-SN(1)
      BZ(5)=SN(1)*CUR(K)
      BZ(7)=2.0D0*DSN(2)/ELEN(K)
      BZ(10)=-SN(2)
      BZ(11)=SN(2)*CUR(K)
      BZ(13)=2.0D0*DSN(3)/ELEN(K)
      BZ(16)=-SN(3)
      BZ(17)=SN(3)*CUR(K)
C
      BN(3)=2.0D0*DSN(1)/ELEN(K)
      BN(2)=SN(1)
      BN(9)=2.0D0*DSN(2)/ELEN(K)
      BN(8)=SN(2)
      BN(15)=2.0D0*DSN(3)/ELEN(K)
      BN(14)=SN(3)
C
      DO 32 I=1,18
      DO 34 J=1,I
      C(I,J)=0.5D0*SK*EAREA(K)*G*ELEN(K)*(BZ(I)*BZ(J)+BN(I)*BN(J))
     &*WT(N1,NP2)+C(I,J)
 34   CONTINUE
 32   CONTINUE
C
30    CONTINUE
C
      DO 40 N1=1,NPT
      X1=GAUSS(N1,NPT)
C
      CALL SHAPE(X1,K)
C
      BT(2)=-SN(1)*CUR(K)
      BT(6)=2.0D0*DSN(1)/ELEN(K)
      BT(8)=-SN(2)*CUR(K)
      BT(12)=2.0D0*DSN(2)/ELEN(K)
```

```
        BT(14)=-SN(3)*CUR(K)
        BT(18)=2.0D0*DSN(3)/ELEN(K)
C
        DO 42 I=1,18
        DO 44 J=1,I
        D(I,J)=0.5D0*G*EIT(K)*ELEN(K)*BT(I)*BT(J)*WT(N1,NPT)+D(I,J)
44      CONTINUE
42      CONTINUE
C
40      CONTINUE
        DO 60 I=1,18
        DO 60 J=1,I
        EK(I,J)=B(I,J)+C(I,J)+D(I,J)
60      CONTINUE
C
        DO 65 I=1,18
        DO 65 J=I+1,18
        EK(I,J)=EK(J,I)
65      CONTINUE
C
        RETURN
        END
C-----------------------------------------------------------------------
        SUBROUTINE SHAPE(X1,K)
C
C       SN--------------element shape functions N at X1
C
C       DSN-----------------first derivative of N at X1
C
        COMMON/FDATA1/ELEN(50),EAREA(50),EIN(50),EIZ(50),EIT(50),
     &CUR(50),E,G,SK
        COMMON/SHP/SN(3),DSN(3),SNU(18),SNV(18),SNW(18),SNTHN(18),
     &SNTHZ(18),SNBT(18),SNF(18)
        IMPLICIT DOUBLE PRECISION (A-H,O-Z)
C
        DO 10 I=1,3
        SN(I)=0.0D0
        DSN(I)=0.0D0
10      CONTINUE
C
        DO 20 I=1,18
        SNU(I)=0.0D0
        SNV(I)=0.0D0
        SNW(I)=0.0D0
        SNTHN(I)=0.0D0
        SNTHZ(I)=0.0D0
        SNBT(I)=0.0D0
        SNF(I)=0.0D0
20      CONTINUE
C
        SN(1)=-0.5D0*X1*(1.0D0-X1)
        SN(2)=1.0D0-X1**2
        SN(3)=0.5D0*X1*(1.0D0+X1)
C
```

```
      DSN(1)=X1-0.5D0
      DSN(2)=-2.0D0*X1
      DSN(3)=X1+0.5D0
C
      SNU(1)=SN(1)
      SNU(7)=SN(2)
      SNU(13)=SN(3)
C
      SNV(3)=SN(1)
      SNV(9)=SN(2)
      SNV(15)=SN(3)
C
      SNW(5)=SN(1)
      SNW(11)=SN(2)
      SNW(17)=SN(3)
C
      SNTHN(4)=SN(1)
      SNTHN(10)=SN(2)
      SNTHN(16)=SN(3)
C
      SNTHZ(2)=SN(1)
      SNTHZ(8)=SN(2)
      SNTHZ(14)=SN(3)
C
      SNBT(6)=SN(1)
      SNBT(12)=SN(2)
      SNBT(18)=SN(3)
C
        SNF(2)=-0.25D0*ELEN(K)*CUR(K)*(-0.5D0*(X1**2)+(X1**3)/3.0D0
     &+5.0D0/6.0D0)
        SNF(8)=-0.5D0*ELEN(K)*CUR(K)*(X1-(X1**3)/3.0D0+2.0D0/3.0D0)
        SNF(14)=-0.25D0*ELEN(K)*CUR(K)*(0.5D0*(X1**2)+(X1**3)/3.0D0
     &-1.0D0/6.0D0)
C
        RETURN
        END
C-----------------------------------------------------------------------
        SUBROUTINE ASSEM1(NDA,ERO)
        COMMON/EDATA/EK(18,18),EM(18,18)
        COMMON/SDATA/SSTIFF(500,500),SMASS(500,500)
        COMMON/FDATA2/NE,NN,ND,IDE,INOD,NOD(50,3),ID(50,18)
        IMPLICIT DOUBLE PRECISION (A-H,O-Z)
C
        NNE=INOD*IDE
        DO 40 I=1,NE
C
C       for element I, generate element stiffness matrix EK,
C       mass matrix EM
C
        CALL ESTIFF(I)
C
        CALL EMASS(I,ERO)
C
        DO 35 J=1,NNE
```

```
        IJ=ID(I,J)
        IF (IJ.GT.NDA) GOTO 35
        DO 30 K=1,NNE
        IK=ID(I,K)
        IF (IK.GT.NDA) GOTO 30
        SSTIFF(IJ,IK)=SSTIFF(IJ,IK)+EK(J,K)
        SMASS(IJ,IK)=SMASS(IJ,IK)+EM(J,K)
30      CONTINUE
35      CONTINUE
40      CONTINUE
        RETURN
        END
C-----------------------------------------------------------------------
        SUBROUTINE EMASS(K,ERO)
C
        COMMON/FDATA1/ELEN(50),EAREA(50),EIN(50),EIZ(50),EIT(50),
     &CUR(50),E,G,SK
        COMMON/FDATA3/NP1,NP2,NPM,NPB,NPT,NP4
        COMMON/EDATA/EK(18,18),EM(18,18)
        COMMON/SHP/SN(3),DSN(3),SNU(18),SNV(18),SNW(18),SNTHN(18),
     &SNTHZ(18),SNBT(18),SNF(18)
        DIMENSION GAUSS(4,4),WT(4,4),A(18,18),B(18,18),D(18,18)
        IMPLICIT DOUBLE PRECISION (A-H,O-Z)
C
        DATA GAUSS/4*0.0D0,0.5773502692D0,-0.5773502692D0,2*0.0D0,
     &0.0D0,0.7745966692D0,-0.7745966692D0,0.0D0,
     &0.3399810436D0,-0.3399810436D0,0.8611363116D0,-0.8611363116D0/
        DATA WT/2.0D0,3*0.0D0,2*1.0D0,2*0.0D0,0.8888888889D0,
     &2*0.5555555556D0,0.0D0,2*0.6521451549D0,2*0.3478548451D0/
C
        DO 10 I=1,18
        DO 10 J=1,18
        A(I,J)=0.0D0
        B(I,J)=0.0D0
        D(I,J)=0.0D0
        EM(I,J)=0.0D0
 10     CONTINUE
C
        CONST1=ERO*EAREA(K)*ELEN(K)/2.0D0
        CONST2=ERO*ELEN(K)/2.0D0
        CONST3=ERO*EIT(K)*ELEN(K)/2.0D0
C
        DO 20 N1=1,NPM
        X1=GAUSS(N1,NPM)
C
        CALL SHAPE(X1,K)
C
        DO 50 I=1,18
        DO 50 J=1,18
        A(I,J)=A(I,J)+(SNU(I)*SNU(J)+SNV(I)*SNV(J)+SNW(I)*SNW(J))
     &*WT(N1,NPM)
        B(I,J)=B(I,J)+(EIN(K)*SNTHN(I)*SNTHN(J)+
     &EIZ(K)*SNTHZ(I)*SNTHZ(J))*WT(N1,NPM)
50      CONTINUE
```

```
20      CONTINUE
C
        DO 30 N1=1,NP4
        X1=GAUSS(N1,NP4)
C
        CALL SHAPE(X1,K)
C
        DO 40 I=1,18
        DO 40 J=1,18
        D(I,J)=D(I,J)+(SNBT(I)+SNF(I))*(SNBT(J)+SNF(J))*WT(N1,NP4)
40      CONTINUE
30      CONTINUE
C
        DO 60 I=1,18
        DO 60 J=1,18
        EM(I,J)=CONST1*A(I,J)+CONST2*B(I,J)+CONST3*D(I,J)
60      CONTINUE
        RETURN
        END
C-------------------------------------------------------------
        SUBROUTINE ECURVA(CUR,ELEN)
        COMMON/FDATA2/NE,NN,ND,IDE,INOD,NOD(50,3),ID(50,18)
        COMMON/FDATA4/X(100),Y(100),XN(100),YN(100)
        DIMENSION CUR(50),ELEN(50),TH(3),XP(3),YP(3)
        IMPLICIT DOUBLE PRECISION (A-H,O-Z)
C
        DO 5 I=1,NN
        XN(I)=X(I)
5       YN(I)=Y(I)
        PI=3.1415926D0
        DO 10 I=1,NE
        X2=XN(NOD(I,2))-XN(NOD(I,1))
        X3=XN(NOD(I,3))-XN(NOD(I,1))
        Y2=YN(NOD(I,2))-YN(NOD(I,1))
        Y3=YN(NOD(I,3))-YN(NOD(I,1))
        C=2.0D0*(Y2*X3-Y3*X2)
        A=(-Y3*X2**2+Y2*X3**2-Y2**2*Y3+Y3**2*Y2)/C
        B=(X3*X2**2-X2*X3**2+Y2**2*X3-Y3**2*X2)/C
        R=DSQRT(A**2+B**2)
        CUR(I)=1.0D0/R
C
        XP(1)=-A
        YP(1)=-B
        XP(2)=X2-A
        YP(2)=Y2-B
        XP(3)=X3-A
        YP(3)=Y3-B
C
        DO 30 I1=1,3
        THT=DATAN(DABS(YP(I1)/XP(I1)))
        IF(XP(I1).EQ.0) GOTO 40
        IF(XP(I1).GT.0) GOTO 50
        IF(XP(I1).LT.0) GOTO 60
C
```

```
40      IF(YP(I1).GT.0) TH(I1)=PI/2.0D0
        IF(YP(I1).LT.0) TH(I1)=-PI/2.0D0
C
50      IF(YP(I1).GT.0) TH(I1)=THT
        IF(YP(I1).LT.0) TH(I1)=-THT
        IF(YP(I1).EQ.0) TH(I1)=0.0D0
C
60      IF(YP(I1).GT.0) TH(I1)=PI-THT
        IF(YP(I1).LT.0) TH(I1)=PI+THT
        IF(YP(I1).EQ.0) TH(I1)=PI
30      CONTINUE
        THN2=(TH(1)+TH(3))/2.0D0
        XPN2=R*DCOS(THN2)
        YPN2=R*DSIN(THN2)
        X2N=XPN2+A
        Y2N=YPN2+B
        XN(NOD(I,2))=XN(NOD(I,1))+X2N
        YN(NOD(I,2))=YN(NOD(I,1))+Y2N
        ELEN(I)=(DABS(TH(3)-TH(1)))*R
10      CONTINUE
C
        WRITE(20,80) (I,XN(I),YN(I),I=1,NN)
80      FORMAT(1X,'NODE',I3,2X,'XN=',F10.4,2X,'YN=',F10.4)
        RETURN
        END
C-----------------------------------------------------------------------
        SUBROUTINE SOLVEQ(N,A,B,EVAL,EVEC)
        DIMENSION A(N,N),B(N,N),EVAL(N),EVEC(N,N)
        IMPLICIT DOUBLE PRECISION (A-H,O-Z)
C
        CALL DGVCSP(N,A,N,B,N,EVAL,EVEC,N)
C
        RETURN
        END
```

```
C  ***********************************************************************
C  *                                                                     *
C  *         Program Name: DYNA                                          *
C  *         Description:  dynamic response of beams by using            *
C  *                       3-node curved beam element(6-DOF)             *
C  *                       (including shear deformation)                 *
C  *                        tapered pole                                 *
C  *                                                                     *
C  ***********************************************************************
C
C  Definition
C
C        NE--------number of elements
C        NN--------total number of nodes
C        ND--------total number of degrees of freedom
C        E,G-------modulus of elasticity
C        SK--------shear correction factor
C        NP1~NPB---the number of Gauss integral points
C        ELEN------beam element length
C        EAREA-----beam element cross-sectional area
C        EIN,EIZ
C        EIT-------element cross-sectional moments of inertia
C        SSTIFF----system stiffness matrix
C        SMASS-----system mass matrix
C        SDAMP-----system damping matrix
C        SLOAD-----system load column
C        SDISP-----system displacement column
C        SDISPB----system displacement boundary condition column
C        SVELO-----system velocity column
C        SACCE-----system acceleration column
C        EK--------element stiffness matrix
C        EM--------element mass matrix
C        X1--------local coordinate
C        CUR(I)----curvature(1/R) of Ith element
C        NOD(I,J)--global node number of Ith element
C        ID(I,J)---global freedom number corresponding to Ith element
C        IDE-------number of degrees of freedom of each node
C        INOD------number of nodes of each element
C        WIN-------wind speed
C        PZ,PN,PX,
C        PMZ,PMN,PMX---nodal distributed load (N/m)
C        ARO-------air density
C        ERO-------material density
C        CD0,CD etc.--------aerodynamic coefficients
C        BCD0,BCD etc.--------aerodynamic parameters
C        DD--------dimension of the cross-section
C        NNE=INOD*IDE
C        unknown displacement: input 500.0
C
C     subroutine name                  function
C
C
C      ESTIFF              calculate element stiffness matrix
C
```

```
C       EMASS                calculate element mass matrix
C
C       CELOAD               calculate element equivalent load column
C
C       SHAPE                evaluation of the interpolation function
C                            and the derivatives at the Gauss points
C
C       ASSEM1               assemble system stiffness, mass and
C                            damping matrices
C
C       ASSEM2               assemble system load column
C
C       BNDY                 impose boundary conditions
C
C       SOLVEQ               solve linear equations by using IMSL
C
C-----------------------------------------------------------------------
C
        COMMON/SDATA/SSTIFF(500,500),SMASS(500,500),SDAMP(500,500),
     &SLOAD(500),SDISP(500)
        COMMON/FDATA1/ELEN(50),RO(500),DD(500),CUR(50),E,G,SK
        COMMON/FDATA2/NE,NN,ND,IDE,INOD,NOD(50,3),ID(50,18)
        COMMON/FDATA3/NP1,NP2,NPM,NPM1,NPB,NPT,NP4
        COMMON/FDATA4/X(100),Y(100),XN(100),YN(100)
        COMMON/EDATA/EK(18,18),EM(18,18)
        COMMON/SHP/SN(3),DSN(3),SNU(18),SNV(18),SNW(18),SNTHN(18),
     &SNTHZ(18),SNTHX(18),SNF(18)
        DIMENSION TK1(250000),SDISPB(500),SVELO(500),TT(50),
     &SACCE(500),SDISP0(500),SVELO0(500),SACCE0(500),SLOAD0(500),
     &SA(500,500),AA(500),Q(500),R(500),FAI(500),BCD0(4,11),
     &BCS0(4,11),BCD(4,11),BCS(4,11),BCL(4,11),BCMR(4,11),
     &BCMY(4,11),BCMP(4,11),BREAK(11)
        IMPLICIT DOUBLE PRECISION (A-H,O-Z)
        OPEN(UNIT=10,FILE='DYNA.dat')
        OPEN(UNIT=20,FILE='DYNA.out')
C
C       read general data and initialize variables
C
        IDE=6
        INOD=3
        WRITE(20,10)
10      FORMAT(1X,'input data')
        NP1=2
        NP2=2
        NPM=3
        NPM1=4
        NPB=4
        NPT=4
        NP4=5
        WRITE(20,8) NP1,NP2,NPM,NPM1,NPB,NPT,NP4
8       FORMAT(1X,'NP1=',I3,2X,'NP2=',I3,2X,'NPM=',I3,2X,'NPM1=',I3,
     &2X,'NPB=',I3,2X,'NPT=',I3,2X,'NP4=',I3)
        READ(10,*) NE,NN,E,G,SK
        WRITE(20,20) NE,NN,E,G,SK
```

```
20      FORMAT(1X,'NE=',I5,2X,'NN=',I5,2X,'E=',E15.6,2X,'G=',
     &E15.6,2X,'SK=',F10.6)
        READ(10,*) N0,N1,NH,CML
        WRITE(20,11) N0,N1,NH,CML
11      FORMAT(1X,'N0=',I5,2X,'N1=',I5,2X,'NH=',I5,2X,'CML=',F8.3)
C
        READ(10,*) RO(1),RO(N1),RO(N0),RO(NN)
        READ(10,*) ABLL,BCLL,CELL
        DO 62 I=2,N1-1
        XX=(I-1)*ABLL/(N1-1)
62      RO(I)=RO(N1)+(RO(1)-RO(N1))*(ABLL-XX)/ABLL
        DO 64 I=N1+1,N0-1
        XX=(I-N1)*BCLL/(N0-N1)
64      RO(I)=RO(N0)+(RO(N1)-RO(N0))*(BCLL-XX)/BCLL
        DO 66 I=N0+1,NN-1
        XX=(I-N0)*CELL/(NN-N0)
66      RO(I)=RO(NN)+(RO(N0)-RO(NN))*(CELL-XX)/CELL
        PI=3.1415926D0
        DO 68 I=1,NN
68      DD(I)=2.0D0*RO(I)
        WRITE(20,22)
22      FORMAT(1X,'DD=')
        WRITE(20,*) (DD(I),I=1,NN)
C
        READ(10,*) (ELEN(I),TT(I),I=1,NE)
        WRITE(20,12) (I,ELEN(I),TT(I),I=1,NE)
12      FORMAT(1X,'I=',I3,2X,'ELEN=',E14.6,2X,'TT=',E14.6)
C
        READ(10,*) ERO,ARO,AC0,AC1
        WRITE(20,15) ERO,ARO,AC0,AC1
15      FORMAT(1X,'ERO=',F10.5,2X,'ARO=',F10.5,2X,'AC0=',
     &F10.5,2X,'AC1=',F10.5)
C
        READ(10,*) ((BCD0(I,J),I=1,4),J=1,11)
        READ(10,*) ((BCS0(I,J),I=1,4),J=1,11)
        READ(10,*) ((BCD(I,J),I=1,4),J=1,11)
        READ(10,*) ((BCL(I,J),I=1,4),J=1,11)
        READ(10,*) ((BCS(I,J),I=1,4),J=1,11)
        READ(10,*) ((BCMY(I,J),I=1,4),J=1,11)
        READ(10,*) ((BCMP(I,J),I=1,4),J=1,11)
        READ(10,*) ((BCMR(I,J),I=1,4),J=1,11)
C
        READ(10,*) BREAK
C
        READ(10,*) (CUR(I),I=1,NE)
C
        DO 24 I=1,N0
24      FAI(I)=PI/2.0D0
        DO 26 I=1,NH-N0
        I1=N0+I
26      FAI(I1)=PI/2.0D0 -I*PI/(2.0D0*(NH-N0))
        DO 27 I=1,NN-NH
        I1=NH+I
27      FAI(I1)=0.0D0
```

```
C
      ND=IDE*NN
C
      READ(10,*) ((NOD(I,J),J=1,INOD),I=1,NE)
C
      DO 32 I=1,ND
      SDISPB(I)=500.0
      SDISP0(I)=0.0D0
      SVELO0(I)=0.0D0
      SACCE0(I)=0.0D0
32    SLOAD0(I)=0.0D0
C
      READ(10,*) (SDISPB(I),I=1,6)
C
      READ(10,*) BETA,GAMMA,DT,WIN,NUM
      WRITE(20,48) BETA,GAMMA,DT,WIN,NUM
48    FORMAT(1X,'BETA=',F8.4,2X,'GAMMA=',F8.4,2X,'DT=',F8.4,
     &2X,'WIN=',F10.6,2X,'NUM=',I5)
C
      NUM1=1
C
      READ(10,*) EBS
      WRITE(20,51) EBS
51    FORMAT(1X,'EBS=',F15.6)
      DO 50 I=1,ND
      DO 60 J=1,ND
      SMASS(I,J)=0.0D0
60    SSTIFF(I,J)=0.0D0
50    CONTINUE
C
C     generate ID according to NOD
C
      DO 70 I=1,NE
      DO 80 J=1,INOD
      I0=(NOD(I,J)-1)*IDE
      IE0=(J-1)*IDE
      DO 90 II=1,IDE
      ID(I,IE0+II)=I0+II
90    CONTINUE
80    CONTINUE
70    CONTINUE
C
      WRITE(20,85)
85    FORMAT(1X,'ID=')
      WRITE(20,88) ((ID(I,J),J=1,18),I=1,NE)
88    FORMAT(1X,9I5)
C
      CALL ASSEM1(ERO,AC0,AC1,CML,TT)
C
      C1=1.0D0/(BETA*DT*DT)
      C2=GAMMA/(BETA*DT)
      C3=1.0D0/(BETA*DT)
      C4=1.0D0/(2.0D0*BETA)-1.0D0
      C5=GAMMA/BETA-1.0D0
```

```
      C6=DT*(GAMMA/(2.0D0*BETA)-1.0D0)
C
      DO 400 I=1,ND
      DO 400 J=1,ND
400   SA(I,J)=SSTIFF(I,J)+C1*SMASS(I,J)+C2*SDAMP(I,J)
C
      WRITE(20,480)
480   FORMAT(1X,'Nodal Displacements:')
      WRITE(20,482) NN
482   FORMAT(1X,'NODE',I3)
      WRITE(20,484)
C484   FORMAT(1X,'T',16X,'V')
C484   FORMAT(1X,'T',16X,'THN',20X,'W',20X,'THX')
484   FORMAT(1X,'T',16X,'V',20X,'THZ',20X,'U')
C
405   DO 407 I=1,ND
407   SLOAD(I)=0.0D0
C
      CALL ASSEM2(ELEN,FAI,WIN,SDISP0,SVELO0,ARO,DD,
     &BCD0,BCS0,BCD,BCS,BCL,BCMR,BCMY,BCMP,BREAK,
     &SLOAD,N0,NH,EBS)
C
      DO 410 I=1,ND
      Q(I)=C1*SDISP0(I)+C3*SVELO0(I)+C4*SACCE0(I)
410   R(I)=C2*SDISP0(I)+C5*SVELO0(I)+C6*SACCE0(I)
      DO 420 I=1,ND
      SUM=0.0D0
      DO 430 K=1,ND
430   SUM=SUM+SMASS(I,K)*Q(K)+SDAMP(I,K)*R(K)
420   AA(I)=SUM+SLOAD(I)
C
      CALL BNDY(ND,SA,AA,SDISPB)
C
      DO 440 J=1,ND
      DO 440 I=1,ND
440   TK1(ND*(J-1)+I)=SA(I,J)
C
      CALL SOLVEQ(ND,TK1,AA,SDISP)
C
      DO 450 I=1,ND
      SACCE(I)=C1*SDISP(I)-Q(I)
450   SVELO(I)=C2*SDISP(I)-R(I)
C
C     print solutions
C
      IF(MOD(NUM1,5).NE.0) GOTO 550
C      WRITE(20,470) NUM1*DT
C470   FORMAT(1X,'T=',F10.2)
      I=NN
C      WRITE(20,490) NUM1*DT,SDISP(6*I-3)
      WRITE(20,490) NUM1*DT,SDISP(6*I-3),SDISP(6*I-4),
     &SDISP(6*I-5)
C      WRITE(20,490) NUM1*DT,SDISP(6*I-2),SDISP(6*I-1),
C     &SDISP(6*I)
```

```
490     FORMAT(1X,F6.2,2X,E18.8,2X,E18.8,2X,E18.8)
C        WRITE(20,490) I,SDISP(6*I-5),SDISP(6*I-4),SDISP(6*I-3)
C        WRITE(20,495) SDISP(6*I-2),SDISP(6*I-1),SDISP(6*I)
C490     FORMAT(1X,'NODE',I5,2X,'U=',D17.10,2X,'THZ=',D17.10,2X,
C      &'V=',D17.10)
C495     FORMAT(1X,'THN=',D17.10,2X,'W=',D17.10,2X,'THX=',D17.10)
C        DO 520 I=1,NN
C        WRITE(20,500) I
C500     FORMAT(1X,'Node',I3)
C        WRITE(20,510) SDISP(6*I-5),SDISP(6*I-4),SDISP(6*I-3)
C        WRITE(20,530) SDISP(6*I-2),SDISP(6*I-1),SDISP(6*I)
C510     FORMAT(1X,'U=',D17.10,2X,'THZ=',D17.10,2X,'V=',D17.10)
C530     FORMAT(1X,'THN=',D17.10,2X,'W=',D17.10,2X,'THX=',D17.10)
C        WRITE(20,560) SVELO(6*I-5),SVELO(6*I-4),SVELO(6*I-3)
C        WRITE(20,570) SVELO(6*I-2),SVELO(6*I-1),SVELO(6*I)
C560     FORMAT(1X,'VU=',D17.10,2X,'VTHZ=',D17.10,2X,'VV=',D17.10)
C570     FORMAT(1X,'VTHN=',D17.10,2X,'VW=',D17.10,2X,'VTHX=',D17.10)
C520     CONTINUE
550     DO 610 I=1,ND
        SDISP0(I)=SDISP(I)
        SVELO0(I)=SVELO(I)
610     SACCE0(I)=SACCE(I)
        NUM1=NUM1+1
        IF(NUM1.LE.NUM) GOTO 405
        END
C-----------------------------------------------------------------------
        SUBROUTINE ESTIFF(K,NOD,TT)
C
C       SN------------------element shape functions N
C       DSN-----------------first derivative of N
C       GAUSS---------------matrix of Gauss points
C       WT------------------Gauss weights corresponding to
C                           the Gauss points
C       B,C,D---------------element matrices needed to calculate EK
C
        COMMON/FDATA1/ELEN(50),RO(500),DD(500),CUR(50),E,G,SK
        COMMON/FDATA3/NP1,NP2,NPM,NPM1,NPB,NPT,NP4
        COMMON/EDATA/EK(18,18),EM(18,18)
        COMMON/SHP/SN(3),DSN(3),SNU(18),SNV(18),SNW(18),SNTHN(18),
      &SNTHZ(18),SNTHX(18),SNF(18)
        DIMENSION GAUSS(4,4),WT(4,4),B(18,18),C(18,18),BZ(18),
      &BN(18),BT(18),D(18,18),NOD(50,3),TT(50)
        IMPLICIT DOUBLE PRECISION (A-H,O-Z)
C
        DATA GAUSS/4*0.0D0,0.5773502692D0,-0.5773502692D0,2*0.0D0,
      &0.0D0,0.7745966692D0,-0.7745966692D0,0.0D0,
      &0.3399810436D0,-0.3399810436D0,0.8611363116D0,-0.8611363116D0/
        DATA WT/2.0D0,3*0.0D0,2*1.0D0,2*0.0D0,0.8888888889D0,
      &2*0.5555555556D0,0.0D0,2*0.6521451549D0,2*0.3478548451D0/
C
        K1=NOD(K,1)
        K3=NOD(K,3)
C
        DO 10 I=1,18
```

```
      BZ(I)=0.0D0
      BN(I)=0.0D0
      BT(I)=0.0D0
      DO 10 J=1,18
      B(I,J)=0.0D0
      C(I,J)=0.0D0
      D(I,J)=0.0D0
      EK(I,J)=0.0D0
10    CONTINUE
C
      DO 20 N1=1,NP1
      X1=GAUSS(N1,NP1)
C
      DX=DD(K3)+0.5D0*(1.0D0-X1)*(DD(K1)-DD(K3))-TT(K)
      BB=0.57735D0*DX
      EAREA=6.0D0*BB*TT(K)
C      WRITE(20,33) K,EAREA
C33    FORMAT(1X,'ELEMENT',I3,2X,'EAREA=',D15.6)
      B1=0.5D0*E*EAREA*ELEN(K)*CUR(K)**2
      B3=-E*EAREA*CUR(K)
      B4=2.0D0*E*EAREA/ELEN(K)
C
C     call SUBROUTINE SHAPE to evaluate the interpolation
C     functions and their derivatives at Gauss point X1
C
      CALL SHAPE(X1,K)
C
      B(1,1)=WT(N1,NP1)*SN(1)**2*B1+B(1,1)
      B(5,1)=WT(N1,NP1)*DSN(1)*SN(1)*B3+B(5,1)
      B(5,5)=WT(N1,NP1)*DSN(1)**2*B4+B(5,5)
      B(7,1)=WT(N1,NP1)*SN(1)*SN(2)*B1+B(7,1)
      B(7,5)=WT(N1,NP1)*SN(2)*DSN(1)*B3+B(7,5)
      B(7,7)=WT(N1,NP1)*SN(2)**2*B1+B(7,7)
      B(11,1)=WT(N1,NP1)*SN(1)*DSN(2)*B3+B(11,1)
      B(11,5)=WT(N1,NP1)*DSN(1)*DSN(2)*B4+B(11,5)
      B(11,7)=WT(N1,NP1)*SN(2)*DSN(2)*B3+B(11,7)
      B(11,11)=WT(N1,NP1)*DSN(2)**2*B4+B(11,11)
      B(13,1)=WT(N1,NP1)*SN(1)*SN(3)*B1+B(13,1)
      B(13,5)=WT(N1,NP1)*SN(3)*DSN(1)*B3+B(13,5)
      B(13,7)=WT(N1,NP1)*SN(2)*SN(3)*B1+B(13,7)
      B(13,11)=WT(N1,NP1)*SN(3)*DSN(2)*B3+B(13,11)
      B(13,13)=WT(N1,NP1)*SN(3)**2*B1+B(13,13)
      B(17,1)=WT(N1,NP1)*SN(1)*DSN(3)*B3+B(17,1)
      B(17,5)=WT(N1,NP1)*DSN(1)*DSN(3)*B4+B(17,5)
      B(17,7)=WT(N1,NP1)*SN(2)*DSN(3)*B3+B(17,7)
      B(17,11)=WT(N1,NP1)*DSN(2)*DSN(3)*B4+B(17,11)
      B(17,13)=WT(N1,NP1)*SN(3)*DSN(3)*B3+B(17,13)
      B(17,17)=WT(N1,NP1)*DSN(3)**2*B4+B(17,17)
20    CONTINUE
C
      DO 25 N1=1,NPB
      X1=GAUSS(N1,NPB)
C
      DX=DD(K3)+0.5D0*(1.0D0-X1)*(DD(K1)-DD(K3))-TT(K)
```

```
        BB=0.57735D0*DX
        EIN=2.0D0*(BB-0.577D0*TT(K))*TT(K)*(0.5D0*DX)**2
     &+4.0D0*BB*TT(K)*(0.25D0*DX)**2
        EIT=6.0D0*BB*TT(K)*(0.5D0*DX)**2
        EIZ=EIT-EIN
C
        B2=2.0D0*E*EIN/ELEN(K)
        B5=2.0D0*E*EIZ/ELEN(K)
        B6=E*EIZ*CUR(K)
        B7=0.5D0*E*ELEN(K)*EIZ*CUR(K)**2
C
        CALL SHAPE(X1,K)
C
        B(4,4)=WT(N1,NPB)*DSN(1)**2*B2+B(4,4)
        B(2,2)=WT(N1,NPB)*DSN(1)**2*B5+B(2,2)
        B(6,2)=WT(N1,NPB)*SN(1)*DSN(1)*B6+B(6,2)
        B(6,6)=WT(N1,NPB)*SN(1)**2*B7+B(6,6)
        B(10,4)=WT(N1,NPB)*DSN(1)*DSN(2)*B2+B(10,4)
        B(10,10)=WT(N1,NPB)*DSN(2)**2*B2+B(10,10)
        B(8,2)=WT(N1,NPB)*DSN(1)*DSN(2)*B5+B(8,2)
        B(8,6)=WT(N1,NPB)*SN(1)*DSN(2)*B6+B(8,6)
        B(8,8)=WT(N1,NPB)*DSN(2)**2*B5+B(8,8)
        B(12,2)=WT(N1,NPB)*SN(2)*DSN(1)*B6+B(12,2)
        B(12,6)=WT(N1,NPB)*SN(1)*SN(2)*B7+B(12,6)
        B(12,8)=WT(N1,NPB)*SN(2)*DSN(2)*B6+B(12,8)
        B(12,12)=WT(N1,NPB)*SN(2)**2*B7+B(12,12)
        B(16,4)=WT(N1,NPB)*DSN(1)*DSN(3)*B2+B(16,4)
        B(16,10)=WT(N1,NPB)*DSN(2)*DSN(3)*B2+B(16,10)
        B(16,16)=WT(N1,NPB)*DSN(3)**2*B2+B(16,16)
        B(14,2)=WT(N1,NPB)*DSN(1)*DSN(3)*B5+B(14,2)
        B(14,6)=WT(N1,NPB)*SN(1)*DSN(3)*B6+B(14,6)
        B(14,8)=WT(N1,NPB)*DSN(2)*DSN(3)*B5+B(14,8)
        B(14,12)=WT(N1,NPB)*SN(2)*DSN(3)*B6+B(14,12)
        B(14,14)=WT(N1,NPB)*DSN(3)**2*B5+B(14,14)
        B(18,2)=WT(N1,NPB)*SN(3)*DSN(1)*B6+B(18,2)
        B(18,6)=WT(N1,NPB)*SN(1)*SN(3)*B7+B(18,6)
        B(18,8)=WT(N1,NPB)*SN(3)*DSN(2)*B6+B(18,8)
        B(18,12)=WT(N1,NPB)*SN(2)*SN(3)*B7+B(18,12)
        B(18,14)=WT(N1,NPB)*SN(3)*DSN(3)*B6+B(18,14)
        B(18,18)=WT(N1,NPB)*SN(3)**2*B7+B(18,18)
25      CONTINUE
C
        DO 30 N1=1,NP2
        X1=GAUSS(N1,NP2)
C
        CALL SHAPE(X1,K)
C
        BZ(1)=2.0D0*DSN(1)/ELEN(K)
        BZ(4)=-SN(1)
        BZ(5)=SN(1)*CUR(K)
        BZ(7)=2.0D0*DSN(2)/ELEN(K)
        BZ(10)=-SN(2)
        BZ(11)=SN(2)*CUR(K)
        BZ(13)=2.0D0*DSN(3)/ELEN(K)
```

```
        BZ(16)=-SN(3)
        BZ(17)=SN(3)*CUR(K)
C
        BN(3)=2.0D0*DSN(1)/ELEN(K)
        BN(2)=SN(1)
        BN(9)=2.0D0*DSN(2)/ELEN(K)
        BN(8)=SN(2)
        BN(15)=2.0D0*DSN(3)/ELEN(K)
        BN(14)=SN(3)
C
        DX=DD(K3)+0.5D0*(1.0D0-X1)*(DD(K1)-DD(K3))-TT(K)
        BB=0.57735D0*DX
        EAREA=6.0D0*BB*TT(K)
        DO 32 I=1,18
        DO 34 J=1,I
        C(I,J)=0.5D0*SK*EAREA*G*ELEN(K)*(BZ(I)*BZ(J)+BN(I)*BN(J))
     &*WT(N1,NP2)+C(I,J)
 34     CONTINUE
 32     CONTINUE
C
30      CONTINUE
C
        DO 40 N1=1,NPT
        X1=GAUSS(N1,NPT)
C
        CALL  SHAPE(X1,K)
C
        BT(2)=-SN(1)*CUR(K)
        BT(6)=2.0D0*DSN(1)/ELEN(K)
        BT(8)=-SN(2)*CUR(K)
        BT(12)=2.0D0*DSN(2)/ELEN(K)
        BT(14)=-SN(3)*CUR(K)
        BT(18)=2.0D0*DSN(3)/ELEN(K)
C
        DX=DD(K3)+0.5D0*(1.0D0-X1)*(DD(K1)-DD(K3))-TT(K)
        BB=0.57735D0*DX
        EIT=6.0D0*BB*TT(K)*(0.5D0*DX)**2
        DO 42 I=1,18
        DO 44 J=1,I
        D(I,J)=0.5D0*G*EIT*ELEN(K)*BT(I)*BT(J)*WT(N1,NPT)+D(I,J)
44      CONTINUE
42      CONTINUE
C
40      CONTINUE
        DO 60 I=1,18
        DO 60 J=1,I
        EK(I,J)=B(I,J)+C(I,J)+D(I,J)
60      CONTINUE
C
        DO 65 I=1,18
        DO 65 J=I+1,18
        EK(I,J)=EK(J,I)
65      CONTINUE
C
```

```
      RETURN
      END
C-----------------------------------------------------------------------
      SUBROUTINE SHAPE(X1,K)
C
C     SN--------------element shape functions N at X1
C
C     DSN-----------------first derivative of N at X1
C
      COMMON/FDATA1/ELEN(50),RO(500),DD(500),CUR(50),E,G,SK
      COMMON/SHP/SN(3),DSN(3),SNU(18),SNV(18),SNW(18),SNTHN(18),
     &SNTHZ(18),SNTHX(18),SNF(18)
      IMPLICIT DOUBLE PRECISION (A-H,O-Z)
C
      DO 10 I=1,3
      SN(I)=0.0D0
      DSN(I)=0.0D0
10    CONTINUE
C
      DO 20 I=1,18
      SNU(I)=0.0D0
      SNV(I)=0.0D0
      SNW(I)=0.0D0
      SNTHN(I)=0.0D0
      SNTHZ(I)=0.0D0
      SNTHX(I)=0.0D0
      SNF(I)=0.0D0
20    CONTINUE
C
      SN(1)=-0.5D0*X1*(1.0D0-X1)
      SN(2)=1.0D0-X1**2
      SN(3)=0.5D0*X1*(1.0D0+X1)
C
      DSN(1)=X1-0.5D0
      DSN(2)=-2.0D0*X1
      DSN(3)=X1+0.5D0
C
      SNU(1)=SN(1)
      SNU(7)=SN(2)
      SNU(13)=SN(3)
C
      SNV(3)=SN(1)
      SNV(9)=SN(2)
      SNV(15)=SN(3)
C
      SNW(5)=SN(1)
      SNW(11)=SN(2)
      SNW(17)=SN(3)
C
      SNTHN(4)=SN(1)
      SNTHN(10)=SN(2)
      SNTHN(16)=SN(3)
C
      SNTHZ(2)=SN(1)
```

```
        SNTHZ(8)=SN(2)
        SNTHZ(14)=SN(3)
C
        SNTHX(6)=SN(1)
        SNTHX(12)=SN(2)
        SNTHX(18)=SN(3)
C
        SNF(2)=-0.25D0*ELEN(K)*CUR(K)*(-0.5D0*X1**2+(X1**3)/3.0D0
     &+5.0D0/6.0D0)
        SNF(8)=-0.5D0*ELEN(K)*CUR(K)*(X1-(X1**3)/3.0D0+2.0D0/3.0D0)
        SNF(14)=-0.25D0*ELEN(K)*CUR(K)*(0.5D0*X1**2+(X1**3)/3.0D0
     &-1.0D0/6.0D0)
C
        RETURN
        END
C-----------------------------------------------------------------
        SUBROUTINE EMASS(K,ERO,NOD,TT)
C
        COMMON/FDATA1/ELEN(50),RO(500),DD(500),CUR(50),E,G,SK
        COMMON/FDATA3/NP1,NP2,NPM,NPM1,NPB,NPT,NP4
        COMMON/EDATA/EK(18,18),EM(18,18)
        COMMON/SHP/SN(3),DSN(3),SNU(18),SNV(18),SNW(18),SNTHN(18),
     &SNTHZ(18),SNTHX(18),SNF(18)
        DIMENSION GAUSS(5,5),WT(5,5),A(18,18),B(18,18),D(18,18),
     &NOD(50,3),TT(50)
        IMPLICIT DOUBLE PRECISION (A-H,O-Z)
C
        DATA GAUSS/5*0.0D0,0.5773502692D0,-0.5773502692D0,3*0.0D0,
     &0.0D0,0.7745966692D0,-0.7745966692D0,2*0.0D0,0.3399810436D0,
     &-0.3399810436D0,0.8611363116D0,-0.8611363116D0,
     &0.0D0,0.0D0,0.5384693101D0,-0.5384693101D0,0.9061798459D0,
     &-0.9061798459D0/
        DATA WT/2.0D0,4*0.0D0,2*1.0D0,3*0.0D0,0.8888888889D0,
     &2*0.5555555556D0,2*0.0D0,2*0.6521451549D0,2*0.3478548451D0,
     &0.0D0,0.5688888889D0,2*0.4786286705D0,2*0.2369268851D0/
C
        K1=NOD(K,1)
        K3=NOD(K,3)
        DO 10 I=1,18
        DO 10 J=1,18
        A(I,J)=0.0D0
        B(I,J)=0.0D0
        D(I,J)=0.0D0
        EM(I,J)=0.0D0
 10     CONTINUE
C
        CONST1=ERO*ELEN(K)/2.0D0
C
        DO 20 N1=1,NPM
        X1=GAUSS(N1,NPM)
C
        DX=DD(K3)+0.5D0*(1.0D0-X1)*(DD(K1)-DD(K3))-TT(K)
        BB=0.57735D0*DX
        EAREA=6.0D0*BB*TT(K)
```

```
C
        CALL SHAPE(X1,K)
C
        DO 50 I=1,18
        DO 50 J=1,18
        A(I,J)=A(I,J)+(SNU(I)*SNU(J)+SNV(I)*SNV(J)+SNW(I)*SNW(J))
     &*EAREA*WT(N1,NPM)
50      CONTINUE
20      CONTINUE
C
        DO 22 N1=1,NPM1
        X1=GAUSS(N1,NPM1)
C
        DX=DD(K3)+0.5D0*(1.0D0-X1)*(DD(K1)-DD(K3))-TT(K)
        BB=0.57735D0*DX
        EIN=2.0D0*(BB-0.577D0*TT(K))*TT(K)*(0.5D0*DX)**2
     &+4.0D0*BB*TT(K)*(0.25D0*DX)**2
        EIT=6.0D0*BB*TT(K)*(0.5D0*DX)**2
        EIZ=EIT-EIN
C
        CALL SHAPE(X1,K)
C
        DO 52 I=1,18
        DO 52 J=1,18
        B(I,J)=B(I,J)+(EIN*SNTHN(I)*SNTHN(J)+EIZ*SNTHZ(I)*SNTHZ(J))
     &*WT(N1,NPM1)
52      CONTINUE
22      CONTINUE
C
        DO 30 N1=1,NP4
        X1=GAUSS(N1,NP4)
C
        DX=DD(K3)+0.5D0*(1.0D0-X1)*(DD(K1)-DD(K3))-TT(K)
        BB=0.57735D0*DX
        EIT=6.0D0*BB*TT(K)*(0.5D0*DX)**2
C
        CALL SHAPE(X1,K)
C
        DO 40 I=1,18
        DO 40 J=1,18
        D(I,J)=D(I,J)+EIT*(SNTHX(I)+SNF(I))*(SNTHX(J)+SNF(J))*WT(N1,NP4)
40      CONTINUE
30      CONTINUE
C
        DO 60 I=1,18
        DO 60 J=1,18
        EM(I,J)=CONST1*(A(I,J)+B(I,J)+D(I,J))
60      CONTINUE
        RETURN
        END
C-----------------------------------------------------------------------
        SUBROUTINE ASSEM1(ERO,AC0,AC1,CML,TT)
        COMMON/EDATA/EK(18,18),EM(18,18)
        COMMON/SDATA/SSTIFF(500,500),SMASS(500,500),SDAMP(500,500),
```

```
      &SLOAD(500),SDISP(500)
        COMMON/FDATA2/NE,NN,ND,IDE,INOD,NOD(50,3),ID(50,18)
        DIMENSION TT(50)
        IMPLICIT DOUBLE PRECISION (A-H,O-Z)
C
        NNE=INOD*IDE
        DO 40 I=1,NE
C
C       for element I,generate element stiffness matrix EK,
C       mass matrix EM
C
        CALL ESTIFF(I,NOD,TT)
C
        CALL EMASS(I,ERO,NOD,TT)
C
        IF (I.LT.NE) GOTO 20
        EM(13,13)=EM(13,13)+CML
        EM(15,15)=EM(15,15)+CML
        EM(17,17)=EM(17,17)+CML
20      DO 35 J=1,NNE
        IJ=ID(I,J)
        DO 30 K=1,NNE
        IK=ID(I,K)
        SSTIFF(IJ,IK)=SSTIFF(IJ,IK)+EK(J,K)
        SMASS(IJ,IK)=SMASS(IJ,IK)+EM(J,K)
30      CONTINUE
35      CONTINUE
40      CONTINUE
C
        DO 60 I=1,ND
        DO 60 J=1,ND
60      SDAMP(I,J)=AC0*SMASS(I,J)+AC1*SSTIFF(I,J)
        RETURN
        END
C-----------------------------------------------------------------------
        SUBROUTINE BNDY(ND,TK,TF,TSB)
        DIMENSION TK(500,500),TF(500),TSB(500)
        IMPLICIT DOUBLE PRECISION (A-H,O-Z)
C
        DO 70 I=1,ND
        IF(TSB(I).GT.400.0) GOTO 70
        DO 40 J=1,ND
        IF(J.EQ.I) GOTO 40
        TF(J)=TF(J)-TK(J,I)*TSB(I)
        TK(I,J)=0.0D0
        TK(J,I)=0.0D0
40      CONTINUE
        TK(I,I)=1.0D0
        TF(I)=TSB(I)
70      CONTINUE
        RETURN
        END
C-----------------------------------------------------------------------
        SUBROUTINE ASSEM2(ELEN,FAI,WIN,SDISP0,SVELO0,ARO,DD,
```

```
     &BCD0,BCS0,BCD,BCS,BCL,BCMR,BCMY,BCMP,BREAK,SLOAD,N0,NH,EBS)
       COMMON/FDATA2/NE,NN,ND,IDE,INOD,NOD(50,3),ID(50,18)
       DIMENSION ELOAD(18),SLOAD(500),ELEN(50),FAI(500),SDISP0(500),
     &SVELO0(500),DD(500),BCD0(4,11),BCS0(4,11),BCD(4,11),BCS(4,11),
     &BCL(4,11),BCMR(4,11),BCMY(4,11),BCMP(4,11),BREAK(11)
       IMPLICIT DOUBLE PRECISION (A-H,O-Z)
C
       NNE=INOD*IDE
       DO 30 I=1,NE
C
C      generate element load matrix ELOAD
C
       CALL CELOAD(I,ELEN(I),FAI,WIN,SDISP0,SVELO0,ARO,DD,
     &BCD0,BCS0,BCD,BCS,BCL,BCMR,BCMY,BCMP,BREAK,ELOAD,N0,NH,EBS)
C
C      for element I
C
       DO 40 J=1,NNE
       IJ=ID(I,J)
       SLOAD(IJ)=SLOAD(IJ)+ELOAD(J)
40     CONTINUE
30     CONTINUE
       RETURN
       END
C-----------------------------------------------------------------------
       SUBROUTINE CELOAD(K,ELEN,FAI,WIN,SDISP0,SVELO0,ARO,DD,
     &BCD0,BCS0,BCD,BCS,BCL,BCMR,BCMY,BCMP,BREAK,ELOAD,N0,NH,EBS)
       COMMON/FDATA2/NE,NN,ND,IDE,INOD,NOD(50,3),ID(50,18)
       DIMENSION PZ(3),PN(3),PX(3),PMN(3),PMZ(3),PMX(3),
     &SDISP0(500),SVELO0(500),ELOAD(18),K1(3),DD(500),
     &BCD0(4,11),BCS0(4,11),BCD(4,11),BCS(4,11),BCL(4,11),
     &BCMR(4,11),BCMY(4,11),BCMP(4,11),BREAK(11),FAI(500)
       IMPLICIT DOUBLE PRECISION (A-H,O-Z)
C
       C1=ELEN/4.0D0
C
       ALF0=0.174533D-01
       DO 5 I=1,18
5      ELOAD(I)=0.0D0
C
       K1(1)=NOD(K,1)
       K1(2)=NOD(K,2)
       K1(3)=NOD(K,3)
C
C      calculate forces per unit length at node J
C
       DO 20 J=1,3
       I=K1(J)
       I1=6*I-5
       I2=6*I-4
       I3=6*I-3
       I4=6*I-2
       I5=6*I-1
       I6=6*I
```

```
      FI=FAI(I)
      WINV=WIN+SVELO0(I3)
      WINE=WIN*EBS
      IF (I.LT.N0) GOTO 50
      IF (I.GE.N0 .AND. I.LE.NH) GOTO 60
      IF (I.GT.NH .AND. I.LE.NN) GOTO 70
C
50    ALF=-SDISP0(I6)+SVELO0(I1)/WINV-EBS
53    UREL2=WINV**2+(SVELO0(I1)-WINE)**2
      CD0=DCSVAL(ALF,10,BREAK,BCD0)
      CS0=DCSVAL(ALF,10,BREAK,BCS0)
      FD=0.5D0*ARO*UREL2*DD(I)*CD0
      FS=0.5D0*ARO*UREL2*DD(I)*CS0
      PZ(J)=-FD*DSIN(ALF)-FS*DCOS(ALF)
      PN(J)=FD*DCOS(ALF)-FS*DSIN(ALF)
      PX(J)=0.0D0
      PMZ(J)=0.0D0
      PMN(J)=0.0D0
      PMX(J)=0.0D0
      GOTO 20
60    UY=SVELO0(I1)*DSIN(FI)-SVELO0(I5)*DCOS(FI)
      THZ=SDISP0(I2)*DCOS(FI)+SDISP0(I6)*DSIN(FI)
      ALF=-THZ+UY/WINV-EBS
63    UREL2=WINV**2+(UY-WINE)**2
      CD=DCSVAL(ALF,10,BREAK,BCD)
      CS=DCSVAL(ALF,10,BREAK,BCS)
      CL=DCSVAL(ALF,10,BREAK,BCL)
      CMR=DCSVAL(ALF,10,BREAK,BCMR)
      CMP=DCSVAL(ALF,10,BREAK,BCMP)
      CMY=DCSVAL(ALF,10,BREAK,BCMY)
      FD=0.5D0*ARO*UREL2*DD(I)*CD
      FS=0.5D0*ARO*UREL2*DD(I)*CS*DSIN(FI)
      FL=0.5D0*ARO*UREL2*DD(I)*CL*DCOS(FI)
      FMR=0.5D0*ARO*UREL2*DD(I)**2*CMR
      FMYA=0.5D0*ARO*UREL2*DD(I)**2*CMY*DSIN(FI)
      FMP=0.5D0*ARO*UREL2*DD(I)**2*CMP*DCOS(FI)
      PY=-FD*DSIN(ALF)-FS*DCOS(ALF)
      PMY=FMR*DSIN(ALF)-FMP*DCOS(ALF)
      PZ(J)=PY*DSIN(FI)+FL*DCOS(FI)
      PN(J)=FD*DCOS(ALF)-FS*DSIN(ALF)
      PX(J)=-PY*DCOS(FI)+FL*DSIN(FI)
      PMZ(J)=PMY*DSIN(FI)-FMYA*DCOS(FI)
      PMN(J)=-FMR*DCOS(ALF)-FMP*DSIN(ALF)
      PMX(J)=-PMY*DCOS(FI)-FMYA*DSIN(FI)
      GOTO 20
70    ALF=-SDISP0(I6)+SVELO0(I1)/WINV
      UREL2=WINV**2+SVELO0(I1)**2
73    CD0=DCSVAL(ALF,10,BREAK,BCD0)
      CS0=DCSVAL(ALF,10,BREAK,BCS0)
      FD=0.5D0*ARO*UREL2*DD(I)*CD0
      FL=0.5D0*ARO*UREL2*DD(I)*CS0
      PZ(J)=-FD*DSIN(ALF)+FL*DCOS(ALF)
      PN(J)=FD*DCOS(ALF)+FL*DSIN(ALF)
      PX(J)=0.0D0
```

```
        PMZ(J)=0.0D0
        PMN(J)=0.0D0
        PMX(J)=0.0D0
20      CONTINUE
C
        ELOAD(1)=PZ(1)
        ELOAD(2)=PMZ(1)
        ELOAD(3)=PN(1)
        ELOAD(4)=PMN(1)
        ELOAD(5)=PX(1)
        ELOAD(6)=PMX(1)
        ELOAD(7)=2.0D0*PZ(2)
        ELOAD(8)=2.0D0*PMZ(2)
        ELOAD(9)=2.0D0*PN(2)
        ELOAD(10)=2.0D0*PMN(2)
        ELOAD(11)=2.0D0*PX(2)
        ELOAD(12)=2.0D0*PMX(2)
        ELOAD(13)=PZ(3)
        ELOAD(14)=PMZ(3)
        ELOAD(15)=PN(3)
        ELOAD(16)=PMN(3)
        ELOAD(17)=PX(3)
        ELOAD(18)=PMX(3)
C
        DO 30 I=1,18
30      ELOAD(I)=C1*ELOAD(I)
        RETURN
        END
C-----------------------------------------------------------------------
        SUBROUTINE SOLVEQ(N,A,B,X)
        DIMENSION A(N,N),B(N),X(N)
        IMPLICIT DOUBLE PRECISION (A-H,O-Z)
C
        CALL DLSASF(N,A,N,B,X)
C
        RETURN
        END
```

Appendix D

Verification of Program DYNA

The computer program DYNA is written to take advantage of the Newmark-β method [36]. First, the program FREEVIB is utilized to calculate the natural frequencies, and then DYNA is used to calculate the dynamic response. Several examples are used to corroborate the output of DYNA. Example D.1 is used to test the time integration; Examples D.2 and D.3 are used to test the whole program. However, there are no previously published results for Examples D.2 and D.3. In the following dynamic calculations, $\beta_1 = 0.6$ and $\beta_2 = 0.3025$ are always used.

Example D.1 (Example 6-9 given in [42])

A five-story building is modeled by the system shown in Figure D.1. $k_i \ (i = 1,2,\cdots 5)$ are the stiffness constants and $m_i \ (i = 1,2,\cdots 5)$ are the lumped masses. The structural stiffness and the lumped mass matrices, as well as the lowest three natural frequencies, can be found in [42]. The building is exposed to a tornado which is described by the concentrated force, $P(t)$, given in Table D.1.

The displacements $u_i \ (i = 1,2,\cdots 5)$ are obtained by using the program DYNA. The results are presented in Table D.2 where δ=0.01 and Δt=0.002s. Table D.3 gives the corresponding results from [42]. Here, the unit inch is used to conform with the unit

employed in [42]. It can be seen that u_1 and u_2 in Table D.2 are a little different from the results presented in Table D.3. But, for the tip displacement u_5, the maximum discrepancy is only 0.4%. The difference may be because the mode-superposition method and Runge-Kutta method are used in [42].

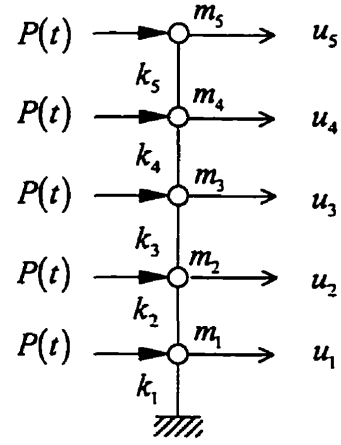

Figure D.1 Model for Example D.1

Table D.1 Data for tornado loading [42]

Time (s)	0.01	0.02	0.03	0.04	0.05	0.06	0.07	0.08	0.09	0.10
$P(t)\times 10^7$ lb.	0.2	0.4	0.6	0.8	1.0	1.2	1.4	1.6	1.8	2.0

Table D.2 Displacements (in) of Example D.1

Time (s)	u_1	u_2	u_3	u_4	u_5
0.01	0.001	0.001	0.001	0.001	0.001
0.02	0.004	0.004	0.004	0.005	0.006
0.03	0.013	0.014	0.014	0.015	0.020
0.04	0.029	0.033	0.034	0.037	0.047
0.05	0.054	0.064	0.066	0.072	0.090
0.06	0.087	0.108	0.114	0.125	0.153
0.07	0.128	0.169	0.181	0.199	0.238
0.08	0.177	0.245	0.270	0.298	0.350
0.09	0.234	0.339	0.384	0.425	0.489
0.10	0.298	0.449	0.525	0.582	0.660

Table D.3 Displacements (in) of Example D.1 taken from [42]

Time (s)	u_1	u_2	u_3	u_4	u_5
0.01	0.000	0.001	0.001	0.001	0.001
0.02	0.003	0.005	0.004	0.004	0.006
0.03	0.011	0.015	0.014	0.015	0.020
0.04	0.025	0.036	0.033	0.035	0.047
0.05	0.047	0.068	0.064	0.069	0.090
0.06	0.078	0.114	0.112	0.120	0.153
0.07	0.118	0.175	0.179	0.193	0.239
0.08	0.166	0.253	0.268	0.291	0.350
0.09	0.222	0.346	0.382	0.417	0.490
0.10	0.286	0.456	0.522	0.574	0.660

Example D.2

Figure D.2 shows a traffic pole that is the same as the one illustrated in Figure 4.3 but the cross section is circular now. Dimension D and the thickness h are the same as those described in Section 4.3. The uniformly distributed force per unit length, $F_0 = 2H(t)\ N/m$, acts on the pole, where $H(t)$ is the unit Heaviside step function, shown below.

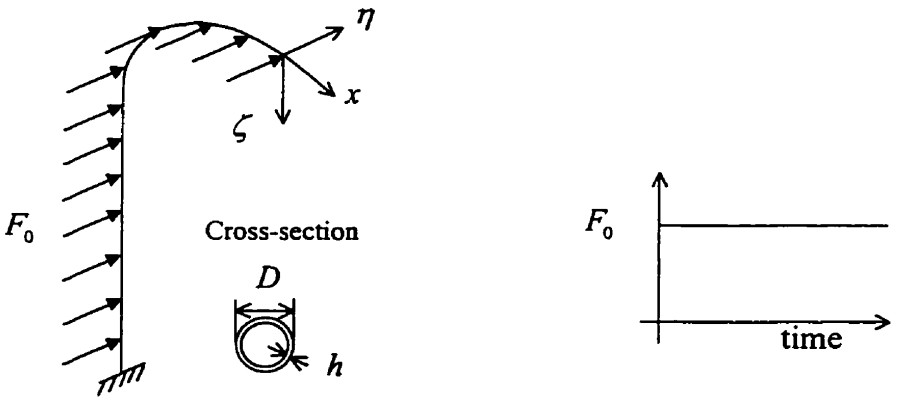

Figure D.2 Example D.2.

The lowest six natural frequencies are given in Table D.4. The mass of the lamp is 39 *kg* (as in Chapter 4). The lowest six frequency mode shapes are very similar to those for the octagonal cross-section. The dynamic responses are computed and they are shown in Figures D.3 and D.4. (Other deflections, which are not shown, are zero.) Here δ=0.005 and Δt=0.02s. Also, when F_0 is a static load, the deformations are calculated by using the program STATIC. The deformations at the tip are:

$$\theta_\zeta = -0.0001043\ rad \qquad v = 0.002759\ m \qquad \theta_x = -0.0003675\ rad\ .$$

These static values are noted at the right hand side of Figures D.3 and D.4. At 26s, the mean values of dynamic responses are within 0.7% of the static data for the pole with a lamp and within 0.05% for the pole without a lamp. The dynamic results tend to the static solution when $t \to \infty$, as indicated from the trends in these figures. On the other hand, the damping ratio, δ, obtained in a standard fashion [43] from the envelope curves of the response histories is within 15% of the input δ.

Table D.4 Lowest natural frequencies, $\omega_n\ (rad/s)$, for Example D.2

Mode number	Circular cross-section	
n	With a lamp	Without a lamp
1	7.15513 out-of-plane*	11.36140 out-of-plane
2	7.41811 in-plane	11.36528 in-plane
3	21.14463 in-plane	40.69759 out-of-plane
4	24.81257 out-of-plane	41.50057 in-plane
5	52.06839 in-plane	78.66159 out-of-plane
6	60.89361 out-of-plane	86.55806 in-plane

* predominant motion

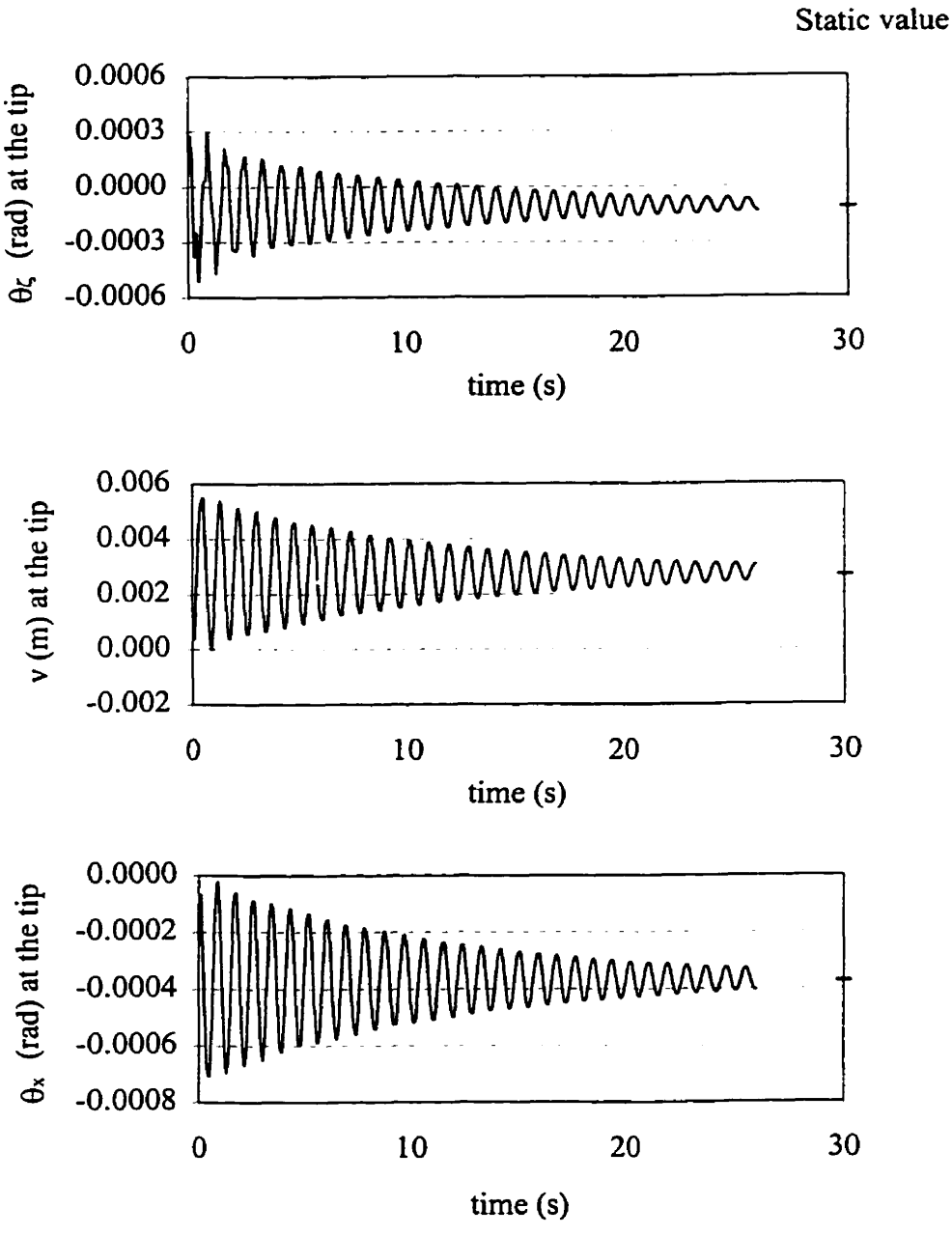

Figure D.3 Dynamic responses of Example D.2 with a lamp.

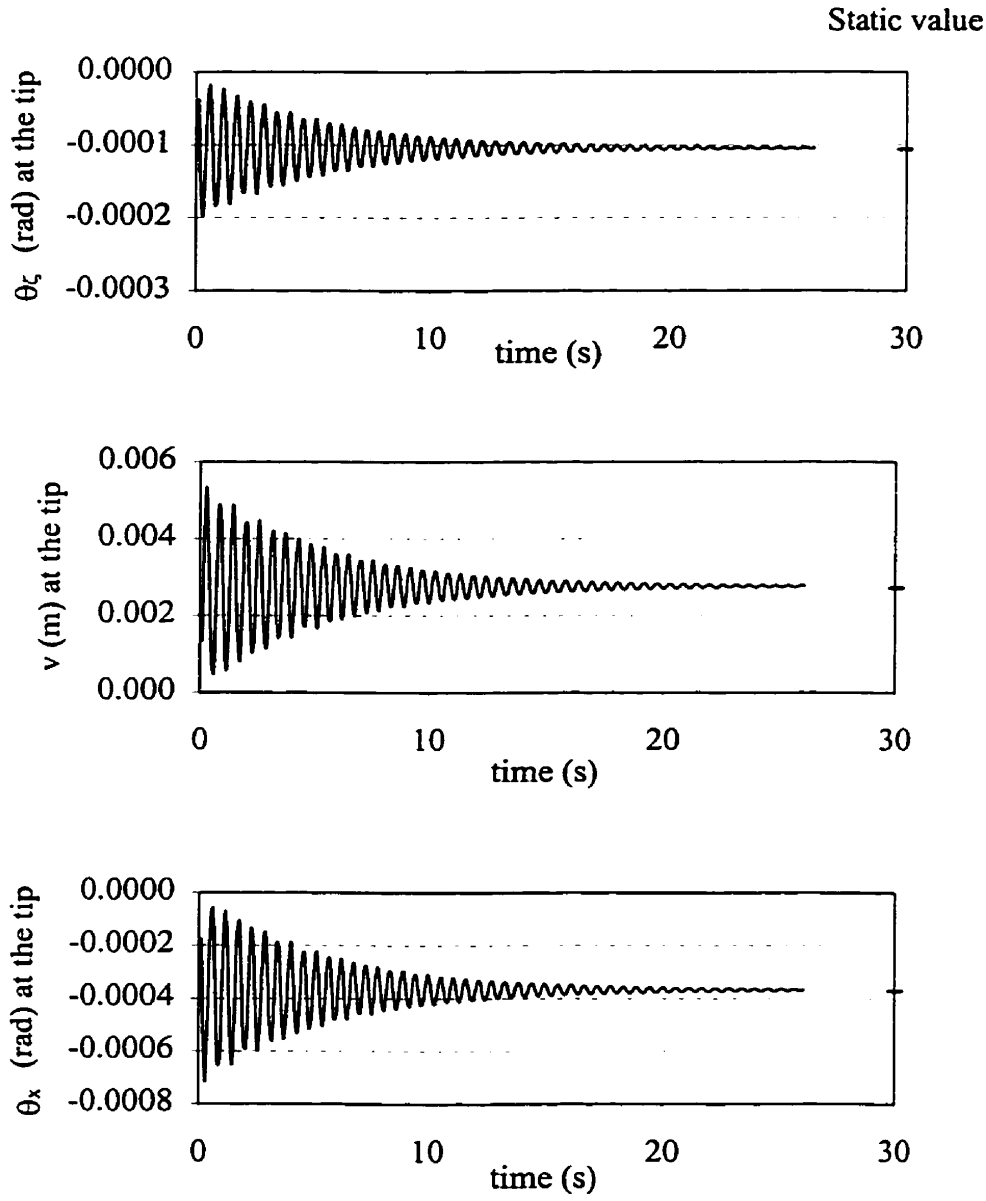

Figure D.4 Dynamic responses of Example D.2 without a lamp.

Example D.3

The pole of Example D.2 is reconsidered but a concentrated point force, $P = 38.2\ N$, is exerted at the free end. This example is shown in Figure D.5. The force is in the $\zeta - \eta$ plane, and it is located eccentrically from the axis with $e = 0.056\ m$. The force in the η direction is the same as the total force employed in Example D.2. Dynamic response histories are computed by using the data of the previous example. The results are shown in Figures D.6 through D.9. The static deformations are calculated as before, and at the tip they are:

$$u = 0.002274\ m \qquad \theta_\zeta = -0.001354\ rad \qquad v = 0.009013\ m$$

$$\theta_\eta = 0.001174\ rad \qquad w = 0.002650\ m \qquad \theta_\xi = -0.001142\ rad\ .$$

Again, the static values are marked in the related figures. After 26s, the mean values of the dynamic responses are within 0.2% of the static data for the pole with a lamp and

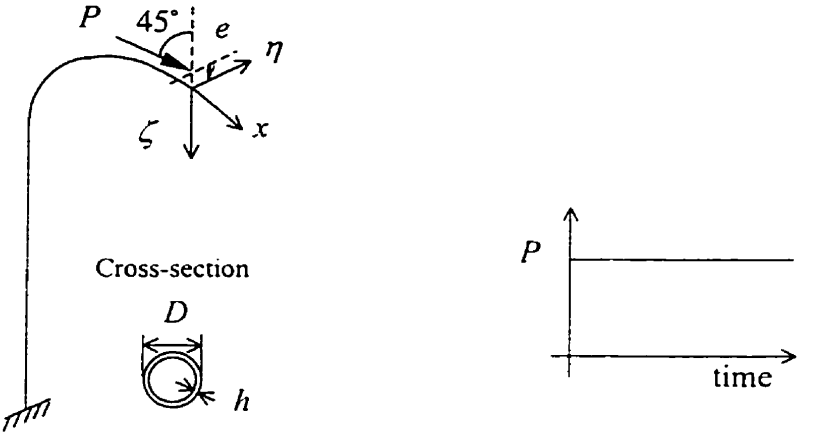

Figure D.5 Example D.3.

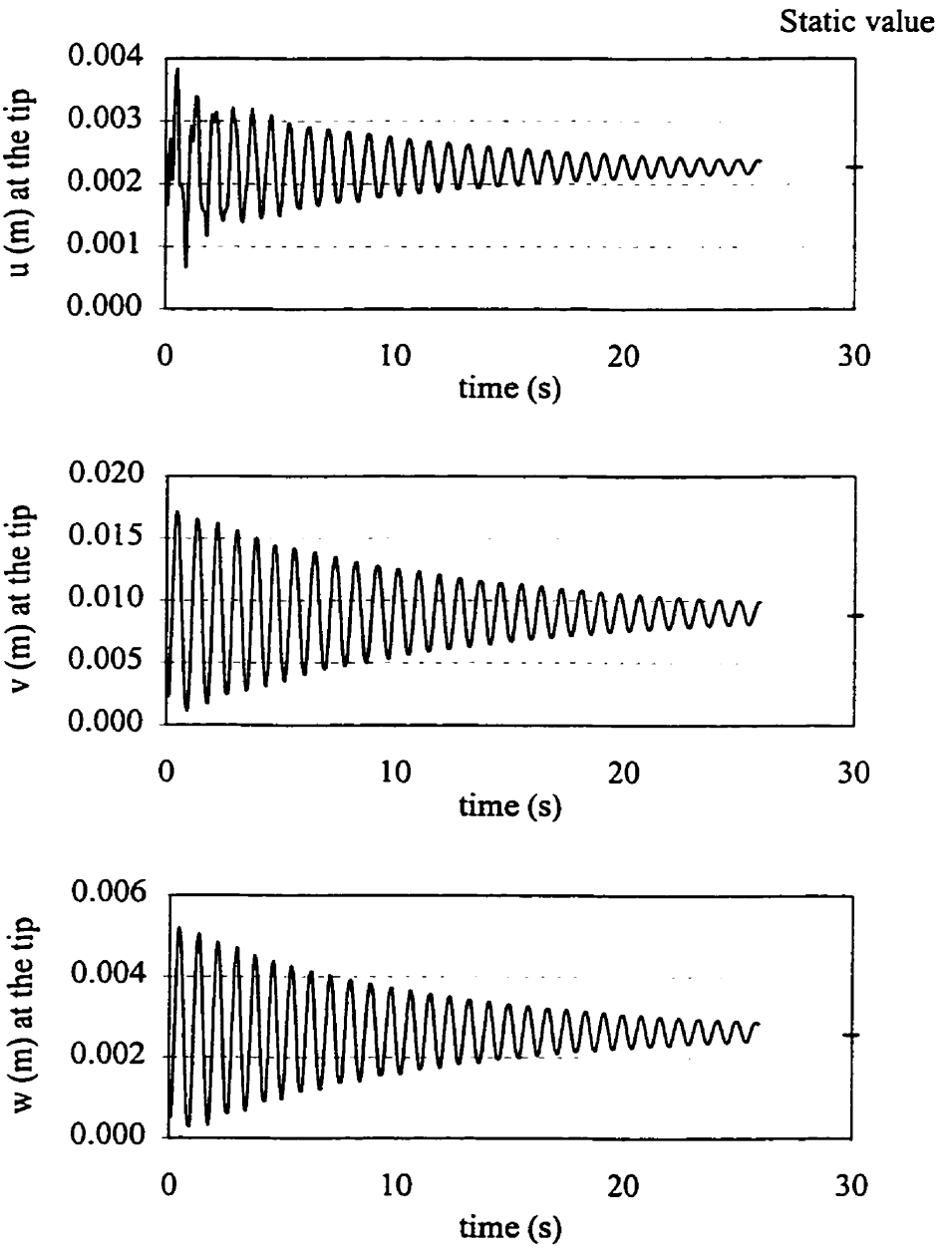

Figure D.6 Dynamic deflections for Example D.3 with a lamp.

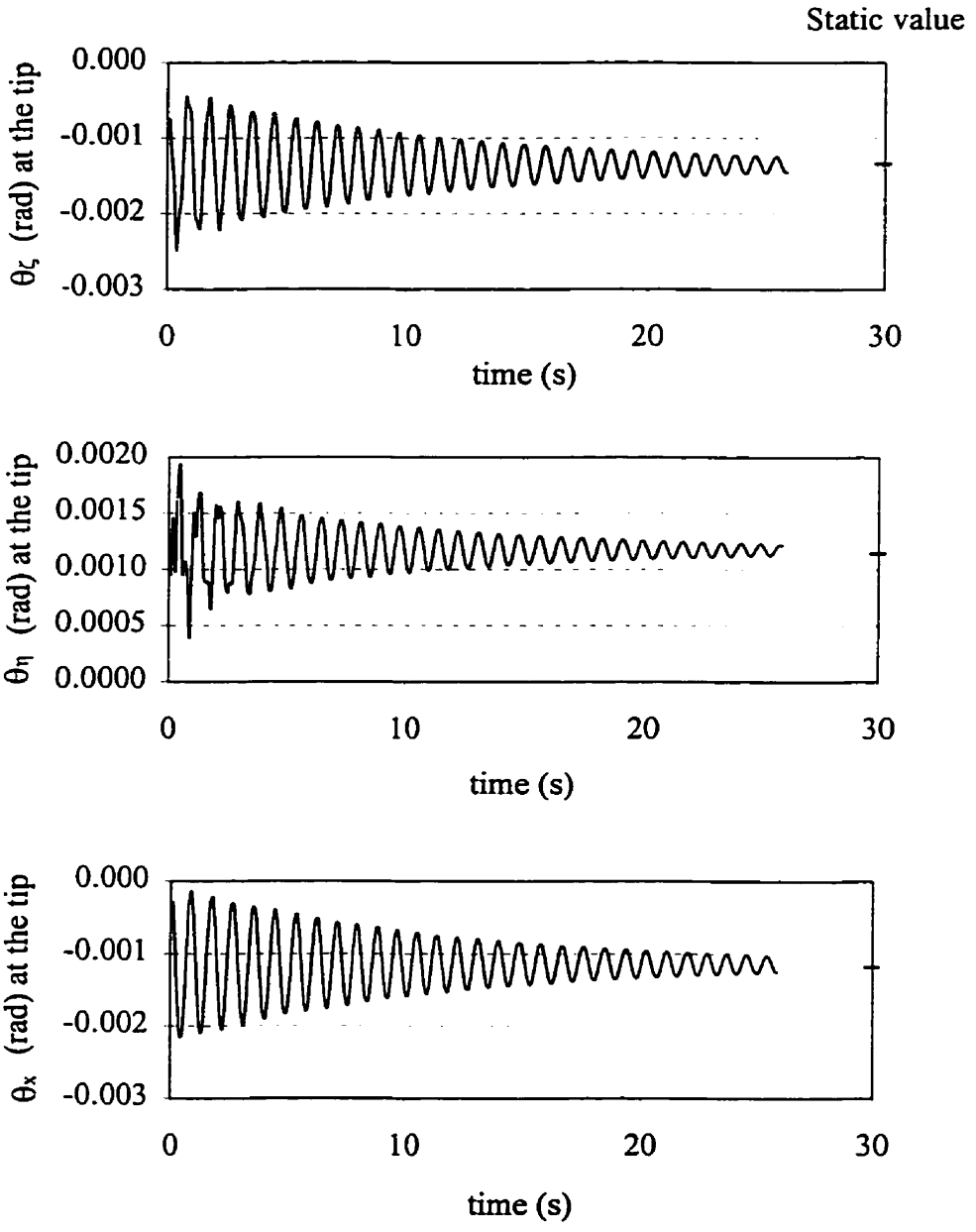

Figure D.7 Dynamic rotations for Example D.3 with a lamp.

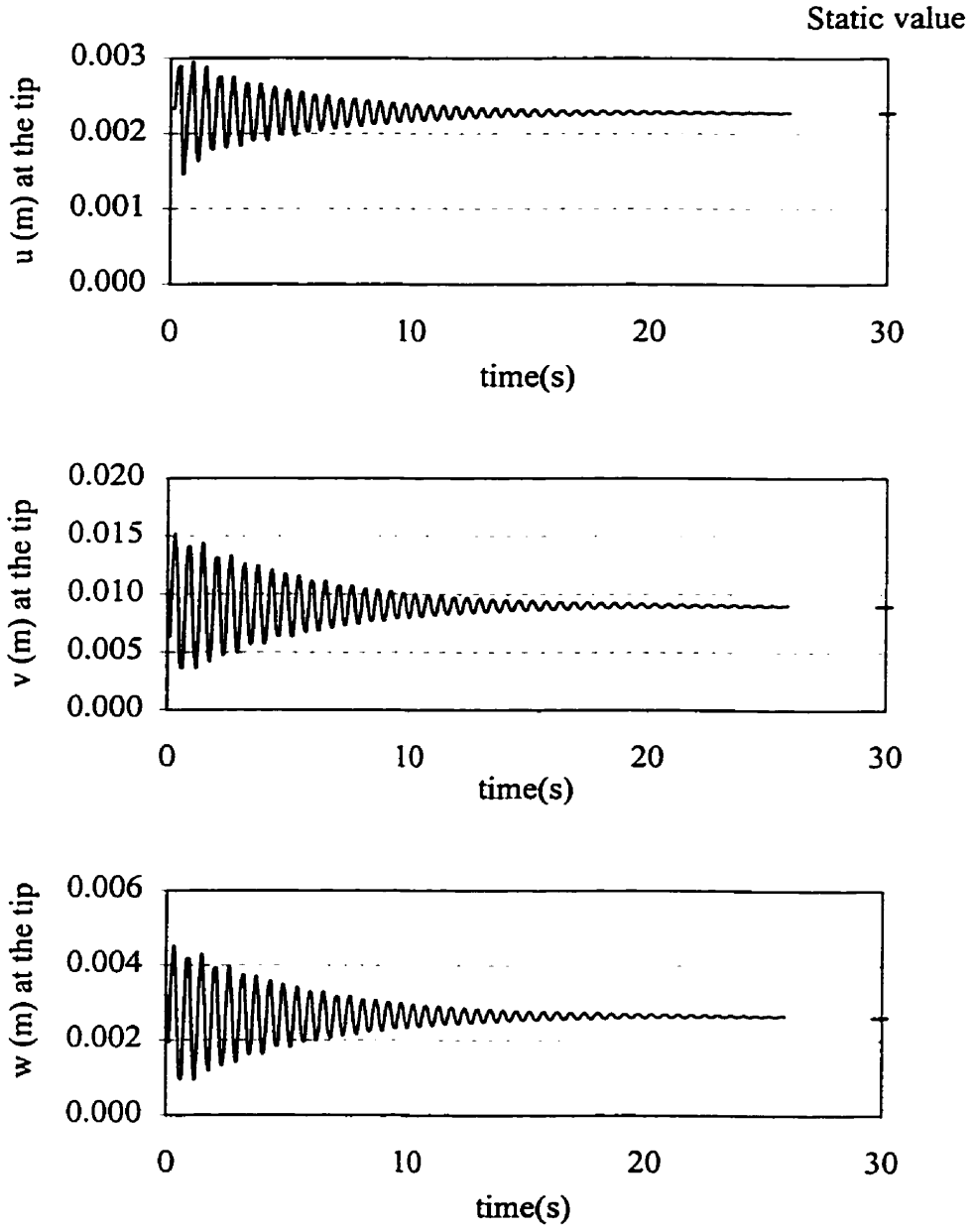

Figure D.8 Dynamic deflections for Example D.3 without a lamp.

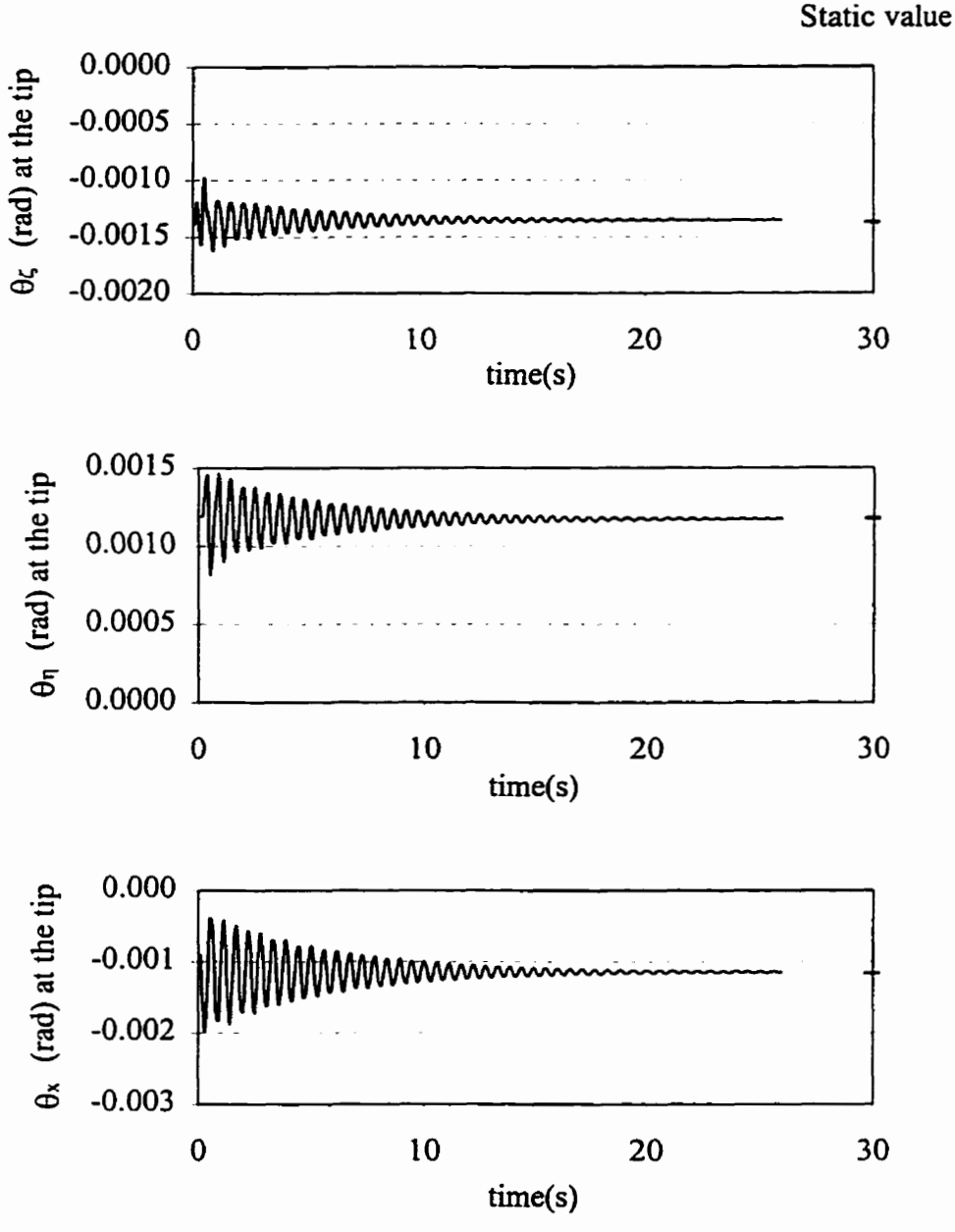

Figure D.9 Dynamic rotations for Example D.3 without a lamp.

within 0.03% for the pole without a lamp. As before, the dynamic results approach the static solutions as $t \to \infty$. The damping ratio, δ, obtained from the envelopes of the dynamic responses is still within 15% of the input δ. Compared with the results of Example D.2, it can be seen that, when the total load is the same in the η direction, the dynamic displacements due to the uniformly distributed load are smaller than those from the concentrated load.

These three examples suggest that the results obtained from DYNA are reasonable.

Appendix E

Calculation of Aerodynamic Coefficients

The following section relates to the calculation of the aerodynamic coefficients for the purely curved part, CD, of a pole.

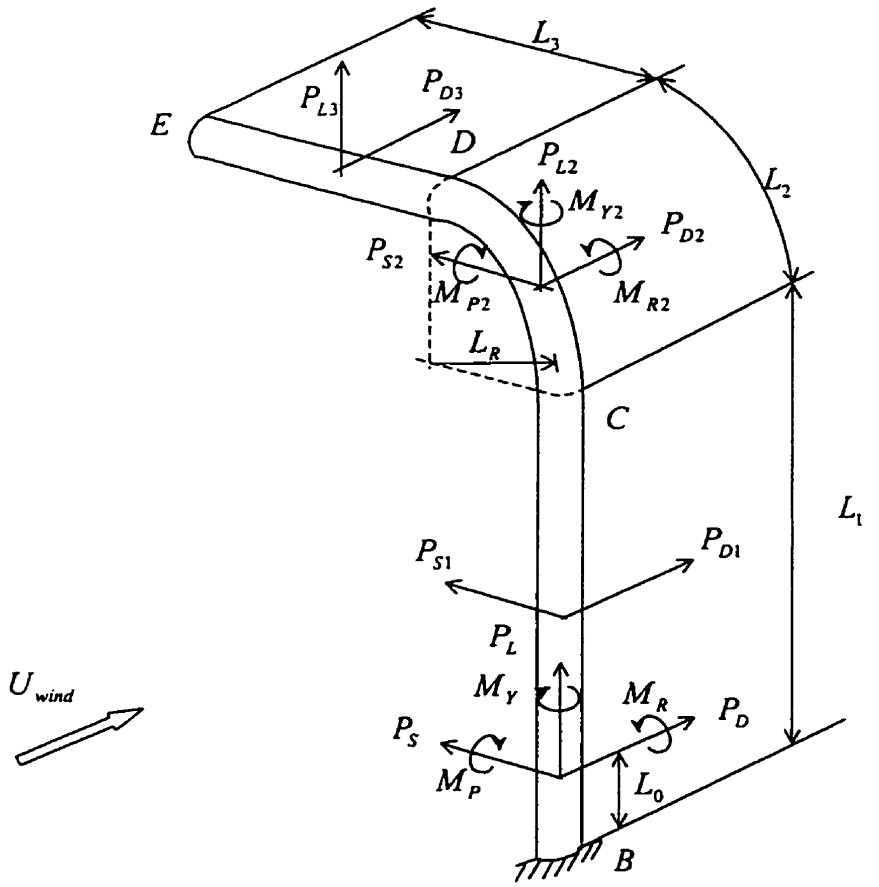

Figure E.1 Aerodynamic forces on the small scale model BE.

The curved pole model consists of three parts, one vertical straight part BC, one horizontal straight part, DE, and the joining, curved part, CD, shown in Figure E.1. Hexagonal and octagonal cross-sections are considered. Because the measured data include the effects of the three parts, the main idea in the following derivation is to subtract the effects of the two straight parts from the measured data to obtain the aerodynamic coefficients corresponding to the purely curved part, CD. This procedure permits a somewhat more detailed representation of the aerodynamic loads in the finite element model.

The following data are used experimentally:

$$L_1 = 290\ mm \quad L_2 = 320\ mm \quad L_3 = 100\ mm$$

$$L_R = 198\ mm \quad L_0 = 195.58\ mm$$

and $D = 12.7\ mm$. See Figure 4.3 for clarification.

The drag and side forces acting on part BC are:

$$P_{D1} = \frac{1}{2}\rho_{air}U_{wind}^2 DC_D L_1$$

and (E.1)

$$P_{S1} = \frac{1}{2}\rho_{air}U_{wind}^2 DC_S L_1 .$$

where C_D and C_S are the drag and side force coefficients for the straight pole. They are given in Figure 4.8. Similarly, for part DE, the drag and lift forces are:

$$P_{D3} = \frac{1}{2}\rho_{air}U_{wind}^2 DC_D L_3$$

and (E.2)

$$P_{L3} = \frac{1}{2}\rho_{air}U_{wind}^2 DC_S L_3 .$$

For the curved part CD, assume that the air pressures in the P_{L2} and P_{S2} directions are

distributed uniformly. Then the forces are:

$$\begin{aligned} P_{D2} &= \frac{1}{2}\rho_{air}U_{wind}^2 DC_D^*(\pi L_R / 2) \\ P_{L2} &= \frac{1}{2}\rho_{air}U_{wind}^2 DC_L^* L_R \\ P_{S2} &= \frac{1}{2}\rho_{air}U_{wind}^2 DC_S^* L_R \,. \end{aligned} \tag{E.3}$$

where C_D^*, C_L^* and C_S^* are the drag, lift and side force coefficients for the curved part CD, respectively. They are defined in Section 4.7. For the model of BE, the total measured forces are (see Section 4.6):

$$\begin{aligned} P_D &= \frac{1}{2}\rho_{air}U_{wind}^2 DC_{DC}L_{BE} \\ P_L &= \frac{1}{2}\rho_{air}U_{wind}^2 DC_{LC}L_{BE} \\ P_S &= \frac{1}{2}\rho_{air}U_{wind}^2 DC_{SC}L_{BE} \end{aligned} \tag{E.4}$$

C_{DC}, C_{LC} and C_{SC} are presented in Figures 4.6 and 4.7, where $L_{BE} = L_1 + L_2 + L_3$. On the other hand,

$$\begin{aligned} P_D &= P_{D1} + P_{D2} + P_{D3} \\ P_L &= P_{L2} + P_{L3} \\ P_S &= P_{S1} + P_{S2} \,. \end{aligned} \tag{E.5}$$

By combining equations (E.1) through (E.5), the following results can be obtained:

$$\begin{aligned} C_D^* &= \frac{2}{\pi L_R}\left[C_{DC}L_{BE} - C_D(L_1 + L_3)\right] \\ C_L^* &= \frac{1}{L_R}(C_{LC}L_{BE} - C_S L_3) \\ C_S^* &= \frac{1}{L_R}(C_{SC}L_{BE} - C_S L_1) \,. \end{aligned} \tag{E.6}$$

For the moment coefficients, the measured total yawing moment of the complete model BE is M_Y. Now

$$M_Y = M_{Y2} + M_Y^D \tag{E.7}$$

where M_{Y2} is the yawing moment on part CD and M_Y^D is the moment contribution from the drag force. Furthermore:

$$M_Y = \frac{1}{2}\rho_{air} U_{wind}^2 D^2 C_{MYC} L_{BE} \tag{E.8}$$

and

$$M_{Y2} = \frac{1}{2}\rho_{air} U_{wind}^2 D^2 C_{MY}^* L_R \ . \tag{E.9}$$

The C_{MYC} is given in Figures 4.6 and 4.7. C_{MY}^* is the yawing moment coefficient of the curved part CD. Also,

$$M_Y^D = M_{Y2}^D + M_{Y3}^D \tag{E.10}$$

where M_{Y2}^D and M_{Y3}^D are the moment contributions from parts CD and DE, respectively. From Figure E.2, it can be shown that:

$$M_{Y2}^D = \int_0^{\pi L_R/2} \frac{1}{2}\rho_{air} U_{wind}^2 D C_D^* X' ds \tag{E.11}$$

and

$$M_{Y3}^D = \int_{L_R}^{L_R+L_3} \frac{1}{2}\rho_{air} U_{wind}^2 D C_D X' dX' \ . \tag{E.12}$$

The following result can be obtained from equations (E.7) through (E.12):

$$C_{MY}^* = \frac{1}{L_R}\left(C_{MYC} L_{BE} - C_D^* L_{C0} - C_D L_{C1}\right) \tag{E.13a}$$

where

$$L_{C0} = \frac{L_R^2}{D}\left(\frac{\pi}{2} - 1\right) \tag{E.13b}$$

and

$$L_{C1} = \frac{1}{2D}\left[(L_R + L_3)^2 - L_R^2\right]. \tag{E.13c}$$

Similarly, the total pitching moment is:

$$M_P = M_{P2} + M_P^D \tag{E.14}$$

where M_{P2} is the pitching moment on part CD and M_P^D is the moment contribution

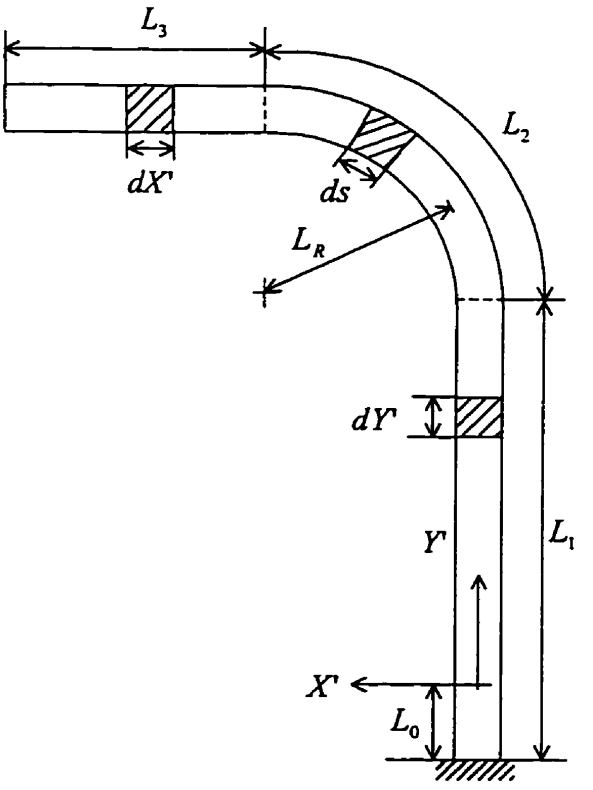

Figure E.2 Coordinate system X'–Y'.

from the drag force. Also

$$M_P = \frac{1}{2}\rho_{air}U_{wind}^2 D^2 C_{MPC} L_{BE} \tag{E.15}$$

and

$$M_{P2} = \frac{1}{2}\rho_{air}U_{wind}^2 D^2 C_{MP}^{*} L_R \tag{E.16}$$

C_{MPC} is presented in Figures 4.6 and 4.7. C_{MP}^{*} is the pitching moment coefficient of the curved part CD whose derivation is found from:

$$M_P^D = M_{P1}^D + M_{P2}^D + M_{P3}^D \tag{E.17}$$

$$M_{P1}^D = \int_{-L_0}^{L_1-L_0} \frac{1}{2}\rho_{air}U_{wind}^2 D C_D Y' dY' \tag{E.18}$$

$$M_{P2}^D = \int_0^{\pi L_R/2} \frac{1}{2}\rho_{air}U_{wind}^2 D C_D^{*} Y' ds \tag{E.19}$$

and

$$M_{P3}^D = \frac{1}{2}\rho_{air}U_{wind}^2 D C_D L_3 (L_1 - L_0 + L_R). \tag{E.20}$$

From equations (E.14) through (E.20), it can be shown that:

$$C_{MP}^{*} = \frac{1}{L_R}\left(C_{MPC}L_{BE} - C_D L_{C2} - C_D^{*} L_{C3}\right) \tag{E.21a}$$

where

$$L_{C2} = L_{C4} + \frac{L_3}{D}(L_1 - L_0 + L_R) \tag{E.21b}$$

$$L_{C3} = \frac{L_R}{D}\left[\frac{\pi}{2}(L_1 - L_0) + L_R\right] \tag{E.21c}$$

$$L_{C4} = \frac{1}{2D}\left[(L_1 - L_0)^2 - L_0^2\right]. \tag{E.21d}$$

Next, the total rolling moment for the model of BE is:

$$M_R = M_R^S - M_R^L + M_{R2} \tag{E.22}$$

where M_R^S is the moment contribution from the side force, M_R^L is the moment contribution from the lift force and M_{R2} is the rolling moment on part CD. Furthermore,

$$M_R = \frac{1}{2}\rho_{air} U_{wind}^2 D^2 C_{MRC} L_{BE} \tag{E.23}$$

and

$$M_{R2} = \frac{1}{2}\rho_{air} U_{wind}^2 D^2 C_{MR}^* (\pi L_R / 2) \tag{E.24}$$

where C_{MRC} is given in Figures 4.6 and 4.7 again. C_{MR}^* is the rolling moment coefficient of the curved part CD which can be found from:

$$M_R^S = M_{R1}^S + M_{R2}^S \tag{E.25}$$

$$M_{R1}^S = \int_{-L_0}^{L_1 - L_0} \frac{1}{2}\rho_{air} U_{wind}^2 D C_S Y' \, dY' \tag{E.26}$$

and

$$M_{R2}^S = \int_{L_1 - L_0}^{L_1 - L_0 + L_R} \frac{1}{2}\rho_{air} U_{wind}^2 D C_S^* Y' dY' \,. \tag{E.27}$$

Similarly,

$$M_R^L = M_{R2}^L + M_{R3}^L \tag{E.28}$$

$$M_{R2}^L = \int_0^{L_R} \frac{1}{2}\rho_{air} U_{wind}^2 D C_L^* X' \, dX' \tag{E.29}$$

and

$$M_{R3}^{L} = \int_{L_R}^{L_R+L_1} \frac{1}{2}\rho_{air} U_{wind}^2 D C_S X' dX' \tag{E.30}$$

By combining equations (E.22) through (E.30), $C_{MR}^{\bullet}$ can be obtained as:

$$C_{MR}^{\bullet} = \frac{2}{\pi L_R}\left[C_{MRC} L_{BE} + C_S(L_{C1} - L_{C4}) - C_S^{\bullet} L_{C5} + C_L^{\bullet} L_{C6}\right] \tag{E.31a}$$

where

$$L_{C5} = \frac{L_R}{D}\left[(L_1 - L_0) + L_R/2\right] \tag{E.31b}$$

$$L_{C6} = L_R^2/(2D)\,. \tag{E.31c}$$

Therefore, the aerodynamic coefficients of the curved part *CD* can be calculated from equations (E.6), (E.13), (E.21) and (E.31). The results are presented in Figures 4.10 and 4.11.

Appendix F

Additional Aerodynamic Figures

Figures F.1 through F.3 present the effects of Reynolds number, the wind speed and a simulated lamp which is located at the tip of a pole, as described in Section 4.6. From Figure F.1, it can be seen that C_{DC} is nearly the same when Re is between 10^4 and 2×10^4 for the hexagonal pole. However, C_{DC} varies with Re for the octagonal pole. Figure F.2 shows that aerodynamic coefficients are very close when the wind speed changes in a small range. Furthermore, it can be seen from Figure F.3 that the effect of the simulated lamp on the aerodynamic coefficients is small.

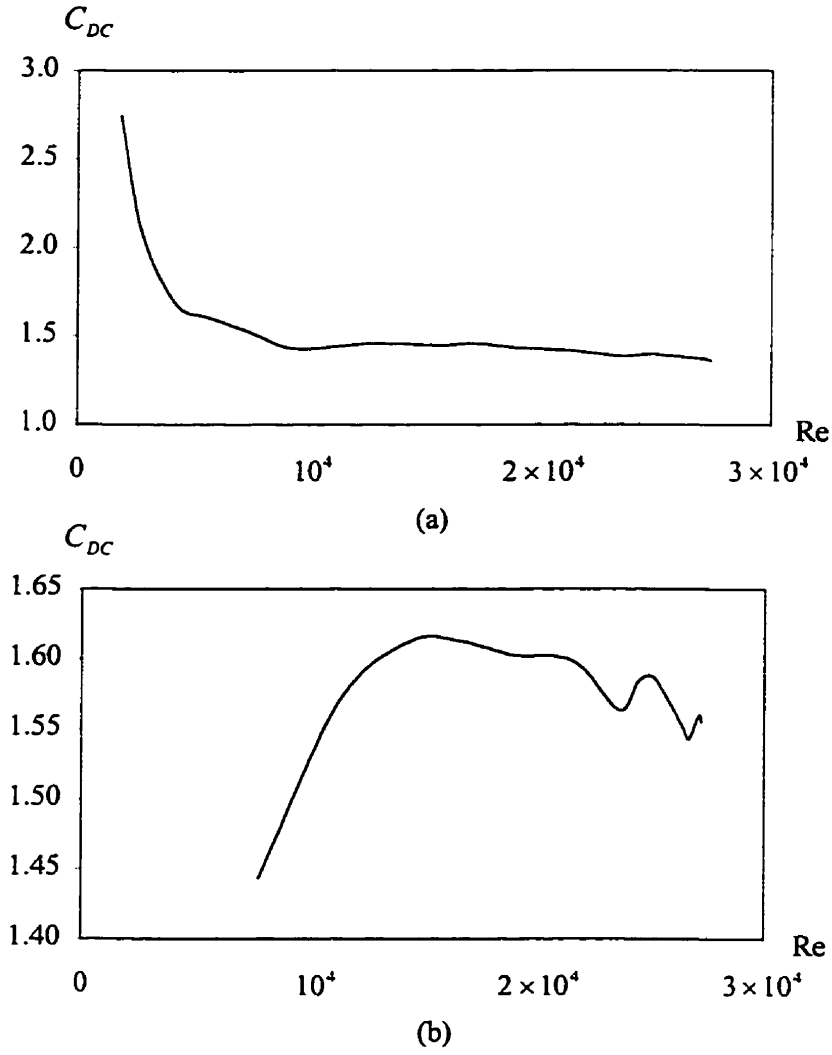

Figure F.1 Drag coefficient, C_{DC}, for $\bar{\alpha}_m = 90°$ but different Reynolds numbers. Results for the (a) hexagonal and (b) octagonal cross-section.

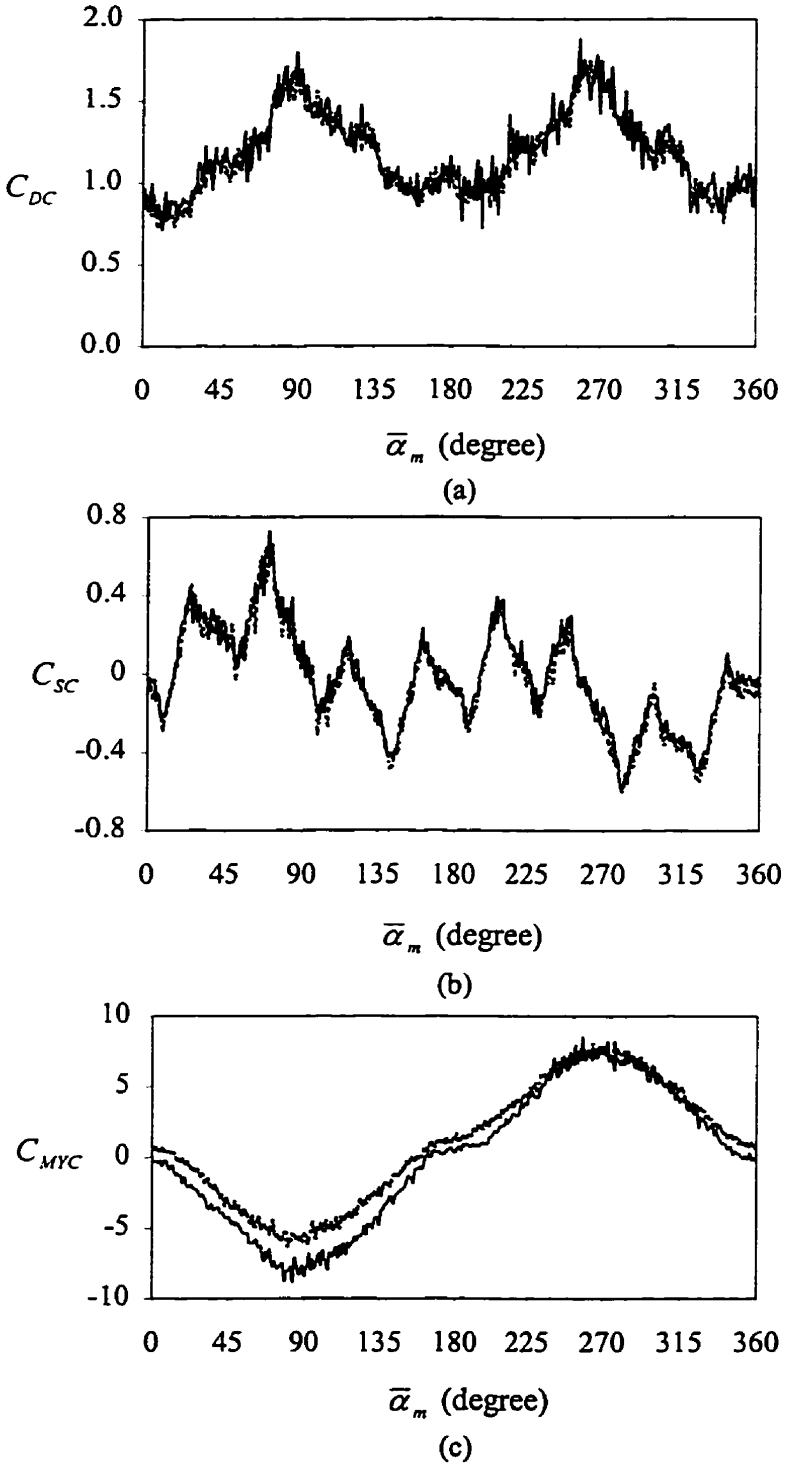

Figure F.2 The effect of the wind speed on aerodynamic coefficients for the octagonal curved model. — U_{wind}=29.5m/s; ---- U_{wind}=31.4 m/s.

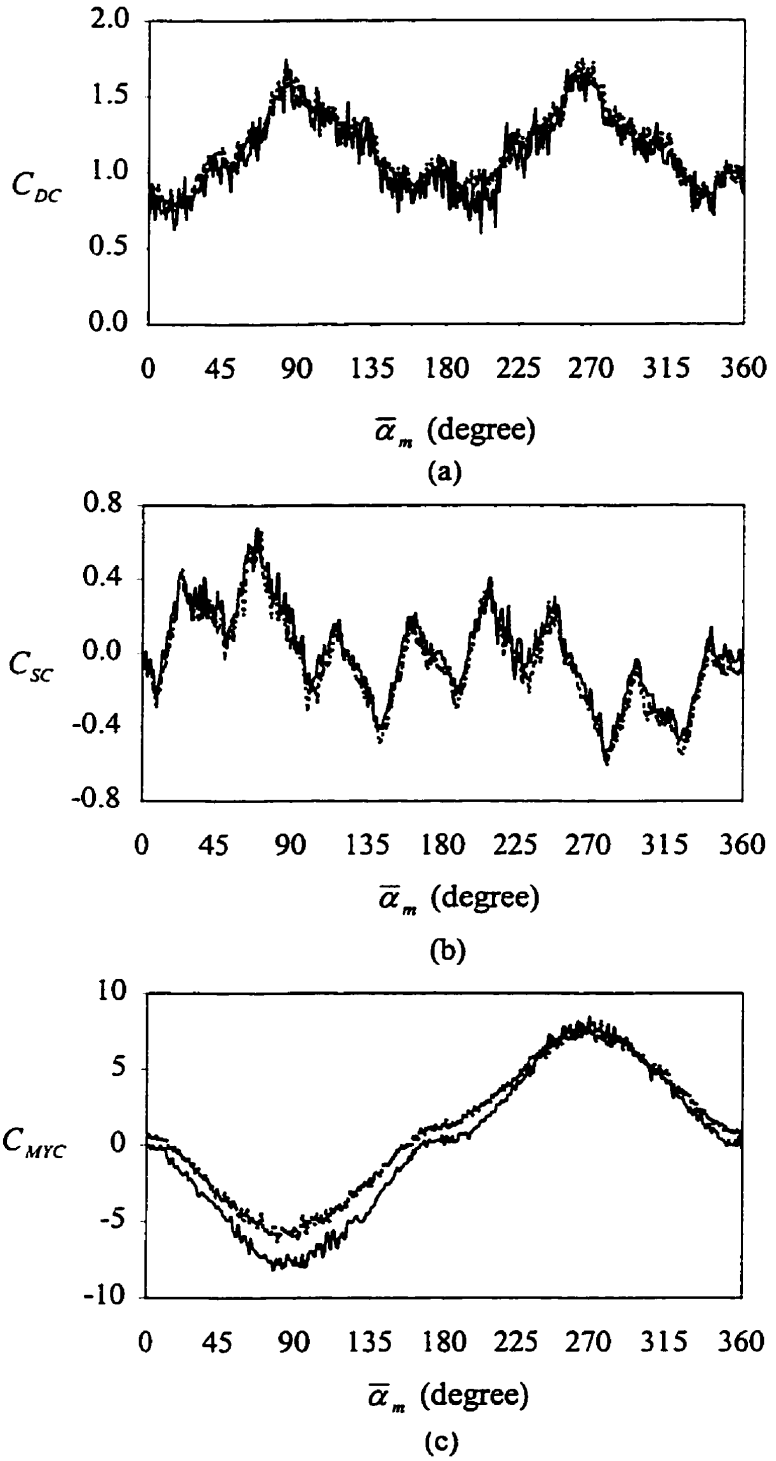

Figure F.3 The effect of the simulated lamp on aerodynamic coefficients for the octagonal curved model. — with the simulator; ---- without the simulator.

IMAGE EVALUATION
TEST TARGET (QA-3)

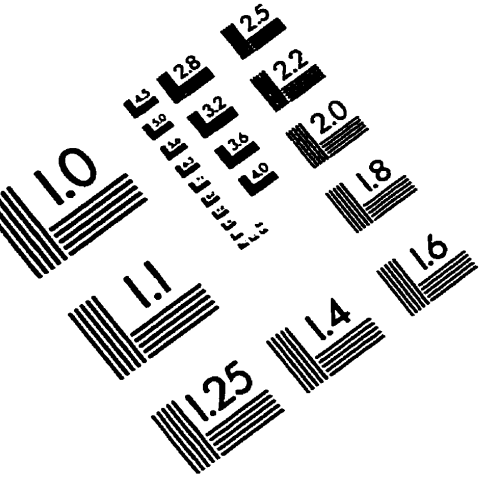

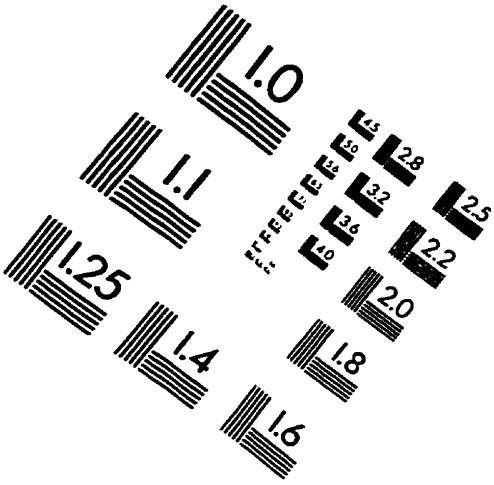

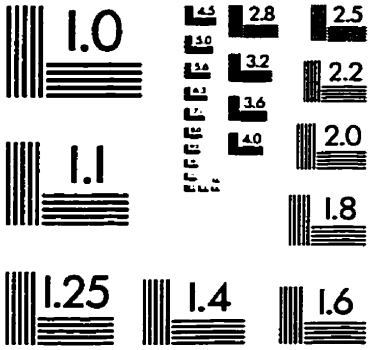

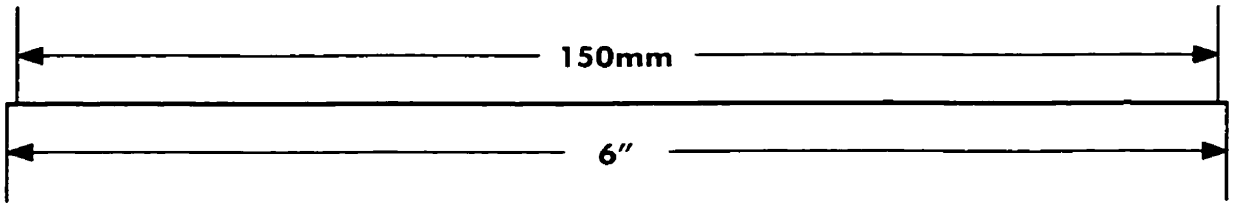

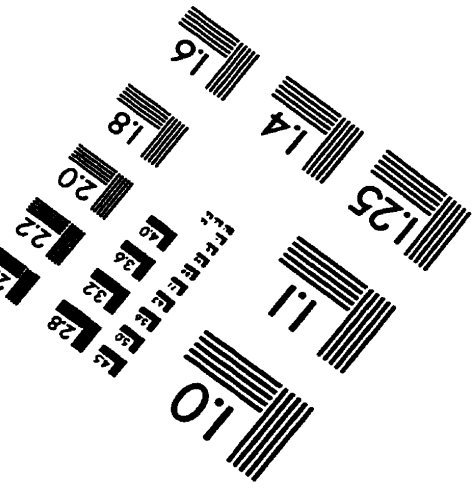

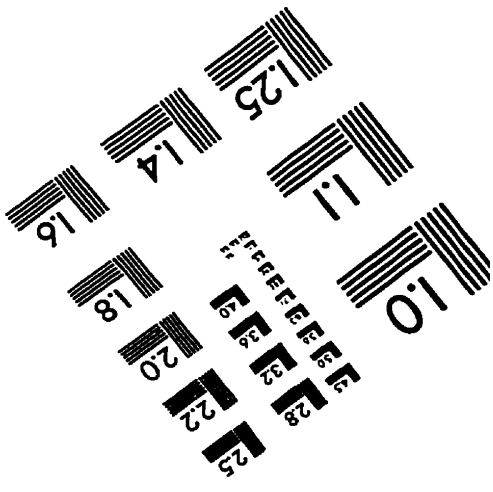

APPLIED IMAGE, Inc
1653 East Main Street
Rochester, NY 14609 USA
Phone: 716/482-0300
Fax: 716/288-5989